Nanomechanotransduction of Human Mesenchymal Stem Cells
an Application of Medical Nanobiotechnology

Habib Nikukar
MD

This thesis is submitted for the degree of Doctor of Philosophy at the University of Glasgow

Centre for Cell Engineering
Institute for Molecular, Cell and System Biology
College of Medical, Veterinary and Life Sciences
University of Glasgow
United Kingdom
G12 8QQ

September 2013


بسم الله الرحمن الرحيم

Abstract

In this project the influences on human adult mesenchymal stem cells using nanomechanical stimulation techniques has been explored. It is expected that human mesenchymal stem cells will find use in many autologous regenerative therapies and in tissue engineering. However, the ability to control stem cell growth and differentiation is presently limited, and this is a major hurdle to the clinical use of these multipotent cells especially when considering the desire not to use soluble factors or complex media formulations in culture. Also, unpredictable number of cells required to be clinically useful is currently a hurdle to using materials-based (stiffness, chemistry, nanotopography, etc.) culture substrates.

According to known cellular reactions to environmental stimuli, it was expected that human cells show some reactions to nanoscale vibration that in the case of stem cells it could be a differentiation response. This thesis gives a first demonstration of using nanoscale mechanotransductive protocols (10-14 nm vertical displacements at 1 kHz frequency), “nanokicking”, to promote osteoblastogenesis in human mesenchymal stem cell cultures. On the basis of application of the reverse piezo effect, laser interferometry was used to develop the optimal stem cell stimulation conditions, allowing delivery of nanoscale cues across the entire surface of the Petri dishes used.

A combination of biological techniques has then been used to demonstrate osteoblastogenesis. Furthermore, RhoA has been implicated as being central to osteoblastic differentiation in agreement with materials-based strategies. We validate this with pharmacological inhibition of RhoA kinase.

It is easy to envisage such stimulation protocols being up-scaled to form large-scale osteoblast bioreactors as standard cell culture plates and incubators are used in the protocol.

Table of contents

List of Tables

List of Figures

List of Abbreviations

2D	Two-dimensional
2X	Two times
3D	Three-dimensional
Al	Aluminium
ANOVA	Analysis of variance
BMP	Bone Morphogenic Protein
bp	Base pair
BSA	Bovine serum albumin
cDNA	complementary DNA
CO_2	Carbon dioxide
CS	Coverslip
DNA	Deoxyribonucleic acid
ECM	Extracellular matrix
ERK	Extracellular signal-regulated kinases
ESC	Embryonic stem cell
FAK	Focal Adhesion Kinase
FA	Focal adhesion
GAPDH	Glyceraldehyde 3-phosphate dehydrogenase
hr	hour
iPSC	induced pluripotent stem cell
kPa	Kilopascal
lt	Litre
LINC	Linker of nucleoskeleton & cytoskeleton
MAPK	Mitogen-activated protein kinases
mM	mili Molar
MSC	Mesenchymal stem cell
mRNA	Messenger RNA
MW	Molecular weight
NASA	The National Aeronautics and Space Administration
nm	Nanometer
P	Piezo actuator
PBS	Phosphate Buffer Saline

PCR	Polymerase Chain Reaction
pN	pico-Newton
PPARγ	Peroxisome proliferator-activated receptor gamma
RhoA	Ras homolog gene family, member A
RNA	Ribonucleic acid
ROCK	Rho-associated protein kinase
rpm	Revolutions per minute
Runx2	Runt-related transcription factor 2
SD	Standard deviation
SEM	Scanning Electron Microscopy
TCP	Tissue culture plastic dish
TE	Tissue engineering
v/v	Volume by volume
w/v	Weight by volume

Presentations and publications

Poster presentations:

1. Nanomechanotransduction of human mesenchymal stem cell

➔ Tissue and Cell Engineering Society (TCES), July 2012, Liverpool, UK

2. Nanoscale mechanical stimulation promotes osteogenesis from mesenchymal stem cells (Nanomechanotransduction of Human Mesenchymal Stem Cells)

➔ 6th Mesenchymal stem cell conference, June 2012, University of Southampton, Southampton, UK

➔ European Molecular Biology Laboratory (EMBL) Conference: Stem Cells in Cancer and Regenerative Medicine, 29 August 2012 - 01 September 2012, Heidelberg, Germany

3. "Nanokicking" of human MSCs could make bone. Possible clinical applications

➔ TCES, July 2013, Cardiff, UK

➔ European Society for Artificial organs (ESAO), September 2013, Glasgow, UK

Oral presentations:

1. Nanomechanotransduction of human mesenchymal stem cell: 8th Royan International congress on stem cell biology and technology, September 2012, Royan Institute, Tehran, I.R. Iran

2. Osteogenesis of mesenchymal stem cells by nanoscale mechanotransduction: European Society for Artificial organs (ESAO), September 2013, Glasgow, UK

Publications:

1. NIKUKAR, H., REID, S., TSIMBOURI, P. M., RIEHLE, M. O., CURTIS, A. S. & DALBY, M. J. 2013. Osteogenesis of mesenchymal stem cells by nanoscale mechanotransduction. *ACS Nano,* 7**,** 2758-67.

2. CURTIS, A., REID, S., MARTIN, I., VAIDYANATHAN, R., SMITH, C. A., NIKUKAR, H. & DALBY, M. J. 2013. Cell Interactions at the nanoscale: piezoelectric stimulation. *IEEE Trans Nanobioscience,* 12**,** 247-54.

Acknowledgements

I would like to take this opportunity to express my sincere gratefulness and best regards to Dr Matthew Dalby for his supervision, patience, advice and constant encouragements throughout this work.

Also I am indebted to Prof Adam Curtis, Dr Mathis Riehle, and Dr Stuart Reid for their supervision, guidance and encouragements.

I would like to thank the late Prof Chris Wilkinson for his interest and invaluable advices.

I would like to give my special thanks to my dear uncle, Mr Kazem Mojibian, whom it was impossible to handle the difficulties of studying and stay abroad for me and my family without.

I am indebted to Prof Kamran Bagheri Lankarani and Dr S Jalil Mirmohammadi for their great supports to award this grant and their encouragements to complete this education.

I am thankful to my colleagues Dr Monica P Tsimbouri, Dr Laura E McNamara, and Dr Lesley-Anne Turner for their help, especially for the review of my thesis and their advices and recommendations.

Thanks to staff, technicians and students in CCE and the University of Glasgow for their great hospitality and helps in all the stages of my study, especially Mr Andrew Hart, Mrs Carol-Anne Smith, Mr Colin Craig, Mrs Margaret Mullin, Mr Peter Chang for their technical support and Mrs Avril McGregor.

Thanks to the Iranian Ministry of Health and Medical Educations for funding this project as well as their brave and helpful administrator, Ms Nikooseresht for all her hard work and supports.

Finally heartfelt thanks to my wife and my daughters for their support, extraordinary patience, and love they afforded me during the years of my study. Also thanks are to my mother, my father and other family members whose good wishes enabled me to complete this research.

Author's Declaration

The research reported within this thesis is the original work of the author except where the assistance of others has been acknowledged and at the time of submission is not being considered elsewhere for any other academic qualification.

Habib Nikukar
September 2013

Dedication

I dedicated this thesis to my dear parents,
and my dear family,
Mahshid, Zeynab, Reyhaneh, and Narges

Chapter I- Introduction

1.1 Introduction

The complexity of the human body and coordinated efficient harmony of various parts of living organisms are reflections of more complex integration at the cellular and molecular level. Thanks to modern microscopy and molecular approaches, biologists are finding inside the smallest parts of living organisms, the cell. Growth, development and repair are continuously occurring to preserve health to the end of life. Medicine, as a science to conserve human health and treat diseases, is always looking for new methods to support us, as we grow older. By progress in the field of very small (micro- and nanosciences), the possibility of finding new techniques for prevention and treatment of diseases is increasing. The hopes for use of the cells directly for cell based therapy, stem cell therapy, gene therapy and understanding cell control and signalling mechanisms will realize regenerative therapy. Use of autologous stem cells to make new tissues and organs to replace or treat those that have become damaged or diseased is one major tissue engineering aim.

1.2 Bionanotechnology

Development and availability of modern technology has facilitated discovery within the very small world at the micro – and nanoscale resulting in the introduction of micro – and nanotechnology (Greco et al., 2005, Kubinova and Sykova, 2010). The desire to find new methods to maintain human health and treat the life threatening diseases in medical sciences linked to nanotechnology defines the field of ‘bionanotechnology’. The term ‘nanomedicine’ (Mason and Dunnill, 2008) sometimes is applied to the usage of high performance nanotechnology for the improvement of medical methods and devices. The basics of these sciences focus on nanoscale (1-100 $\times$ 10^{-9} m) materials such as synthetic nanotubes, nanoparticles, molecular engines and also the study of cellular nanostructures such as pores, chromosomes (DNA), etc (Etheridge et al., 2013). Every little hint could generate new

knowledge about use of nanosciences in medicine and move toward better protection of health and improved treatments (Akhter et al., 2013).

1.3 Regenerative medicine

Health and lifestyle improvements have caused a progressive increase in old age groups around the world (Sandrasagra, 2007). As the result of old age the body and its organs can suffer disease or damage and these global changes cause pressure to discover new methods for replacement of organs, joints etc. to support the aging population. It is further clear that the numbers of human-based tissues (allograft transplants) are not sufficient and the adverse immune reactions with transplanted organs leading to the need for immunosuppressive drugs coupled to shortage in donor organs make regeneration of organs and/or engineered replacements very attractive (Dvir et al., 2011). Regenerative medicine is dealing with production of living and functional tissues to replace lost, diseased, or failed tissue and organs. Aging, accidents and congenital defects are among the common causes that increase the need for regenerative therapy. Since early in the 20th century, musculoskeletal grafting has been within the surgical scope. Orthopedic need for regeneration and replacement of lost extremities is a progressive field of investigation (Evans, 2011, Gruskin et al., 2012, Baddour et al., 2012).

Manipulation of cellular fates is one of the most important aspects of the biologists' interests with hope for regeneration of tissues. Use of these methods in cell therapy and replacement of body tissues or organs using the multipotent stem cells taken from the same patient is a particular focus. This scope of such innovation is constantly expanding as more is discovered about the usefulness of these adult stem cells. Engineering the tissues and making functional and viable organs are major drivers in regenerative medicine (Mimeault et al., 2007, Edalat et al., 2012, Glenn and Boyce, 2012). Making bone tissue (Rust et al., 2007, Rupani et al., 2012), joint (Li et al., 2010, Kock et al., 2012, Oreffo and Triffitt, 1999), tendon (Oreffo and Triffitt, 1999), muscle (Mudera et al., 2009, Haghighipour et al., 2012) , heart (Hansson et al., 2009, Poon et al., 2011, Barile et al., 2007), bladder (Atala et al., 2006), pancreatic island cells, liver

and hepatobilliary system (Fausto, 2004, Allameh and Kazemnejad, 2012), kidney (Chhabra and Brayman, 2009, Zoja et al., 2012), eye layers (Casaroli-Marano et al., 2013), brain and neural tissues (Morando et al., 2012), and many other tissues are under research and at various stages of success / clinical usage (Ehrnet et al., 2009).

1.4 Stem cells

Stem cells are capable of making one or several cell types (plasticity) according to the body needs based on complex messages at different developmental and regenerative stages. The other characteristic aspect of stem cells is the capability to replicate, making a cell similar to themselves (self-renewal) and another daughter cell that will also be a stem cell (symmetrical self-renewal) or a specialized, progenitor cells (asymmetrical self-renewal). As well as pluripotent embryonic stem cells, there are multipotent adult stem cells throughout the body, residing in niches in many tissues and organs. They are supported by a special microenvironment (lacuna or niches) (Scadden, 2006) surrounded by blood vessels, neurons, supportive cells and soft tissue. This environment works to control quiescence (a way of preserving stem cell numbers without DNA damage and self-renewal / differentiation based on tissue demand (Aldahmash et al., 2012, Dmitrieva et al., 2012)). It is hoped that their potential can be tapped to aid with transplantation (Winkler et al., 2012), organ donation and rejection, malfunctioning organs and limbs (Baddour et al., 2012), genetic diseases (Frumkin et al., 2010), cancer treatment (Ferrara et al., 2010), threatening inflammatory diseases (Morando et al., 2012) and many other medical issues.

Types:

The stem cells are usually divided into three groups: adult stem cells, embryonic stem cells (ESCs) and induced pluripotent stem cells (iPSCs). The description of each group will be discussed briefly later after a focus on mesenchymal stem cells (MSCs) and cells of bone. After the initial stages of embryonic life, all the stem cells become known as adult (or tissue) type stem cells. Adult stem cells are named by their origin and usually are multipotent, i.e. capable of differentiation to a limited precursor cells. They do not normally require a feeder

layer *in vitro* and can grow and differentiate on cell culture plastics. MSCs are the best-known stem cells that can achieve *in vitro* growth and differentiation (haematopoietic stem cells have been described for longer but do not expand *ex vivo*). Among the different types of MSCs, such as bone marrow derived, umbilical cord, fat tissue and dental pulp; bone marrow is the richest source for adult stem cells or MSCs.

1.4.1 MSCs

MSCs are a type of adult stem cell, residing since early neonatal (cellular) phase in special niches close to the red bone marrow, and surrounded by neural, vascular and bone tissue. The laboratory characteristics of MSC are: 1) adherence to tissue plastic culture dishes under standard culture conditions, 2) cell surface characterization (positive for e.g. CD73, CD90 and CD105; negative for e.g. CD11b or CD14, CD34, CD45, CD79α or CD19, HLA-DR and 3) *in vitro* mesodermal differentiation (Vemuri et al., 2011, Ribeiro et al., 2012). They are capable of differentiating into fibroblasts, osteoblasts, chondrocytes and adipocytes and in special situations to tenocytes, neuroblasts, hepatocytes and myoblasts (Caterson et al., 2001, Donzelli et al., 2007).

It has been shown that there is a strong correlation between changes in focal adhesion (FA) complex (larger, mature, highest in number) and MSC differentiation toward e.g. osteoblasts and adipocytes with MSCs with very few, small adhesions forming fat and MSCs with super-mature (>5 μm in length) adhesions forming bone (Biggs et al., 2008b, Engler et al., 2007, Holle et al., 2012, Engler et al., 2012, McBeath et al., 2004a) as will be discussed later. This information on adhesions linked to differentiation potential of the MSCs could be used for tissue engineering especially for bone, cartilage and tendon tissue regeneration (Haddad et al., 2013, Kon et al., 2012). Based on this finding, some types of simulation such as topographical (Dalby et al., 2007c), mechanical (Yuan et al., 2013, Wang and Chen, 2013), chemical (Zhai et al., 2013) and ECM construct changes (Tour et al., 2013, Teh et al., 2013) have been introduced to show how the responses of MSCs could be controlled.

Osteoblast: Originating from MSCs, osteoblasts are responsible for precipitation of organic materials in a cartilaginous base, hence forming hard tissue and eventually the closed porous bony area (lacunae) they will encase themselves in before terminal differentiation to osteocytes. Under the microscope the regular shape of calcified materials with central canaliculi for blood vessels and neural fibers, known as the Haversian systems (Figure 1-1) are the end products of osteoblast activity. Inside the lacunae, osteocytes are surrounded by compact bone and make connections with their neighbors by several cell projections. Also involved in bone remodeling are osteoclasts. Myeloid precursor cells are the origin of osteoclasts and they will migrate from the surrounding blood to the area of bone formation when they needed.

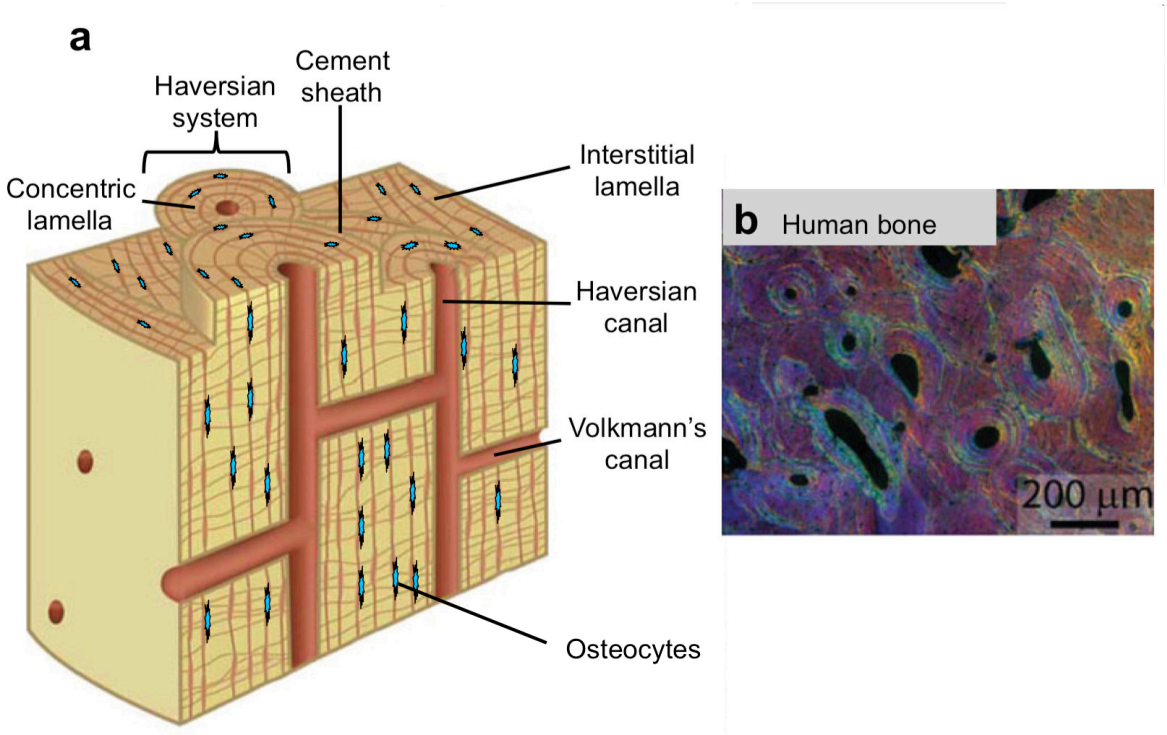

Figure 1-1- human bone structure, a) Schematic diagram of the structure of cortical bone shows the pertinent microstructural features. b) Differential interference contrast (Nomarski) micrograph of a transverse section of compact (cortical) bone of human humerus. Osteocytes are embedded between lamellae and are in contact with each other by several surface processes (Modified from (Launey et al., 2010)).

Chondrocyte: This cell is responsible for synthesis and maintenance of cartilage. After differentiation from MSCs, chondroblasts by secretion of proteoglycan and collagen fibers around themselves will change to chondrocytes. Inside the cartilage in a small closed area they remain alive with secretion of chemicals for maintenance of the tissue (Neumann et al., 2013).

Fibroblast: The main cellular compartment of extracellular matrix (ECM) is fibroblasts. These cells, by secretion of various proteins, mainly collagen fibers, fibrin and other ground substances, help provide structure and integrity of connective tissues. These cells are the most important part of the tissue for adaptation i.e. they sense and respond to the surrounding stimuli by a complex of protein receptors and enzymes. It has been shown that the most important mechanism in these cells is connections between ECM and cell membrane, activation of contractile actin cytoskeleton, activation of chemical pathways such as RhoA and its target kinase (ROCK) in response to mechanical stimuli and finally expression of specific genes inside the nucleus (Chiquet et al., 2007). This cascade is the main core of mechanotransduction in these cells. These characters make fibroblasts good simulators for mechanotransduction.

Adipocyte: the cell that stores lipid is another derivative of MSCs. Low eccentric cytoplasm and a peripheral flat nucleus with a large white or brown fat droplet, make these cells apparent in various tissues. The brown color generated by lots of mitochondria and their architecture helps with heat generation (Schulz and Tseng, 2013). The number of adipocytes increases during the early years of life but in adolescence the volume of stored fat will change by overfeeding or fasting in opposing directions. Sex hormones, androgen and estrogen in addition to leptin, adiponectin and resistin are synthesized by fat cells. Sex hormones make some integration in secondary sex characteristics and leptin with two other proteins are influencing energy balance and homeostasis with some anti-appetite effects. Recently fat tissue has been shown to be a good source of MSCs and multiple researchers have demonstrated isolation of multipotent cells (Zuk et al., 2001, Zuk et al., 2002). During MSC differentiation, soft ECM and low intracellular tension is normally coupled with adipogenic differentiation (Engler et al., 2007, Rehfeldt et al., 2007a).

1.4.2 ESCs

This type of stem cell, deriving from a blastocyst in early embryonic life, is a pluripotent stem cell and capable of making all the tissue precursor cells with ectodermal, mesodermal, or endodermal origin (Watt and Hogan, 2000). In culture, they typically need a mouse embryonic fibroblast layer and growth factors for matrix support and can differentiate to all types of body cells (Amit et al., 2004). For the collection of ESCs, destruction of an early embryo is required. Therefore, many ethical issues for using these cells have been raised. In addition they could differentiate to various cell types after injection to the body and the chance of teratoma and cancer formation with ethical issues made use of ESCs for therapeutic purposes and regenerative therapy very limited (Mathews et al., 2006).

1.4.3 iPSCs

Genetic stimulation for induction of pluripotency is possible for various adult cell types. Reprogramming of a somatic cell for the expression of some specific genes is a new method for generation of induced pluripotent cells. Dermal fibroblasts, hepatic, blood, gastric and exfoliated epithelial cells in the urine (Zhou et al., 2012) have used for this forced genetic expression. The transcriptional regulator genes those used for viral mediated transfer were OCT 3/4, SOX2, cMyc and Klf4 (Takahashi et al., 2007, Yu et al., 2007). It is noteworthy that two of the latter genes, cMyc and Klf4 are oncogenic. Huangfu et al. have since reported this induction without cMyc is possible (Huangfu et al., 2008). These cells are the same as ESCs for differentiation, methylation, teratoma formation, gene and protein expression and many other characteristics. Reprogramming of autologous cells to the iPSCs will be a safe and easy access source with the least ethical issues for stem cell therapy purposes but it is still being assessed due to concerns over genetics and induction practices.

All the types of human stem cells are under investigation for clinical application and therapeutic uses due to their strong potential for differentiation and tissue production (Figure 1-2).

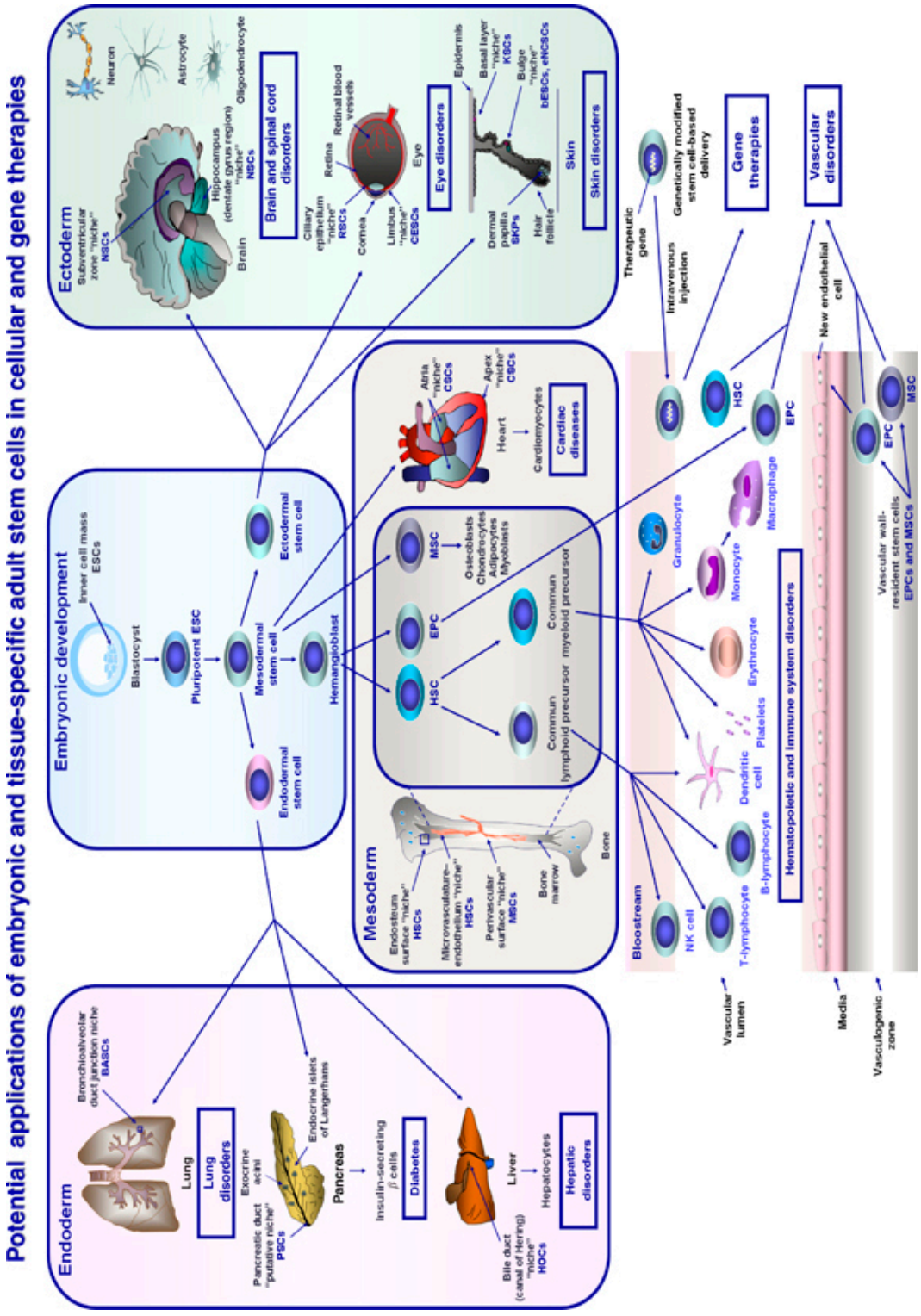

Figure 1-2- Scheme showing the potential therapeutic applications of embryonic and tissue-specific adult stem cells in cellular and gene therapies. Abbreviations: BASCs,

bronchioalveolar stem cells; bESCs, bulge epithelial stem cells; CESCs, corneal epithelial stem cells; CSCs, cardiac stem cells; eNCSCs, epidermal neural crest stem cells; ESCs, embryonic stem cells; EPC, endothelial progenitor cell; HOCs, hepatic oval cells; HSCs, hematopoetic stem cells; KSCs, keratinocyte stem cells; MSCs, mesenchymal stem cells; NSCs, neuronal stem cells; PSCs, pancreatic stem cells; RSCs, retinal stem cells; SKPs, skin-derived precursors. (Adapted from (Mimeault et al., 2007))

1.5 Human cell structure

Eukaryotic cells are microscale in size and generally they consist of two main parts, the cytoplasm and the nucleus (Figure 1-3). The cell cytoplasm is surrounded by a lipid bilayer, plasma membrane, which is highly selective. The entrance and exit to the cell are under the close control by plasma membrane combined with various protein structures or pores. A complex cooperation of cellular parts makes an efficient sensor for a cell to properly make a connection to other cells and its environment. The canaliculi and pores over the cytoplasmic membrane could be affected by various factors from outside such as changes in electrical charges, ECM composition, chemical factors, mechanical interactions, shape of the environment and many other factors (Alberts et al., 2001, Lodish et al., 2013).

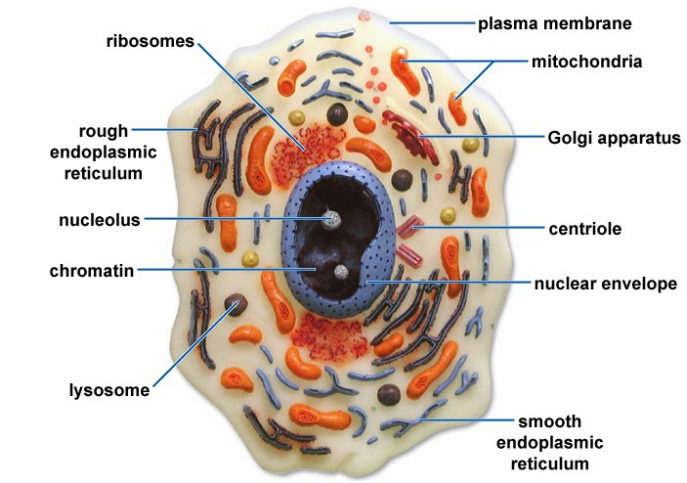

Figure 1-3- a simple scheme showing the most important parts of a human cell (taken from Midlands Technical College, Columbia, South Carolina, USA (http://classes.midlandstech.edu/carterp/Courses/bio101/labquiz2/ss6.htm)).

Throughout the cytoplasm is the cytoskeleton. The cytoskeletal architecture of cells consists of various protein dimers or polymers aiding in structure and shape, division, motility and perhaps environmental sensing (Pierres et al., 2009, Pierres et al., 2008) of the surrounding area and transferal of messages from outside the cell to the nucleus. The cytoskeleton is traditionally categorized to three main fiber types: microtubules, microfilaments and intermediate filaments. An interconnecting network of thin cytoskeletal fibers, the microtubules, helps support the cytoplasmic membrane. They are composed of tubulin and form a polarized meshwork to control protein and organelle passage throughout the cell cytoplasm. They also make special connections for the building of cilia and flagella for some cell types. Actin microfilaments, composed of actin subunits are important in cell movements through making cell protrusions and developing contractile forces through stress fiber formation and myosin interaction (Goldmann et al., 2005, Westhoff et al., 2004, Westphal et al., 1997). It seems that the cortical network of actin microfilaments in contact with membrane proteins is an important factor in cell motility based on cell adhesion and sensing of the surrounding area. Other actin microfilaments, again emanating from focal adhesions, make an internal network and make a connection with the nuclear envelope through LINC complexes (linkers of nucleuskeleton and cytoskeleton) (Crisp et al., 2006). Intermediate filaments are generally considered a more rigid type of cytoskeletal fiber compared to microfilaments and are involved in maintenance of cell shape and cell structural support. The filaments also integrate with the nucleus through LINC complexes (Rothballer et al., 2013, Ostlund et al., 2009).

Inside the cells and between these supportive cytoskeletal networks, various organelles and structures are arranged. The main responsibility of intracytoplasmic organelles is to process and transfer the secretory granules from the cell surface to the inside and from the inside to the surface (protein processing, modification and trafficking). Golgi apparatus, endoplasmic reticulum, vacuoles and vesicles are some major participants in this process. Mitochondria, as the energy making organelles are the only ex-nuclear organelles containing DNA and are presented in various numbers depending to the cell needs and are distributed in different parts of cytoplasm.

The nucleus, the largest and stiffest intracellular organelle, contains the genomic DNA and governs cell activities by transcription of genes and transfer of the resultant mRNA outside the nucleus to the ribosomes for protein translation. The outer layer of the nucleus, the nuclear membrane, is a continuation of the endoplasmic reticulum that encloses all the chromosomes and that has many highly specialized pores to control entrance to the nucleus. Nuclear lamins, as the main part of nucleoskeleton, make an intercalated network inside the nuclear membrane to protect the chromosomal assembly and preserve nuclear shape. Lamins are type V intermediate filaments and are divided into two types: lamin A, C, and AΔ10 from the LMNA gene (lamin C is derived from alternative splicing of this gene) and lamin B from the LMNB1 and LMNB2 genes. The most common type of lamin is lamin A and cells lacking lamin A are able to survive, however, this genetic defect is the cause of laminopathies, a group of human diseases usually known by muscular dystrophy and cardiomyopathy. Lamin B gene knockout could be lethal for animal model embryos. It could be indicative for lethality of knockdown in human embryos as well. Lamin B is present in all eukaryotic cells but Lamin A/C involvement in the lamina is limited to differentiated cells (Dahl et al., 2004, Lammerding et al., 2006, Pajerowski et al., 2007a).

The nucleolus, as the region of ribosome formation, is the largest and stiffest part inside the nucleus. Its liquid structure shows deformation in response to various physical stimuli that could be permanent in high stress. The numbers of nucleoli are different in various cells and some researchers showed that the increase in the number of nucleoli is an indicator for higher cellular activity (Neuburger et al., 1998).

1.6 Cells and mechanical forces

The responses of the body after birth to various types of mechanical forces and stimuli are an important factor for adaptation and growth. The human body is exposed to various types of daily stimuli such as mechanical, electrical, shear stress, thermal, chemical and acoustic waves. Cells could respond individually or in groups to these stimuli (Huang and Ingber, 1999, He and Montell, 2012). Some adaptive responses are necessary for cell maintenance and

some others could perhaps be detrimental. Back disorders due to work with vibrating equipment (Harris et al., 2012) and hypertrophied vasculature and heart muscle in response to hypertension (Pedrinelli et al., 2012) are potentially detrimental mechanoresponsive effects. However, here the focus will be on positive mechanotransduction to allow control of cell fate in a desired manner (Kamkin and Kiseleva, 2008). After the discovery of stem cells, understanding the best way for manipulation, stimulation or conduction of them has been a major scientific focus (Kshitiz et al., 2012, Tay et al., 2013). Research on the effect of chemical, matrix stiffness, topography, electrical, magnetic and mechanical stimuli on stem cell behavior are among them and some of these approaches will be described with a particular focus on mechanical stimulation (as the focus of this thesis) and nanoscale stimulation (as the aim here is to move mechanical stimulation into the nanoscale) (Discher et al., 2009, Guilak et al., 2009, Tay et al., 2013, Clause et al., 2010, Marklein and Burdick, 2010). It is noted that many different types of mechanical stimuli in combination or individually have been tried previously. These include stretching forces (Steward et al., 2010), compression (Maul et al., 2007), shear stress (Stolberg and McCloskey, 2009) and vibration (Gaston et al., 2012, Nikukar et al., 2013) with results demonstrating that the type of stimulus, time-scale and amplitude are all important (Patwari and Lee, 2008, Rehfeldt et al., 2007b, Bukoreshtliev et al., 2013).

1.7 Mechanotransduction

For the purposes of this study, mechanical stimulation will be referred to as mechanotransduction although it is acknowledged that mechanotransduction can be initiated by a wide variety of stimuli that differentially regulate intracellular tension and cell morphology as will be discussed in parallel (e.g. material surfaces). The molecular response of cells to any mechanical stimulus usually is in the shape of altered protein production and changing phenotype. This occurs through a process called mechanotransduction and is a type of adaptation that is necessary for cellular life (Turner and Pavalko, 1998). Briefly, the process starts by sensing changes in the external environment, transfer of this mechanical message by the cytoskeleton to the intracellular organelles and the nucleus, and chromosomal response to the stimulus that will affect transcript to protein synthesis (He and Montell, 2012, Liedert et

al., 2008). This can be indirect (biochemical) or direct (mechanical pulling or pushing of the nucleus). For example, the responses of bones to stimulus during remodeling can determine the strength of ossification, the shape and intrinsic architecture of the resulting tissue (Klein-Nulend et al., 2013). Various mechanisms are involved in the mechanotransductive process. These responses start at the cellular level and are usually driven by cell-matrix interactions, adhesions, as a start point – or at least adhesions are a mechanism of particular interest in the field (Matsuzaka et al., 2003). Indirect (biochemical) and direct (distortion of the nucleus) mechanotransductive events follow as will be described. Both forms, at the nuclear level, will result in different genes being transcribed in response to the changing mechanical environment resulting in differential protein expression typical of different phenotypes e.g. osteocalcin and osteopontin in bone cell differentiation (Liedert et al., 2008, Bukoreshtliev et al., 2013).

This thesis will have a particular focus on the less well-researched direct mechanotransductive effects. For a direct nuclear response, different hypothesized mechanisms have been postulated. Direct transfer of mechanical stimulation to the nuclear envelope or inside the nucleus, changes in nuclear pore complex, lamin responses, interaction via lamin binding proteins, conformational chromatin changes in distinction or chromosomal territories' displacement are among these possibilities (Dahl et al., 2004). Nucleoli, Cajal bodies and PML (promyelocytic leukemia) particles are other parts of nuclear interior that may change their positions in response to mechanical stimuli and this may have implications for e.g. ribosomal formation and function. Some of these will be discussed in more detail shortly.

1.8 Focal adhesion complexes

Without adhesion, tissue cells die through apoptotic mechanisms known as anoikis even quicker than through lack of nutrients (Grossmann, 2002). Attachment of cells to the surfaces is dependent on several factors: cell surface proteins such as integrins, cadherins, selectins and immunoglobulins, to ECM characteristics such as type and concentration of matrix proteins, to matrix stiffness and physical characteristics of the matrix (Selhuber-Unkel et al., 2010). Integrins are considered the most important cell surface proteins in cell/interfacial research as

they form the base of focal adhesion (FA) complexes. FAs are macromolecular structures that serve as mechanical linkages of the cell cytoskeleton to the extra cellular matrix (ECM), and as biochemical signaling hubs involved with the transmission of external mechanical forces through numerous signaling proteins that interact at sites of integrin binding and clustering (Figure 1-4) (Schwartz, 2010). They are a heterodimer consisting of an α and a β subunit, each with three domains: an extracellular domain in contact with ECM, a transmembrane and a cytoplasmic domain. Currently, about eighteen varieties of α subunit and eight of β subunit and twenty-four separate combinations are known. It seems integrins are the major transmitters of biomechanical signals from the ECM to the cell interior. The process of activation starts with pairing of β and α integrins. By the connection of integrins to the ECM proteins, several signaling pathways inside the cell will be activated and more than one hundred proteins share this complex for transmission of signal to the nucleus (Kanchanawong et al., 2010, Wang et al., 2009, Ziegler et al., 2008).

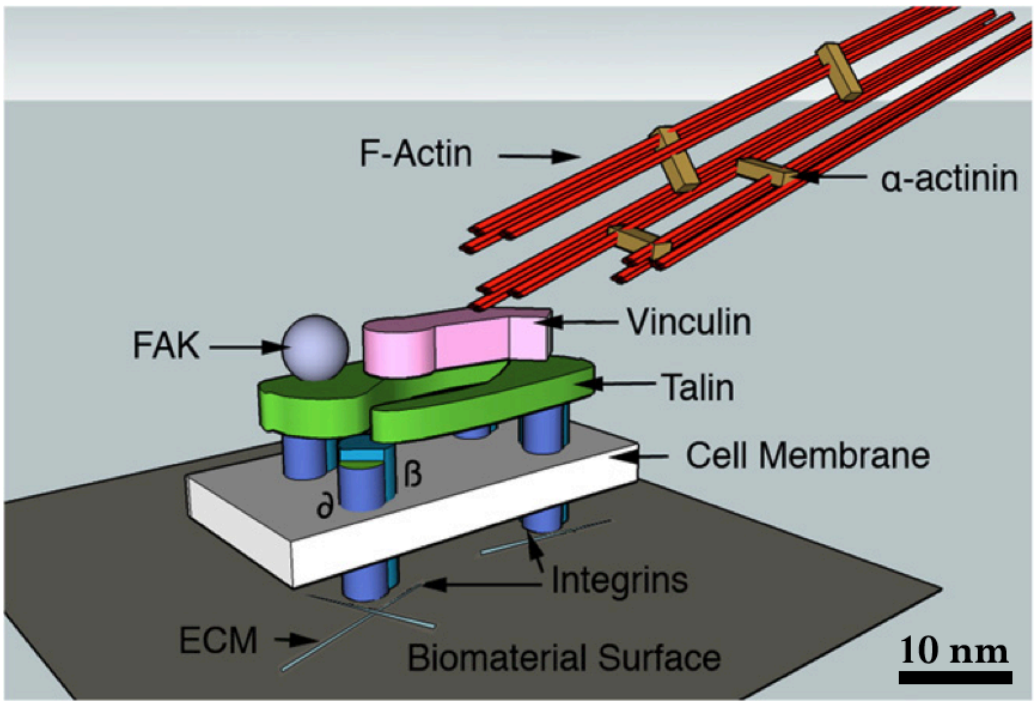

Figure 1-4- a simplified overview of the focal adhesion complex structure. FAs are macromolecular structures that serve as mechanical linkages of the cell cytoskeleton (F-actin microfilaments) to the extra cellular matrix (ECM). This picture is not to scale (Taken from (Biggs et al., 2010)).

Focal adhesion formation by itself needs the integration of more than fifteen proteins that will engage with each other to form a mature adhesion. More than 65 proteins for actomyosin rearrangement and others as various activators, inhibitors and catalysts will be activated. Adhesion can initiate intracellular pathways arising from focal adhesion kinase (FAK) and RhoA kinase (ROCK) leading to transcriptional changes (Leucht et al., 2007, Tay et al., 2013, Kanchanawong et al., 2010). Force and mechanical stress are effective on integrin and its intracytoplasmic proteins' activation. Stiffness of the substrate by changing adhesion-related forces also affects mechanosensations and responses in focal adhesion complexes starting from pairing of α and β subunits upwards (Karamichos et al., 2008, Shih et al., 2011). Integrin response to mechanical stimulation can be considered a type of strain sensing mechanism or response to displacement (Alon and Ley, 2008). Most of intra-cytoplasmic proteins associated with focal adhesion have mechanosensitive properties (Patla et al., 2010). According to these findings, it is currently considered that the cells could sense and transmit all the mechanical forces from the ECM to cell's interior via adhesions (Giannone et al., 2007, Schwartz, 2010, Geiger et al., 2009). Further effects are dependent on biochemical and mechanochemical responses by the cell when it 'senses' these stimuli and the size of FA could be an indicator for the influence of induced forces at the site of attachment (Collin et al., 2008, Schwarz et al., 2006, Wang et al., 2009).

The protein composition of FAs will change by their size. In the smallest FAs, known as focal complexes, at 1μm or less in length, talin, vinculin, paxillin and integrins could be found and they are the point of initial contact between ECM and cell surface receptors. In mature focal adhesions (up to 5 μm in length), paxillin, vinculin, focal adhesion kinase (FAK), zyxin and integrins are present. At the largest size, fibrillar, or super mature FA (> 5 μm in length) greater amounts of these connective proteins and tensin are found. All three types are force sensitive (Schiller and Fassler, 2013). Forces from inside or outside of the cells are triggers for integrin activation and FA formation (Kuo, 2013). Traditionally studies focus on biochemical signals arising from changes in cytoskeletal assembly, especially actin cytoskeleton, as a result of adhesion changes.

FA and FAK directed activation of the g-proteins aid 'cell sensing' of the surface. For example, direction of lamellipodium (from Rac activation) helps cell/surface exploration. A maximum force of 5-7 pN per actin filament is estimated at lamellipodium formation (Wu et al., 2011). Various factors are determining the cell movements such as cell type, chemical attractant, mechanical forces such as gravity, liquid flow, physical shape, ECM stiffness and protein gradient that are more attractive to integrin bonding and formation of advancing lamellipodium will guide cells to these sites. Other activations arise from cdc42 activation causing filopodial formation. These fine membrane protrusions are integrin containing and 'sweep' in front of the cells to locate binding sites for FA growth. The G-protein Rho is also involved in motility and sensing through its role in myosin activation and resultant actin contraction. RhoA inhibition shows significant decreases in cell motility (Miller et al., 2012).

In multipotent MSCs, it has been demonstrated on nanotopography that a shift from stem cell to differentiated osteoblast occurs through changes in adhesion and intracellular tension with osteoblasts being large cells requiring larger adhesions to support the tensile cytoskeletal scaffolding (Tsimbouri et al., 2012). Such effects have also been demonstrated in MSCs cultured on hydrogels (Engler et al., 2006) or forced to confine to morphologies using microcontact printing of fibronectin (McBeath et al., 2004b, Kilian et al., 2010b).

Using changes of gel stiffness, it was seen with very soft gels that neural marker expression was promoted as the cells dissipated adhesive forces into the compliant substrates while on stiffer gels (similar stiffness to pre-calcified bone at 40 kPa) cells were allowed to retain intercellular tension, form large adhesions and differentiate into osteoblasts (Engler et al., 2006). A seminal study on MSC confinement used small adhesive arrays of fibronectin (1000 μm^2) to prevent cell spreading and hence development of intracellular tension and lead to formation of adipose (fat) tissue while when spreading was actively promoted on large, 10,000 μm^2 fibronectin arrays, cells formed large adhesions, well organised cytoskeleton and differentiated to osteoblasts (McBeath et al., 2004b). An elegant update on this study used fibronectin stars and flowers to demonstrate that even if the MSCs are the same size, features that promote adhesion (sharp corners of the stars) promote intracellular tension and

osteogenesis and features that reduce adhesion (soft ‘corners’ of the flower petals) reduce intracellular tension and differentiation (Kilian et al., 2010b).

The presentation of RhoA kinase (ROCK) as a key modulator of osteogenesis is commonality of all the above studies. This is sensible as, as has been described, RhoA is a small G-protein involved in activation of actin/myosin contraction. Cells require this cytoskeletal contraction to spread on to substrates and to migrate. This contraction against focal adhesions allows formation of intracellular tension and motility. Osteoblasts are a large progeny of MSCs and thus are very well spread, thus a highly contractile cytoskeleton is required to support this phenotype and this generates high intracellular tension. In addition, focal adhesion and the cytoskeleton are in a force balance relationship as highly contractile cytoskeleton requires large focal adhesions and focal adhesion require force to gather integrins and hence to grow (Sawada and Sheetz, 2002, Galbraith et al., 2002, Vogel and Sheetz, 2006, Sawada et al., 2006, del Rio et al., 2009). It is notable that osteoblasts have a high proportion of the aforementioned super-mature adhesions(Biggs et al., 2008a, Biggs et al., 2009). Pharmacological inhibition of ROCK prevents osteogenesis and promotes low-tension adipocyte-specific differentiation from MSCs. (Please note that adipocytes are round with few, small adhesions). It is further noteworthy that the MSC phenotype itself appears to be one of intermediate cytoskeletal tension with the stem cells employing many, smaller adhesions; the cells are close to a fibroblastic phenotype, but with fewer adhesions and slightly less intracellular tension (McMurray et al., 2011, Tsimbouri et al., 2012).

The biochemical basis behind these phenotypical changes is not so well understood. Downstream of FAK and the G-proteins are major biochemical signaling hubs such as extracellular-signal related kinase ERK1/2 and other mitogen activated protein kinase modulators such as p38 MAPK and c-jun n-terminal kinase (JNK), all of which have been shown to be important in nanoscale MSC interactions (Tsimbouri et al., 2013, Dalby et al., 2008). Such hubs have also been illustrated as central in other materials approaches such as microcontact printing (Kilian et al., 2010a) and changing substrate stiffness (Engler et al., 2006). It is likely that MSC phenotype is altered through regulation of transcription factors.

For example, the osteogenic transcription factor, Runx2 (runt-related transcription factor 2), requires phosphorylation to be active while the adipogenic transcription factor, PPARγ (peroxisome proliferator-activated receptor gamma), is inactivated by phosphorylation. As adhesion related signaling increases, ERK activation also increases. At very low adhesion, ERK is largely down regulated and thus PPARγ and RUNX2 are un-phosphorylated permissive to adipogenesis. At medium adhesion, ERK is up regulated to a degree permissive for proliferation with little net adipogenesis or osteogenesis. However, if super-mature adhesions are allowed to form, ERK is stimulated to the point of negative feedback and this slows proliferation and allows phosphorylation of the transcription factors, inactivating PPARγ and activating Runx2 that promotes osteogenesis (Biggs et al., 2009, Jang et al., 2012, Ward et al., 2007).

1.9 Linking the cytoskeleton to the nucleus and direct mechanotransduction

Maniotis et al. reported that in reaction to tension, the intermediate filament cytoskeleton re-orients, the nucleus distorts and that the nucleoli rearranged along the applied axis (Maniotis et al., 1997b). Thus, it was concluded that the nucleus is mechanically integrated within the physical entity of the cell via intermediate filaments and that active or passive cell extension can lead to passive nuclear deformation. The lamin-derived nucleoskeleton acts as a mechanical bridge between the cytoskeleton and the nucleus. The nuclear lamina is physically associated with actin and vimentin via nesprins and SUN (Sad1 and *UNC*-84 homology domain) proteins (Haque et al., 2006a, Wang et al., 2009). Micromanipulation experiments have illustrated that transmission of force can occur from the peripheral cytoplasm into the nucleus (Maniotis et al., 1997a), demonstrated the mechanical interconnection of chromosomes and nucleoli (Maniotis et al., 1997c) and shown the importance of the nuclear lamina in force transmission (Pajerowski et al., 2007b, Martin et al., 2009a).

Topography has provided a useful tool in investigation of force transduction into the nucleus and has been used to indicate that redistribution of chromosomal territories, the space occupied by a given chromosome within the nucleus, reviewed by Cremer et al. (Cremer and

Cremer, 2001), or intra-territory loci, the location of particular genes, could affect the cellular transcriptional profile. There are foci of transcriptional activity within the nucleoplasm, where active, transcription-competent RNA polymerase II and transcription factors are clustered. Genes can loop out from chromosome territories to move into these areas, and such repositioning can increase their likelihood of being transcribed ((Osborne et al., 2004b, Chambeyron et al., 2005); discussed in (West and Fraser, 2005)). Alternatively, movement of genes or territories towards the periphery of the nucleus could promote down-regulated transcription. Wang et al. suggested a number of models by which tensile forces from FAs could modulate gene expression (Wang et al., 2009). It was proposed that the assembly or activity of transcription factor complexes could be affected directly or indirectly by tension-mediated alterations in the nucleoskeleton and the telomeric ends of the chromosomes are attached to the lamina via Matrix Attachment Regions (MARs). Also, the authors suggested that gene expression or mRNA transport could also be affected by tension-mediated changes in nuclear pores.

Even at the nanoscale, topography provides a useful means to investigate mechanotransductive effects on the nucleus. Nanocolumn substrates were shown to induce repositioning of chromosome 3 (Dalby et al., 2007b, Dalby et al., 2007a) relative to planar controls. The chromosome 3 centromeres were more closely apposed in cells cultured on the nanocolumns, probably as a consequence of the decreased cell spreading and nuclear area. On hexagonally arrayed nanopits, the inter-centromeric distance was reduced for both chromosomes 3 and 11, and the cells were markedly less spread than controls (Dalby et al., 2007a). As the authors noted, the changes were consistent with the tensegrity model. Tension on the cytoskeleton and nucleus should be reduced, which is likely to have lessened the force exerted on chromosomes (Wang et al., 2009, Maniotis et al., 1997b, Maniotis et al., 1997d, Haque et al., 2006b, Pajerowski et al., 2007a, Martin et al., 2009b).

Furthermore, micro and nanotopography have been used to illustrate movement of large chromosomes in fibroblasts (McNamara et al., 2012) and MSCs (Tsimbouri et al., 2013) with the nuclear lamina indicated as central in conveyance of mechanical signals to permit these

movements. This is particularly interesting with MSCs, which, as has been described, differentiate in response to intracellular tension. If the genome is surveyed with respect to gene positioning in relation to the telomeres (attached to lamins and hence mechanically sensitive) and the centromeres (not attached and thus not mechanically sensitive), it is seen that many osteogenic genes reside on larger chromosomes (which all these studies show to be more mechanically sensitive) at the telomeric regions (e.g. osteocalcin at 1q25-31, osteopontin at 4q22, osteonectin at 5q31 and alkaline phosphatase at 2q37). This indicates that the 'osteogenic' genome of MSCs may be in a position to respond rapidly to changes in tension as the telomeric ends may 'unravel', or at least become less dense and more euchromatic, faster in response to tension. This change in DNA density may be permissive to transcription factor and polymerase access, thus aiding phenotype selection.

A more detailed explanation of the chromosomal architecture would allow further understanding in the effects of chromosomal rearrangements. In the interphase nucleus the main components of nuclear interior are complexes of DNA and histone proteins (chromatin), nucleoli, Cajal bodies and PML. The location, function and structure of chromatin in various areas of nuclear interior are different. Heterochromatin, a dense inactive DNA and histones are usually arranged in the periphery of the nucleus and around the nucleoli. These areas have very low gene expression. Euchromatin shows itself to be 'looser' in density under the microscope and more deformable than heterochromatin and it occupies the spaces between the nuclear periphery and nucleolus. These areas are gene rich and have very active expression. Each chromosome occupies spatial territories inside the internal lamina. The 'territory' for every chromosome is well determined in human cell nuclei. Furthermore, the centre of the nucleus is polymerase rich and these high activity areas are refereed to as 'transcription factories' (Osborne et al., 2004a). Thus, it is easy to imagine that small movements could move chromosomes to active or quiet areas of the nucleus, change access to transcription or more the genes closer towards the transcription factories. Also, it should be considered that polymerase itself, used to transcribe the genes to mRNA, is a motor enzyme that is sensitive to changes in tension (i.e. tension speeds it up, slows it down or even stalls it completely (Bryant et al., 2003, Bustamante et al., 2003)).

1.10 Tensegrity model

In order to convey mechanical signals developed from e.g. changes in focal adhesion signaling and cytoskeletal tension, we need to consider how the cytoskeleton may convey force. Donald Ingber (1993) has proposed tensional integrity as the main mechanism to stabilize the architecture of life. Initially explained by architects, tensegrity in cell biology is defined as interconnection of tension and compression forces inside the cellular cytoskeleton that give the cell its overall stability and integrity. Due to this interconnection, elasticity movements of any part of the cell will be sensed and reacted to by all other parts and they will move or change their position to a new stable position accordingly. This interplay of relaxing and tensing forces (floating compression), provide elasticity and strength for the cells and help permit all the body activities. This result will support the organism to save energy and prevent damage due to various environmental changes and mobility without losing stiffness or stability. Among the components of cytoskeleton in tensegrity, tubulin is considered under compression and actin is considered under tension. These two proteins act in a similar manner to a tent structure in order to make the cell membrane tense and stable, compatible with environmental forces and cell movements (Ingber, 1993).

Down at the individual cell level, the cytoskeleton of the cell is critical for the transmittal of mechanical effects from the substrate to the cell (Ko and McCulloch, 2000). It is thought that microfilaments, intermediate filaments and microtubules form the tensegrity structures in the cell, with microtubules acting as load-bearers and microfilaments and intermediate filaments acting as tensile stiffeners (Ingber, 1993, Charras and Horton, 2002); tensegrity structures are stabilised through continuous tension, rather than compression (such as an arch) (Ingber, 2003b, Ingber, 2003a, Mammoto and Ingber, 2010, Wang et al., 2009).

This area of mechanobiology remains under-researched. Also how the cytoskeleton transduces mechanical signals to the nucleus remains controversial and tensegrity is actually very hard to prove. Nevertheless, the Young's moduli of the individual constituents of the cytoskeleton suggest that mechanical signals would have to be transduced via tension. Secondly, that the cytoskeleton has to work in an integrated manner, as direct mechanotransduction relies on the transmission of force from the focal adhesions to the nucleus. Microfilaments, microtubules

and intermediate filaments are thought to radiate to the cell periphery, however, only cytoskeletal intermediate and microfilaments are linked to the nuclear lamins via the aforementioned LINC complexes. Thirdly, it seems that the inhomogeneity the cytoskeleton provides the cytoplasm is essential for long-distance force propagation (Wang et al., 2001).

1.11 Bone tissue engineering

Bone is characterized by its amazing regenerative potential being a rich source of stem cells (Sirinoglu Demiriz et al., 2012). However, this potential is yet to be realized. By growing needs to replace biological tissues such as bone and cartilage a relatively new multidisciplinary field, called tissue engineering (TE) has evolved i.e. repair or replacement of tissues by engineered functioning tissues made by cooperation of biologists, engineers, and material scientists (Langer and Vacanti, 1993). Replacing the diseased or failed human organs and tissues with 'off the shelf' replacements are the main aims of tissue engineers and that is this scientific group needs cooperation of cell biologists, engineers and medical experts. This triangle makes various connections to other scientists because of the diversity of subjects in this matter. The introduction of stem cells in this field is particularly interesting due to the cells' natural ability to 'engineer' complexity – this is the overarching goal now of stem cell based tissue engineering. But first we must learn to engineer one tissue at a time. At the heart of TE is exploration of cellular and molecular mechanisms for growth, repair and tissue formation (Allhoff, 2009). Often mimicry of natural conditions is used, as a cell could grow and replicate in contact with other cells, ECM, various environmental factors when it needs nutrients and also, they may have gas exchange requirements. TE needs a cell source, extracellular architecture for cells' settlement and growth (scaffold), continuous feeding and oxygenation and at the same time continuous waste removal. The cell line usually has been chosen according to their potency and compatibility by the body with the final purpose in mind. Suitable cells could be extracted from blood or tissues such as fat, bone marrow and umbilical tissue using e.g. centrifugation, digestion and selective growing media or even cell sorting. According to the source of the cells they are defined as autologous: from the same person, allogeneic: from the same species, xenogeneic: from another species. Each group has positive and negative points by itself. Stem cells as the autologous and allogeneic source with multi or pluripotency are becoming the main hope for regenerative medicine. Induced

pluripotent stem cells (iPSCs) are another source of cells for TE that is generating interest. However, due to ethical issues (ESCs), issues of e.g. viral transfection protocols and introduction of oncogenes (iPSCs) and concerns of teratoma formation, MSCs remain a main TE focus due to relative ease of isolation for an adult stem cell. They are also immune-privileged or at least immune-modulatory – possibly due to a perivascular origin (Crisan et al., 2008).

For the purposes of this thesis, the focus will be on development of a new type of bone-cell bioreactor for stimulation of MSCs.

1.11.1 Bone bioreactors:

Use of osteoblasts and stem cells to make bone tissue in the lab (*ex vivo*) is possible (Marolt et al., 2012, de Peppo et al., 2013) but for clinical use (massive bone production), a special device to accelerate tissue growth and production is needed. Different research groups have developed different bioreactors (Yeatts et al., 2013). They usually have been used to improve seeding efficiency, proliferation and osteoblast differentiation (Rupani et al., 2012). In these culture chambers the cells will grow, proliferate and differentiate to bone forming cells, all in sterile conditions. These bioreactors mainly fall into mechanical (compressive, rotatory, and spinning) and perfusion (running a flow of fresh media over cells) categories in order to optimize the environment for osteoblast growth and differentiation (Rath et al., 2012, Cartmell et al., 2011). The efficacy and problems with each type are under investigation and it seems the perfusion systems show the best results for osteoblastic differentiation and mineralized matrix deposition (El Haj and Cartmell, 2010).

Some groups divided bone bioreactors into three main groups: 1- Spinner flask is the simplest type and cells on a 3D scaffold are suspended in a media container and stirred by about 50 rpm. The cell viability, proliferation and distribution compared to static group could be improved but the size of produced tissue is limited because by increasing the flow for increasing the tissue perfusion especially deeper cells, generated shear force leading to

necrotic damage in the surface cells (El Haj and Cartmell, 2010). 2- Rotating vessel (sometimes called the NASA bioreactor) is another type of rotational reactor that usually employs horizontal rotation of solid, bubble free, vessels. In this type of vessel the necrotic effect of shear stress is lessened. In one comparison between these two methods and control, osteoblastic activity was increased by spinner flask culture after 21 days due to superior media mixing (Sikavitsas et al., 2002, Sikavitsas et al., 2003). 3- Perfusion method is designed to mimic blood supply. In this method various types of flow with different speeds, frequencies, and continuity (unidirectional, oscillating, pulsatile) could run the media over the growing cells and at the same time gas exchange will be provided by another pump system. Frequency of flow, flow rate and made shear stress are important variables for perfusion system method. It seems bone TE are more responsive to pulsatile flow than continuous flow (Cartmell et al., 2003, El Haj and Cartmell, 2010).

1.12 Hypothesis

It is hypothesised that cells can sense and respond to many environmental stimuli including nanoscale vibrations (Pierres et al., 2009) (Ito et al., 2011). Development of techniques to provide nanoscale undulations, or vibrations, provide the basis for testing this hypothesis. The preliminary research question for this thesis was what is the extent of these reactions and by which pathways do cells process the information? Hence, a piezo ceramics were used to make a precise vibrator for applying nanoscale vertical displacements to cells when they are settled and growing on otherwise normal tissue culture plastic. Possible phenotypical changes and differentiation to a specific lineages due to the transfer of force to mesenchymal stem cells by activation of mechanotransductive pathways was thus tested. The expected response could be measured and statistically analysed to define the stimulator as a small cell bioreactor for MSC stimulation *in vitro*.

1.13 Aims

In this thesis, I focussed on nanoscale mechanical stimulation of MSCs. The ultimate goal is to develop new bone-specific bioreactors. It is acknowledged that the system will be developed

in 2D rather than 3D and so is strictly an osteoblast bioreactor rather than a bone bioreactor. However, it is predicted that 3D platforms will be deliverable in the future. There is very little information on nanoscale mechanical stimulation and the closest parallels, as have been used to illustrate theories in this introduction, borrow from e.g. nanotopographical information. These theories will be expanded on through this thesis with further comparison and contrast to materials techniques.

Chapter II- Materials and methodology

2.1 Introduction

In this section, all the common biological materials and methods used in order to evaluate cellular responses to nanoscale mechanical stimulation will be reviewed. Firstly the methods used for cells treatment were explained. These are standard methods used by many laboratories. Sterile conditions such as using lab coat, gloves, use of class II cabinet, and cleaning by 70% ethanol were always used during the work. All the chemicals and media were stored in proper condition for prevention of contamination. The cells were fed every 2-3 days inside the standard incubators at 37°C temperature and 5% CO_2 concentration before use and thereafter.

The dishes were prepared for cell stimulation as described in Chapter 3 in another lab with special attention not to open the lids and to preserve the sterility of the cell culture space. Then the arranged setup was moved to the cell culture lab and all the cell works were done in a sterile class II hood to prevent contamination. The electrical devices such as generators were arranged beside the incubators and they were connected to the setup through wires that crossed the seal of the incubator door without interfering with the standard conditions. After the stimulation period, the treated and control cell groups used quickly for the planned tests to prevent any possible effects or changes after discontinuation of stimulation. In the case of immunofluorescent staining the cells were fixed immediately and staining proceeded but if the staining was not done at the same time, the samples were stored, added phosphate buffered saline (PBS) in the fridge. In other cases for example RNA or protein work, cells were either lysed directly in the dish or harvested and pelleted and RNA or protein was extracted immediately. Alternatively, the cells/pellets were stored in -80°C for future uses.

2.2 Cell models

Cell culture and treatment:

During development of the nanomechanical stimulation set-up, various cell types were trialled. At the start, Infinity™ Telomerase Immortalised primary human fibroblasts (hTERT-BJ1, Clonetech Laboratories Inc., USA) and the human osteosarcoma cell line (MG- 63) were used as they grew rapidly and were simple to culture. The media used was

71% Dulbecco's modified Eagle's medium (DMEM) (Sigma, UK), 17.5% medium 199 (Sigma, UK) supplemented with 9% fetal bovine serum (FBS) (PAA, Austria), 1.6% 200mM L-Glutamine (Sigma, UK), 0.9% 100mM sodium pyruvate (Sigma, UK), and antibiotics (Penicillin-Streptomycin from Sigma, UK), and Amphotericin B (Gibco, UK). Firstly by replacing 100 ml of DMEM container (contains 500 ml) with 100 ml medium 199, 60 ml FBS was added. 10 ml of the antibiotics and L-Glutamine mixture (150 ml L-Glutamine, 100 ml Penicillin-Streptomycin, 12.5 ml Amphotericin B) and then 5 ml sodium pyruvate were added to have 575 ml complete DMEM media. The media should be stored in 4°C for short-term use and/or aliquoted in the freezer (-20°C) for longer period. The media was replaced every 2-3 days. Fibroblasts (Figure 2-1) have spindle-like morphology and fast replication. After seeding and incubation at 37°C and 5% CO_2 atmosphere they attached easily to petri dishes.

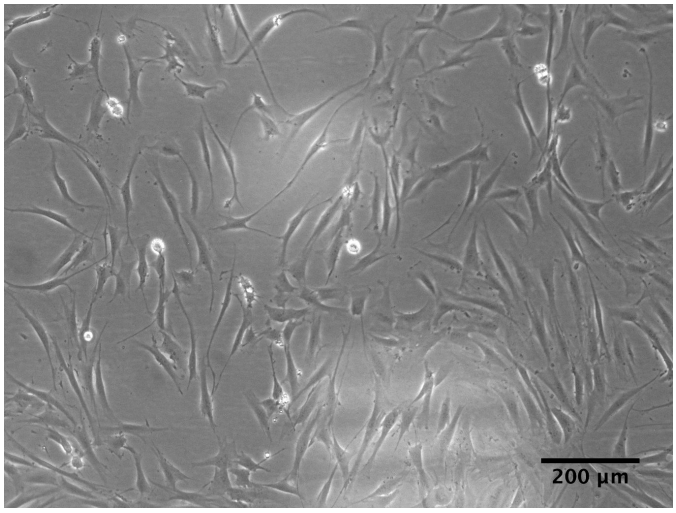

Figure 2-1- human fibroblast (hTERT) after 7 days growth in Petri dish (x10, Motic AE31 with Scion Corporation camera).

Various types of osteosarcoma cell lines are available for laboratory experiments but every type has special characteristics. Among them, MG-63 cells are small and have very quick population doubling time. These cells are resistant to many of environmental changes such as late replacement of media. They sometimes show osteoblastic characteristics with or without stimulation (Clover and Gowen, 1994). After seeding, MG-63 cells always attached to the Petri dish in few minutes and had small, spindle morphologies (Figure 2-2). They continue their replication even without changing the media for more than a week.

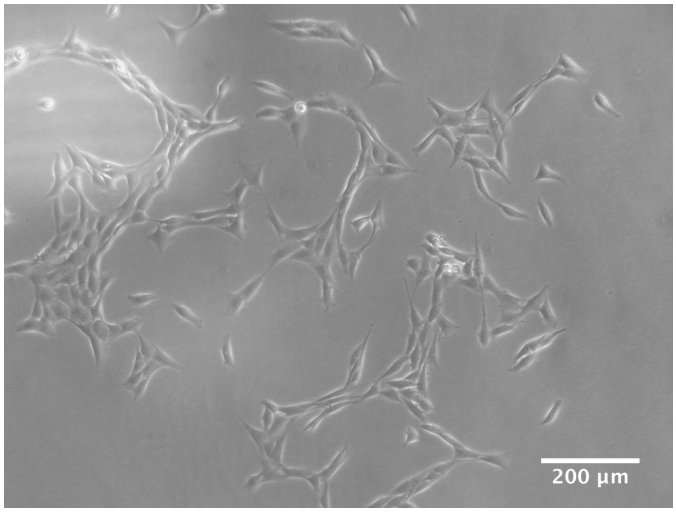

Figure 2-2- human osteosarcoma cells (MG-63) after 24 hours seeding and growth on Petri dish (x10, Motic AE31 with Scion Corporation camera).

Bone marrow derived MSCs (Figure 2-3) purchased from PromoCell® (Heidelberg, Germany) were the cell type selected for more detailed evaluation.

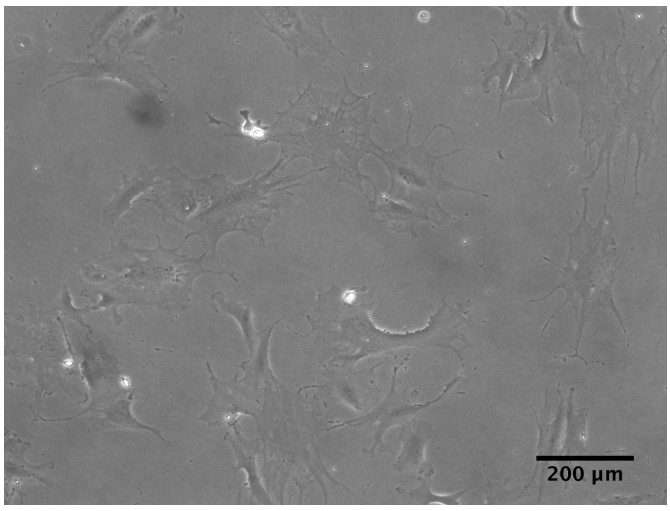

Figure 2-3- human MSCs after 7 days growth in Petri dish, ×10 magnification under the light microscope (Motic AE31 with Scion Corporation camera).

Bone marrow derived MSCs were chosen because they have been shown to have the capability to differentiate into osteoblasts, chondrocytes, myoblasts, adipocytes and fibroblasts *in vitro* (Dominici et al., 2006) and we were looking for any possible phenotypical changes after induction of nanoscale mechanical stimulation. For MSC culture we used alpha-modified Eagle's medium (αMEM) (Sigma, UK) with 9% FBS and antibiotic combination as above, renewing it every 2-3 days. All the experiments were

carried out in a standard cell incubator at 37°C and 5% carbon dioxide/air (v/v) concentration. For initial quantification of phenotypical changes optical and fluorescence microscopy were used.

2.3 Microscopy

In this project according to structures being looked for, several types of microscopes were used:

Light microscope: Motic AE31 with Scion Corporation camera

Fluorescence microscope: Zeiss Axiophot with camera and QCapture™ Suite Plus software (version 3.1.3.10)

Scanning electron microscope: Carl Zeiss Sigma variable-pressure analytical SEM with Oxford Microanalysis® software

2.3.1 Immunofluorescent staining

For better clarification of the cell structures based on antigen- antibody affinity, the immunocytochemical method was used. In this method, after fixation of cells in 4% (v/v) formaldehyde (10 ml of 38% formaldehyde in 90 ml PBS, add 2 gr sucrose and dissolve) for 15 minutes at 37°C, the cell were exposed to a permeabilizing buffer (10.3g sucrose, 0.292g sodium chloride, 0.06g magnesium chloride hexahydrate, and 0.476g HEPES (all from Sigma Aldrich), in phosphate buffered saline (1x PBS, 100ml), PH was adjusted to 7.2 and 0.5 ml of Triton X® added. This was added to the samples for 5 minutes to make the membranes permeable to later antibody incubations. To neutralize other nonspecific proteins the samples were blocked in a 1% (w/v) bovine serum albumin (BSA, 1g in 100ml PBS) for 5 minutes at 37°C. After removing PBS/BSA, monoclonal anti-human (unless stated, raised in mouse) primary antibodies diluted in PBS/BSA were added (Table 2-1). Usual dilution for primary antibodies was 1:50 (20 µl/ml) except for Golgi antibody that the dilution of 1:300 (5 µl/ml) was used. For actin cytoskeleton staining Phalloidin-Rhodamin conjugates (R415, Invitrogen) with dilution of 1:500 (2 µl/ml) was used. The usual volume of antibody solution to cover entire base of a 60 mm Petri dish (21.24 cm^2 surface area) was about 150 µl. After this step all the samples were wrapped in aluminium foil to prevent bleaching by ambient light. After incubating the wrapped samples at 37°C for 1 hour, primary antibody was removed and the samples washed using 0.5% PBST (0.5 ml Tween® 20 in 99.5 ml PBS) for three times, each 5 minutes in duration (3×5 minutes). After removal of washing solution, species-specific biotinylated secondary antibody

diluted in PBS/BSA (1:50 = 20 µl/ml) was added to the samples (anti-mouse: BA 2000, anti-rabbit: BA 1100, Vector Laboratories). After 1-hour incubation at 37°C, removing the excess antibody and washing by PBST (3×5 minutes), the fluorochrome, usually streptavidin conjugated to fluoroisothiocyanate (streptavidin-FITC, SA-5001, Vector Laboratories, USA) (1:50 dilution in PBS/BSA) was added.

Primary antibody	**Company**	**Product number**	**Species origin**	**Dilution**
β3- tubulin	Santa Cruz Biotechnology	SC-51670	Mouse	1:50
Golgi	abcam	ab-27043	Mouse	1:300
Lamin A/C	Santa Cruz Biotechnology	SC-56140	Mouse	1:50
Lamin B	Calbiochem	NA12	Mouse	1:50
MEPE	Santa Cruz Biotechnology	SC-377035	Mouse	1:50
Osteocalcin	Santa Cruz Biotechnology	SC-73464	Mouse	1:50
Runx2	abcam	ab-76956	Mouse	1:50
S-100	abcam	ab-868	Rabbit	1:50
Sox-9	abcam	ab-76997	Mouse	1:50
Stro1	Santa Cruz Biotechnology	SC-47733	Mouse	1:50
Tubulin	Sigma Aldrich	T0198	Mouse	1:50
Vimentin	Sigma Aldrich	V6630	Mouse	1:50
Vinculin	Sigma Aldrich	V9264	Mouse	1:150

Table 2-1- primary monoclonal human antibodies those were used in this project.

The samples were incubated for 30 minutes at 4°C. After washing (3×5 minutes) with 0.5% PBST the immunostaining was complete. The samples were then mounted using VECTASHIELD® mounting medium with DAPI (4', 6-diamidino-2-phenylindole) which stains the nucleus (H-1200, contains 1.5 µg/ml of DAPI, Vector Laboratories, USA). DAPI is a fluorescence marker that strongly binds to A-T regions in DNA and produces a blue colour for the cell nucleus when excited by UV. A small droplet of about 50 µl was placed

on a 35 × 35 mm coverslip which was then placed on top of the stained cells. To prevent drying of the samples they were kept wrapped in aluminium foil in 4°C to view later.

2.3.2 Lamin staining

For lamin staining, after rinsing the cells in warm (37°C) 1x PBS, fixation in cold (-20°C) methanol for 2 minutes was performed. Then the samples were washed (3 times in 1x PBS). After blocking for 1 hour in 3% (w/v) BSA/1x PBS at 37°C, blocking solution had been replaced with primary antibody (mouse anti-lamin A/C or B). Samples were incubated at 37°C for 1.5 hours. After removal of primary antibody and washes in 0.1% PBST (3×5 minutes) cells then were placed in blocking solution for another 10 minutes at 37°C. Then secondary antibody (biotinylated anti-mouse IgG, BA 2000, Vector Laboratories) for 1hr at 37°C was added and then washed in 0.1% PBST (3×5 minutes). Conjugated streptavidin FITC was added in the dark for 30 minutes at 4°C. After the last wash in 0.1% PBST (3×5 minutes) the samples were mounted in DAPI and stored at 4°C after they were wrapped in aluminium foil.

2.3.3 Nucleolar staining

For nucleolar staining, the cells were fixed for 10 minutes in 4% (v/v) formaldehyde. Then using chilled permeabilising buffer (4°C) for 5 minutes the cells were permeabilised. After 10 minutes blocking at 37°C (1% BSA in PBS (w/v)), Alexa-Phalloidin (Alexa 488-labelled Phalloidin, Molecular probes, Invitrogen) was added and incubated (1hr at 37°C). The samples were washed in 5% PBST (v/v) (3×5 minutes) and with propidium iodide (VECTASHIELD, Vector Laboratories) were mounted.
The samples were stored at 4°C, wrapped in foil and viewed by a Zeiss Axiophot fluorescence microscope and camera. The images were captured with QCapture™ Suite Plus software (version 3.1.3.10). ImageJ (version 1.47) software and Microsoft Excel were used for analysis and comparison of pictures.

2.4 Scanning Electron Microscopy

For viewing the phenotypical changes by electron microscopy, the stimulated and control samples underwent fixation and processing as below. Initially the cells were fixed by the addition of buffered fixative (glutaraldehyde 1.5%, sodium cacodylate 0.1M) for 1hr at 4°C followed by sodium cacodylate rinse (0.1 M, 3×5 minutes). Next, the cells were post fixed in osmium tetroxide (1%, 1hr at room temperature), then distilled water washed

(3×10 minutes) followed by addition of aqueous uranyl acetate (for 1hr in the dark) and a quick wash by distilled water. A complete dehydration process was performed by ethanol series (30, 50, 70, 90%, two times, 5 minutes each followed by 100%, four times, 5 minutes each rinse and dried absolute ethanol, four times, 5 minutes each rinse). Finally, the samples were treated in hexamethyl-disilazane (HMDS, 2 times, each for 5 minutes) and were left overnight for slow evaporation of HDMS prior to coating. A thin layer of gold palladium (18 nm) was coated on the cell surface using a Polaron SC515 SEM Coating System (Quorum Technologies, UK). The Petri dishes were cut into circles (15 mm diameter) and stuck onto special aluminium stubs. A Carl Zeiss Sigma variable-pressure analytical SEM with Oxford Microanalysis® software was used to image the samples.

2.5 Polymerase Chain Reaction (PCR)

Looking for any genetic changes initiated by nanomechanical stimulation PCR was used. This technique uses as template either genomic or complementary DNA (cDNA) and makes numerous copies of a particular gene by repeated heating and cooling cycles in the presence of the enzymes called polymerases (Livak and Schmittgen, 2001). In this thesis cDNA was used as template for both qualitative PCR (gel) and reverse transcription real time quantitative qRT-PCR).

2.5.1 RNA extraction and cDNA synthesis:

In an RNAse-free system, RNeasy® Micro Kit (No: 74004, QIAGEN®) was used for RNA extraction. After cessation of mechanical cell stimulation, the medium was removed and the cells were washed in 1xPBS. The cells were then directly lysed on the Petri dishes by adding buffer RLT (according to the manufacturer's guidelines). After transfer of the lysate to sterile Eppendorf tubes (1.5 ml) and vortexing for 1 minute the samples were homogenised. After addition of 70% ethanol to the tubes, to precipitate RNA, all the content was placed in RNeasy® MinElute spin columns within 2 ml collection tubes. This column contains a micro filter that traps the RNA and it is possible to wash the RNA to obtain pure samples. After centrifugation (≥8000 × g or ≥10000 rpm) for 15 seconds and discarding the flow-through, another wash by buffer RW1 was done. After this, DNase I (No: 79254, RNase-Free DNase, QIAGEN) was added to each column for 15 minutes at 20-30°C. In later steps, RW1, RPE buffers and 80% ethanol each followed by centrifugation were used to wash the RNA in the columns. Finally, 14 µl of RNase-free

water was added to each column (over the centre on top of the filter) and the RNA was eluted after a 1-minute full speed centrifugation. To check the efficiency of RNA extraction for the final eluates the optical density (OD) of the samples was measured by spectrophotometry using Nanodrop®. After writing down the samples' ID the templates were stored in -70°C for further experiments.

Omniscript® reverse transcription kit (No: 20511, QIAGEN) was next used for cDNA synthesis. According to the manufacturer's notes, this kit is optimized for use with 50 ng to 2 µg of RNA obtained in the extraction process. Extracted samples were placed on ice for gradual thawing and prevention of RNA degradation. After thawing the components of the kit on ice, a master mix was prepared for every experiment (per reaction: 2µl of 10x Buffer RT, 1µl of 10mM dNTP Mix, 1µl random primer, 1µl RNase inhibitor and 1µl Omniscript® RT) and placed on ice. Based on the Nanodrop® results, the same amount (ng) of extracted RNA was used for all reactions, the final volume to 14µl was made up by RNase free water and heated to 65°C for 5 minutes in a thermal cycler to denature all the RNA. Then 6µl of master mix was added to every reaction making the final reaction volume 20µl. All the samples were put in the thermal cycler programmed for 37°C (for 60 minutes), then 93°C (for 5 minutes to stop the reaction) and then stored at 4°C for 24 hrs or -20°C for prolonged storage.

2.5.2 gel PCR:

Before running a gel to evaluate prominent synthesized DNA fragments, the steps for polymerization were as follows. Firstly, reaction mix containing a heat stable DNA polymerase (GoTaq® Hot Start), gene-specific primers (forward and reverse, 100 µM stock concentration) (Table 2-2) and sterile double distilled water was made (per reaction: 12.5 µl of GoTaq® Hot Start, 0.5 µl of each primers and 9.5 µl of nuclease-free water). It should be prepared for the number of samples plus 2 (or 10% more).

Gene	Forward primer	Reverse primer
GAPDH	TCAAGGCTGAGAACGGGAA	TGGGTGGCAGTGATGGCA
MyoD	TAGTAGGCGCCTTCGTAGCA	AGCACTACAGCGGCGACTC
Nestin	GTGGGAAGATACGGTGGAGA	ACCTGTTGTGATTGCCCTTC
Osteonectin	AGAATGAGAAGCGCCTGGAG	CTGCCAGTGTACAGGGAAGA
PPARγ	TGTGAAGCCCATTGAAGACA	CTGCAGTAGCTGCACGTGTT
Runx2	GGTCAGATGCAGGCGGCCC	TACGTGTGGTAGCGCGTGGC
Sox-9	AGACAGCCCCCTATCGACTT	CGGCAGGTACTGGTCAAACT

Table 2-2- forward and reverse primer details for gel PCR

The cDNA samples were put on ice and 2 µl of each sample was added to the same amount of reaction mix (23 µl) in the small reaction tubes. The PCR programme involved: 1 cycle of initialization (95°C for 2 minutes), 30 cycles of denaturation (95°C for 30 seconds), annealing (55°C for 30 seconds), and extension or elongation (72°C for 30 seconds), and a final single elongation step (72°C for 5 minutes). Synthesised DNA fragments were stored in 4°C for the next step.

Agarose gel (0.6 g Agarose MP (Roche), 60 ml of 1xTBE buffer, 6 µl SYBR® Safe DNA Gel Stain (S-33102, Invitrogen)) with 1×TBE buffer (Tris 21.8 g, boric acid 11 g, EDTA 1.86 g (all from Sigma)), add distilled water to reach 2 lt in total volume) was used to run a larger tank (could carry a 15 well gel). cDNA samples were loaded into the wells along with pure water as an index and a 100 bp ladder with a gel dye (for 1 well used: ladder 2 µl, gel dye 2 µl, distilled water 6 µl). These two index wells could be placed on both sides or in the middle of samples to aid comparison. About forty minutes after connection to a 100V source, the dye reached nearly to the gel edge. After stopping the process the gel was viewed in a UV gel box (GeneSnap 7.08 from Syngene, Cambridge, CB4 1TF, UK). Pictures were scanned and compared with each other (Figure 2-4).

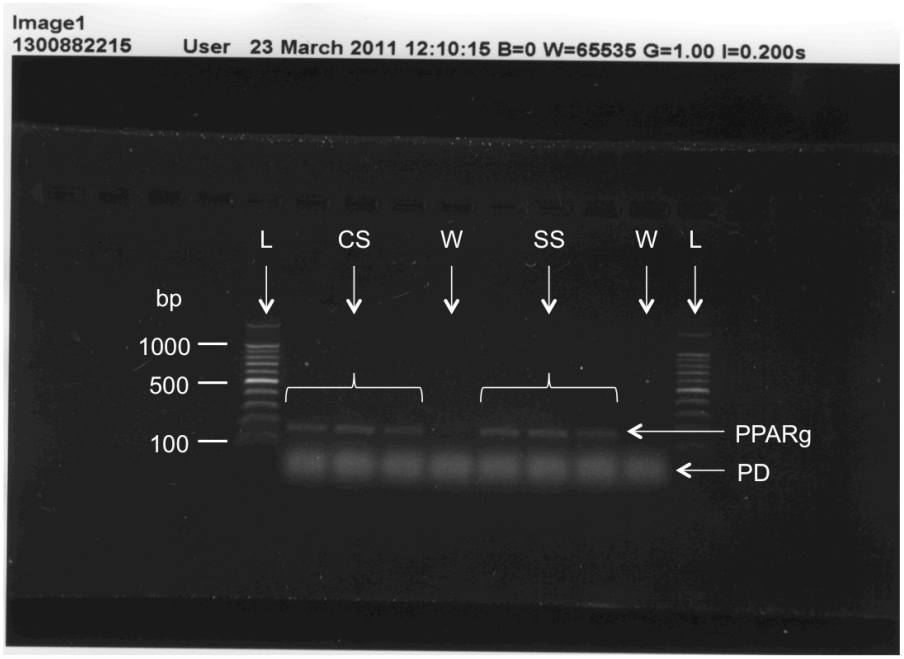

Figure 2-4- a sample of gel PCR view in UV gel box shows ten wells run for PPARγ. From left to right, 100 bp ladder (L), control samples in triplicate (CS), pure water (W), stimulated samples in triplicate (SS), repeated pure water and ladder. Stimulated samples showed a little difference in presentation of this gene. The accurate analysis by densitometry of lines and statistical comparison is possible. PD= primer-dimers, bp= base pair.

2.5.3 Real Time qPCR:

The basics for qPCR are the same as gel PCR but a real time thermocycler is used (7500 Real Time PCR System, Applied Biosystems® by Life Technologies- Invitrogen, USA). Based on principles of sensitive light detection during the thermal cycles of denaturation, annealing and extension of PCR (i.e. amplification of PCR product) via monitoring emitted fluorescence by fluorophores designed as part of the PCR primers. In an RNAse-free system for each reaction 10 µl of the Quantifast® SYBR Green PCR Master Mix (No: 4309155, Applied Biosystem), 1µl of each forward and reverse gene-specific primers (Table 2-3), 6µl RNAse-free water and 1-2 µl cDNA template were mixed. Biophere® Filter Tips (SARSTEDT, Germany) and Applied Biosystems® MicroAmp® Optical 96-Well Reaction Plates were used and 20µl reactions were loaded in each well. After definition of target genes, samples, controls, housekeeping genes and other variables the program was run for about 140 minutes and the results were analysed by the computer (7500 Software, version 2.0.5) or later by statistical software (Microsoft Excel).
The $2^{-\Delta\Delta CT}$ method was used for the result interpretation (Schmittgen and Livak, 2008).

Gene	Forward primer	Reverse primer
Runx2	CAGACCAGCAGCACTCCATA	CAGCGTCAACACCATCATTC
BMP2	ATGGATTCGTGGTGGAAGTG	GTGGAGTTCAGATGATCAGC
GAPDH	GTCAGTGGTGGACCTGACCT	ACCTGGTGCTCAGTGTAGCC

Table 2-3- forward and reverse primer details for qPCR

2.6 Microarray

For this analysis method after one-week experiment, the samples including a triplicate as static control cells and two triplicates for stimulated groups (500 Hz and 1000 Hz) (nine samples in total) were ready for RNA extraction. After extraction and measurement of RNA by Nanodrop® as explained above in section 2.5.1, the samples were measured again for a more accurate measurement of RNA content and evaluation of RNA quality by RNA Nano Chips using an Agilent® 2100 Bioanalyzer (Agilent Technologies, CA). Then a whole transcript expression analysis by using GeneChip® Human Gene 1.0 ST Array (Affymetrix®, US) was performed according to manufacturer's guidelines by the Glasgow Polyomics Facility staff. In this array each well-interpreted gene is signified by about 26 probes on the array spread across the full length of the gene. Estimated number of genes for this array is more than 28,000 genes. The data was analysed by uploading to Ingenuity pathway analysis (http://www.ingenuity.com/products/ipa) and by DAVID Bioinformatics Resources 6.7 (http://david.abcc.ncifcrf.gov).

Chapter III- Application of nanoscale mechanotransductive stimuli

3.1 Introduction

The aim of this project was to generate and apply nanoscale mechanical displacements in the vertical, the Z- axis, consistently across a culture of cells, and to quantify any cell behaviour changes as a consequence. Solid-stacked piezoelectric transducers were chosen to provide repeatable nanoscale displacements within all the experiments carried out. Previous calibration of such piezo devices has been carried out using laser interferometry, as will be discussed later in details in the context of this thesis. Displacement measurement of the upper surface of a typical piezo actuator (as used here - model number 010-05H ring type piezo stacks, distributed by Physik Instrumente® GmbH, Germany) clearly shows (Figure 3-1) that the displacement is linearly proportional to the applied voltage. Also shown here is the fact that the amplitude of displacement decreases as the frequency increases, in the region of approximately 10% (Curtis et al., 2013).

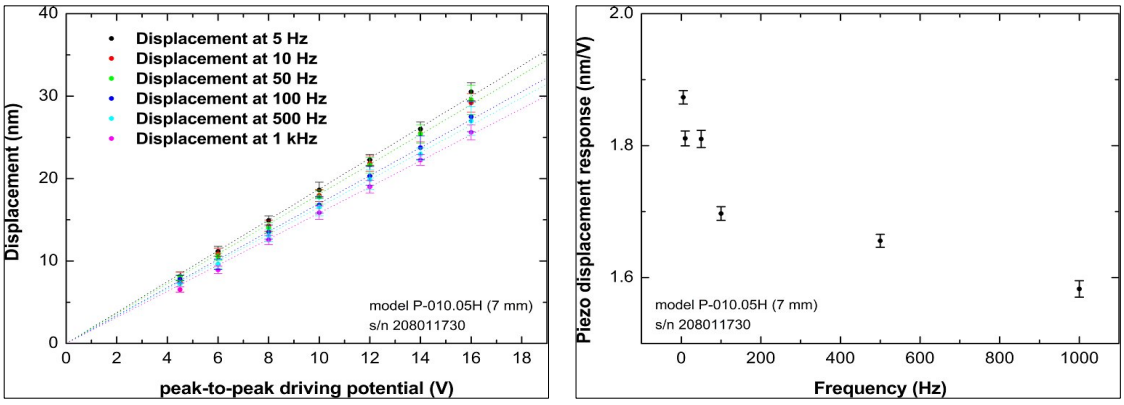

Figure 3-1- Calibration of a piezoelectric device, left: displacement (nm) as function of the peak to peak driving potential (V), and frequency. Right: displacement at a constant driving potential at different frequencies (figure courtesy of A. S. Curtis and S. Reid).

This chapter is therefore devoted to detailing the generation, characterisation and evaluation of the nanoscale displacements.

3.2 Piezoelectricity and Piezo actuator

The Curie brothers first demonstrated piezoelectricity in 1880 (Lang, 1999, Ballato, 1998) through close examination of the crystal *Tourmaline*. Piezoelectricity (arising from the

Greek: *pressure electricity*) is a property of certain classes of crystalline materials including natural crystals of quartz, cane sugar, Rochelle salt (sodium potassium tartrate tetrahydrate), Tourmaline, tooth and bone (collagen) (Minary-Jolandan and Yu, 2009, Halperin et al., 2004) plus manufactured ceramics such as Barium titanate. All these piezoelectric crystals have a non-centrosymmetric structure. Application of force could changes the distribution of electric dipoles in the material resulting in a variation of charge density on the surfaces and thus a variation in the electric field or voltage between the surfaces (direct piezoelectric effect). Opposingly application of electrical field on the material surface could change the charge density, electrical dipoles and resulting a mechanical deformation (indirect piezoelectric effect) i.e. conversion of mechanical energy to an electrical potential and *vice versa*.

When mechanical pressure is applied to one of these materials, the deformation of the crystalline structure produces positive and negative electrical charges to move to the surface of the material. This voltage is proportional to the pressure (direct piezoelectric effect or generator/sensor effect). Conversely, when a voltage is applied on a piezo material, a structural deformation causing a motion is induced (reverse piezoelectric effect). The induced displacement of piezoelectric materials has found use in a very large variety of actuator technology. The magnitude of displacement depends predominantly on the voltage applied. Manufacturers now fabricate various crystal shapes, and by applying voltages across different axes, can induce different forms of displacement across all three dimensions. Lead zirconate titanate composite (PZT) is the most commonly used material with piezoelectric activity for commercial usage. PZT actuators are typically constructed from multiple layers (less than 100 μm each) stacked on top of each other, with electrodes between each layer. This allows an electrical potential to be applied across each of the thin layers and the overall displacement is larger due to the increased electric field within each layer. The alignment of the crystallites in the piezoelectric material, along with the direction of the applied voltage, allows displacements to be longitudinal, shear, contracting, or bending.

3.3 Materials and methods

High-load piezo actuators with inner hole (PICA Thru Ring Actuators) type P-010.00H (Figure 3-2) were used for generation of nanoscale displacements in this project.

Figure 3-2- PICA Thru Ring Actuators type P-010.00H from PI Ceramic®

The characteristics of this type according to its manufacturer are as below:

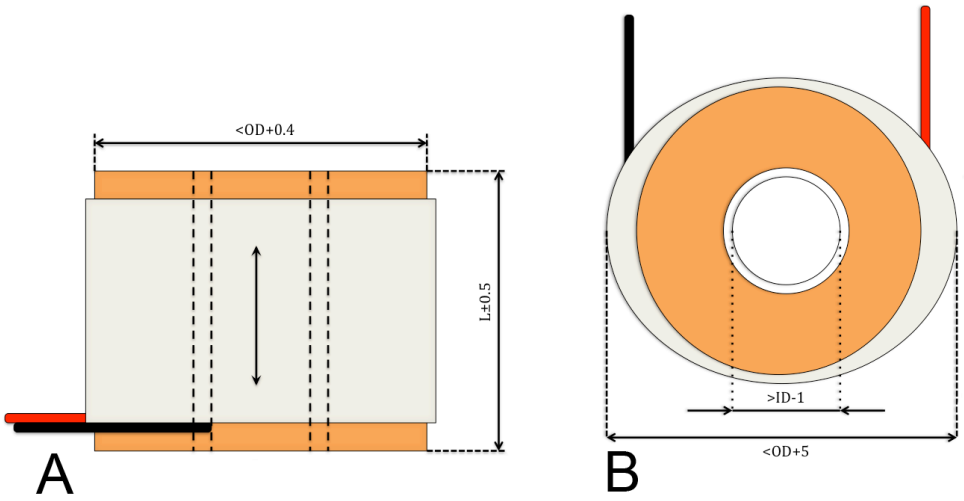

Displacement [µm] (0-1000V) -10/+20%	Diameter OD [mm]	Diameter ID [mm]	Length [mm] ±0.5	Blocking force [N] (0-1000V)	Stiffness [N/µm]	Capacitance [nF] ±20%	Resonant frequency [kHz]
5	10	5	7	1200	230	15	144

Figure 3-3- Piezo actuator (type P-010.00H) characteristics based on PI Ceramic® information; A) lateral view, B) top view, two wires in black and red thick lines, OD: outer diameter, ID: inner diameter, L: length.

The actuators were connected to the base of standard cell culture Petri dishes by all-purpose solvent free water-soluble glue (Bostik Ltd, Leicester, UK). For the first generation configuration, a 20 × 20 mm cover slip was placed at the bottom of each Petri dish. After seeding, the cells rested over the base and in some areas over the glass cover slip (Figures 3-4-A, 3-17). With a suitable sinusoidal potential being applied to the piezo actuator, the entire petri dish assembly, with adhered cells, would move up-and-down at the nanoscale. In order to direct the entire piezo motion towards the Petri dish (and cell cultures), a large aluminium block was placed under the setup. The aluminium block had a mass that was 1,200 times larger than the Petri dish assembly (4200 g versus 3.5 g), which ensured that the vast majority of the displacement was applied to the cell cultures. In a revised setup, to reduce the number of layers between piezo actuator and cell surface and hence to prevent dampening of the very small movements, the cover slip was removed (Figure 3-4 B).

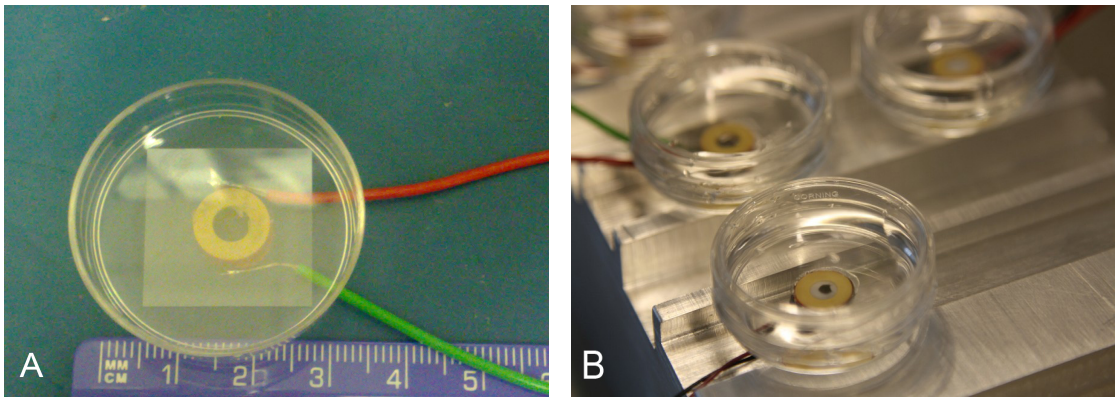

Figure 3-4- setup optimization, A) Initial setup using glass coverslip lying on Petri dish base and piezo actuator attached under the dish. B) Revised setup without coverslips resting on a heavy aluminium block.

3.3.1 Laser vibrometry

In order to accurately calibrate the level of nanoscale movements, laser interferometry was adopted by using a continuous helium-neon laser beam (wavelength: 632.8 nm, CW power: 5mW) and monitoring the beam as it was reflected from the Petri dish surface where the cells were to be cultured. A laser interferometer vibrometer, SIOS Meßtechnik GmbH SP-S 120 (Figure 3-5 A), would reflect the laser beam from a distance of more than 25 cm to the surface (here the Petri dish base) and measure displacement with up to 0.02 nm vertical resolutions.

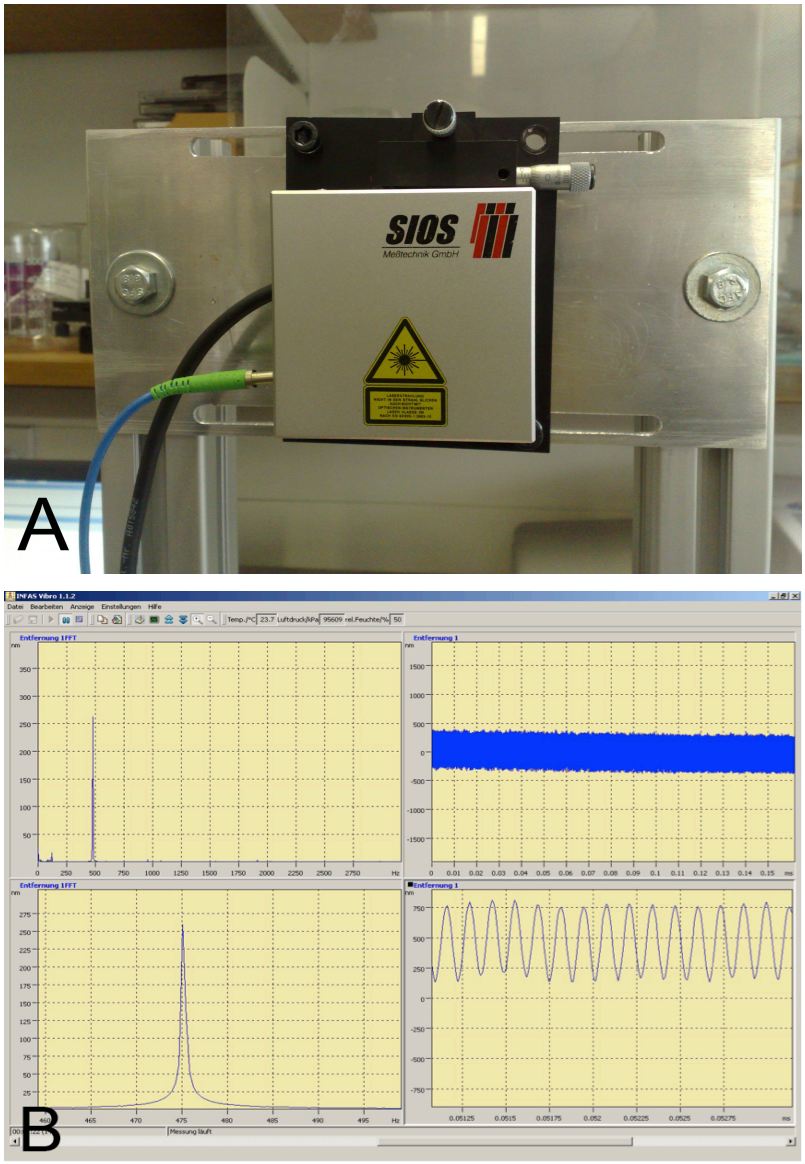

Figure 3-5- Interferometry: A) Laser interferometric vibrometer SP-S series used for measurement of nano scale displacement on the base of Petri dishes, B) a sample of result screen that shows amount of displacement at a chosen frequency (260 nm at 480 Hz).

The reflected beam was directed into an interferometer to create an interference pattern with a reference beam. Alignment was achieved by observing an internal oscillator signal that appeared as a ring shape trace on an oscilloscope. Computer software was used to acquire the interference output from the interferometer, perform a fast fourier transform (FFT), and plot the amplitude of motion in frequency space. SIOS Meßtechnik GmbH's INFAS Vibro (Interferometer Analysis Software for Vibrometers) was used for interpretation of the results (Figure 3-5 B). The FFT spectrum can then be observed.

The measurement setup is shown in Figure 3-6. It consists of a laser source at 75 cm from reflective surface (the dish surface), connected to a data processing unit and an oscilloscope, and finally to a computer that ran the analysis software. The reflected beam from the surface passes through the vibrometer and makes a circular trace on oscilloscope screen. At this situation INFAS program shows displacement curve at chosen frequency. This curve renews every five seconds and for each point we looked for eight renewed measurements and recorded the mean of them in nano meter.

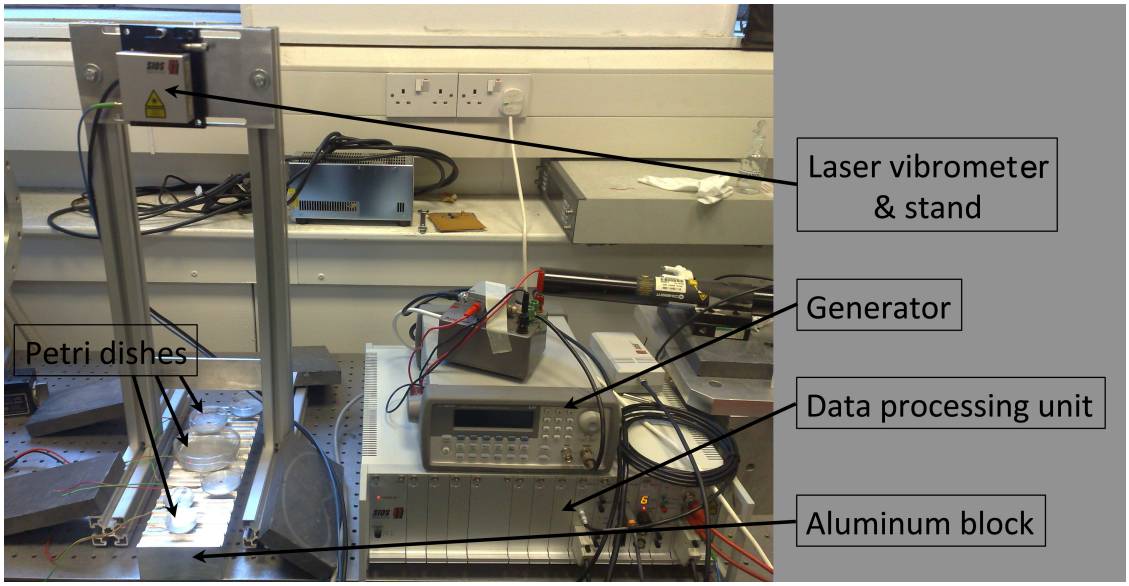

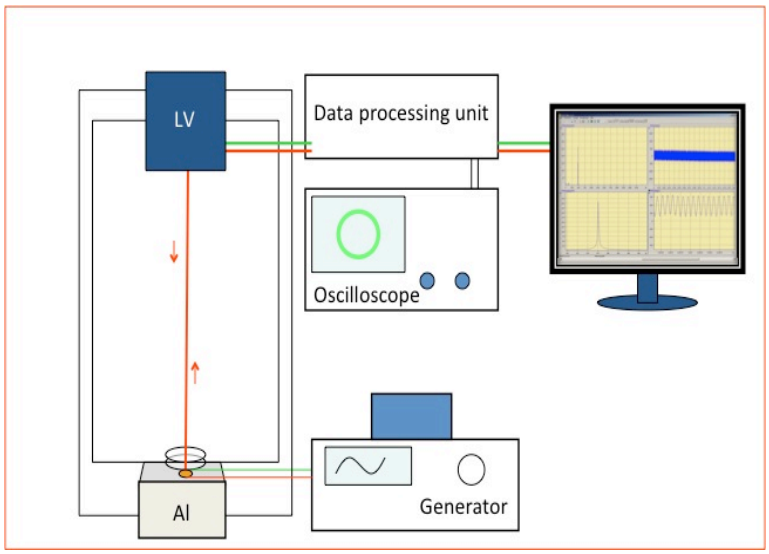

Figure 3-6 - Laser interferometric vibrometry (LV) setup: reflected laser beam from vibrating Petri dish will be analysed by SIOS software and shows the nanometric displacement of the Petri dish base surface every 5 seconds as a plot. Al: aluminium block holding the piezo actuator and attached Petri dish.

Measuring the nanoscale displacements at low frequencies (typically below 25 Hz) was difficult due to the coupling of ground (seismic) motion. Therefore five higher frequencies were chosen, with two amplitudes, to characterise each of the piezo actuator setups with the experiments carried out here (Table 3-1).

	10 Vpp	19 Vpp
25 Hz		
50 Hz		
100 Hz		
500 Hz		
1000 Hz		

Table 3-1- Chosen frequencies and voltages as a blank table

Please note that the highest limit of voltage production for the generators used was 19 volts that is thus used in the results instead of 20 volts.

Four to five radial points from the centre to periphery of dishes were chosen and marked as measurement points (Figure 3-7- A). As the Petri dishes were transparent small square pieces of silicon wafer fragments were attached to act as measurement points over the Petri dish base, the measured displacements were compared between these silicon-tagged points and adjacent points on Petri dishes (Figure 3-7- B).

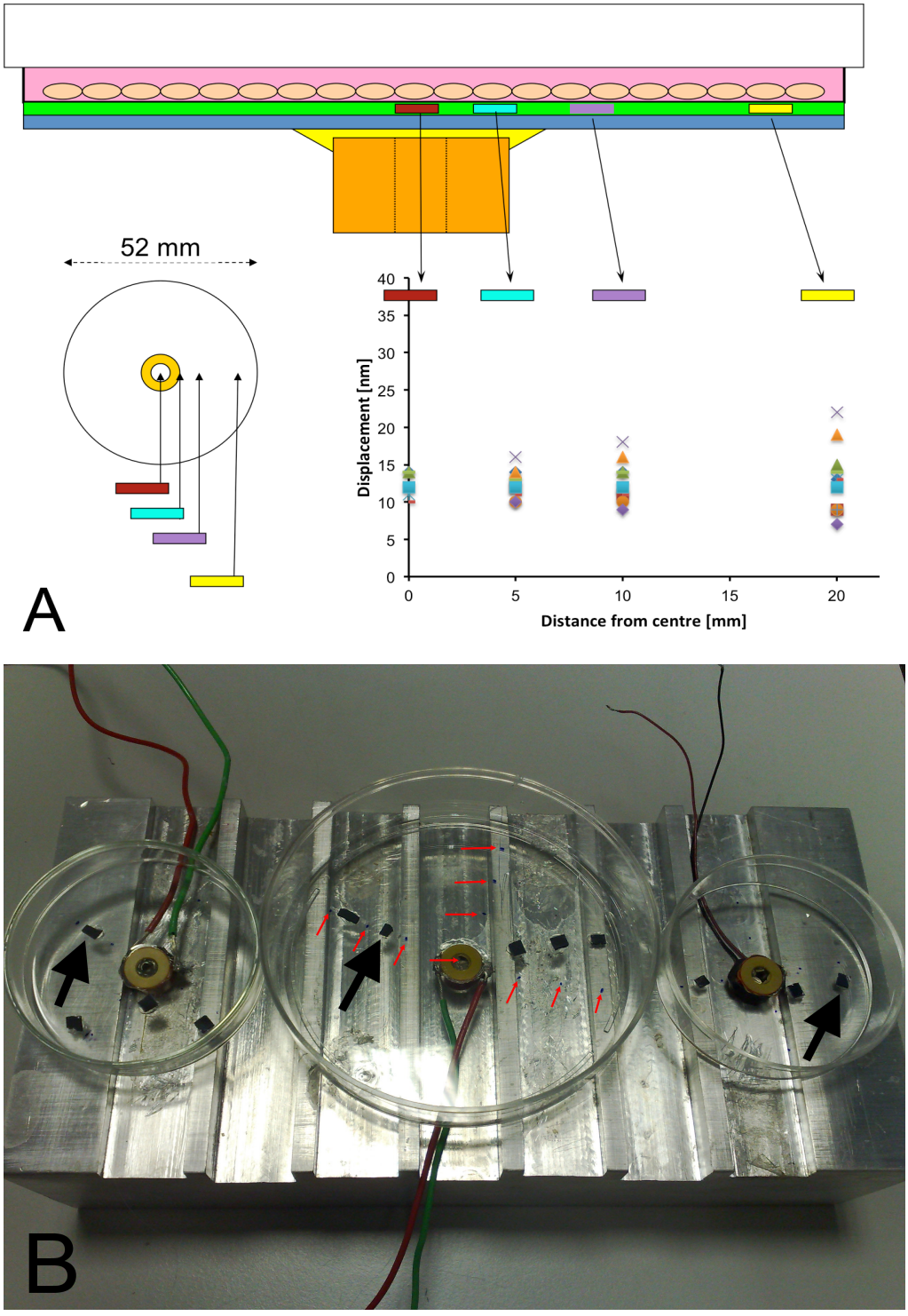

Figure 3-7- Measurement points: A) Schematic image shows 52 mm base Petri dish containing cells is attached by epoxy glue (green) to a glass or aluminium disk (dark blue) with four selected points for vibrometry. B) Small pieces of silicon (black arrows) were attached to the Petri dish bases adjacent to the various points of the base (red arrows) to compare their relative measurements to the next points on the dish surface.

By an additional technique, frequency sweeping can be used to help identify any resonant conditions of the setup. By sweeping up in frequencies, and recording the displacement at each frequency, the possible resonance can be observed as a peak in displacement followed by a return to a lower (expected) displacement (Figure 3-8).

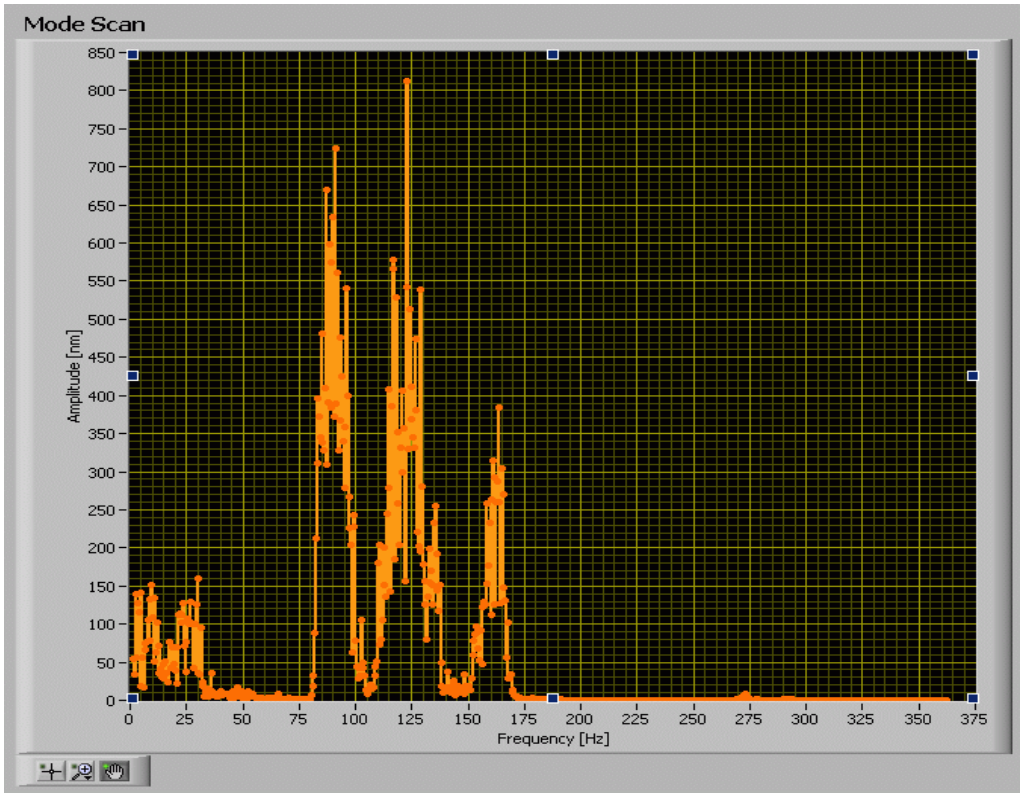

Figure 3-8- Frequency sweeping: possible resonance could be observed between 80-165 Hz frequencies as spiky changes in displacement and return to the expected motion.

By this method the displacements in 35, 60, and 100 mm diameter standard Petri dishes made of surface treated polystyrene attached to piezo actuators were measured.

3.3.2 Thermal Imaging

Since energy will be dissipated into heat through each cycle of the piezo motion, care must be taken to ensure that the cell cultures are not responding to heat shock, particularly as the frequency (the number of cycles per second) increases. In order to probe for any possible thermal change during high frequency vibrations, thermal imaging was performed. An infrared camera (FLIR i7) was used in the hot room (37°C) to examine the setup for any temperature change before and after starting piezo vibration at 500 Hz and 1000 Hz frequencies (Figure 3-9).

Figure 3-9- Thermal imaging setup: Thermal camera is placed in position providing a side-view of two Petri dishes, mounted on top of the piezo actuators and aluminium block respectively. The infrared emission can be observed on the camera display, showing the cold media (D) due to evaporation, a warmer pink point underneath the piezo actuator (P) and yellow background from the aluminium block (A).

Images taken at different time intervals were compared in order to study any colour change that would indicate any rising temperature associated with the piezo actuators and the aluminium disk. The comparisons did not show any heat transmission from the piezoelectric actuators when they were working at 500 Hz and 1 kHz toward the Petri dishes on top. Although temperature difference was apparent (maximum 1.4°C) minutes after connecting the actuators to power source, this difference became negligible after several hours (See part 3.4 for more discussion).

3.3.3 Shear flow

Vibration can also generate fluid waves in any liquid material, which could impose significant viscous forces on the cell cultures. To investigate any flow of media related to piezo stimulation, two experiments were carried out. Firstly, macroscopic particles from

water-soluble dye were introduced and observed before, during and after piezo stimulation. The aim was to observe any change in particle diffusion, or pattern whilst under typical mechanical vibration protocols. Secondly, red fluorescent microspheres (5 μm diameter) were added to create an emulsion in the media and likewise observed before and after mechanical stimulation. These microspheres could be easily viewed under a fluorescent microscope. Video recording was used in both cases to observe and compare the possible shear flow due to piezo stimulation (Figure 3-10).

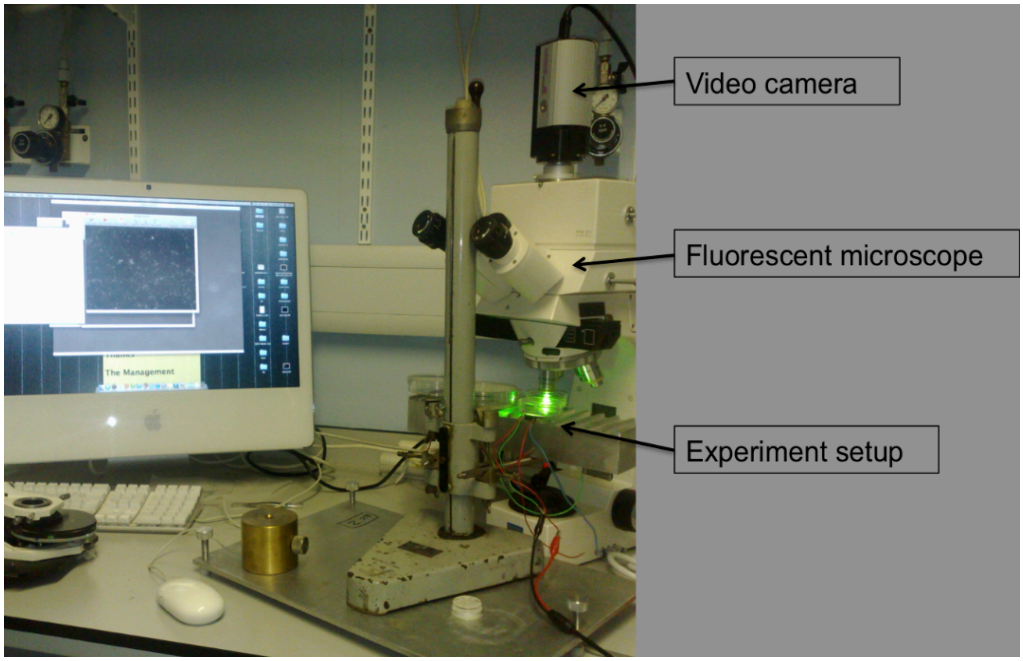

Figure 3-10- Recording fluorescent particles' motion before and after nano scale vibration showed any possible induced motion produced by vibration.

3.4 Results

The initial results from the laser interferometric vibrometry described, reveals a variable displacement across the petri dishes base from the centre to the periphery (Figure 3-11).

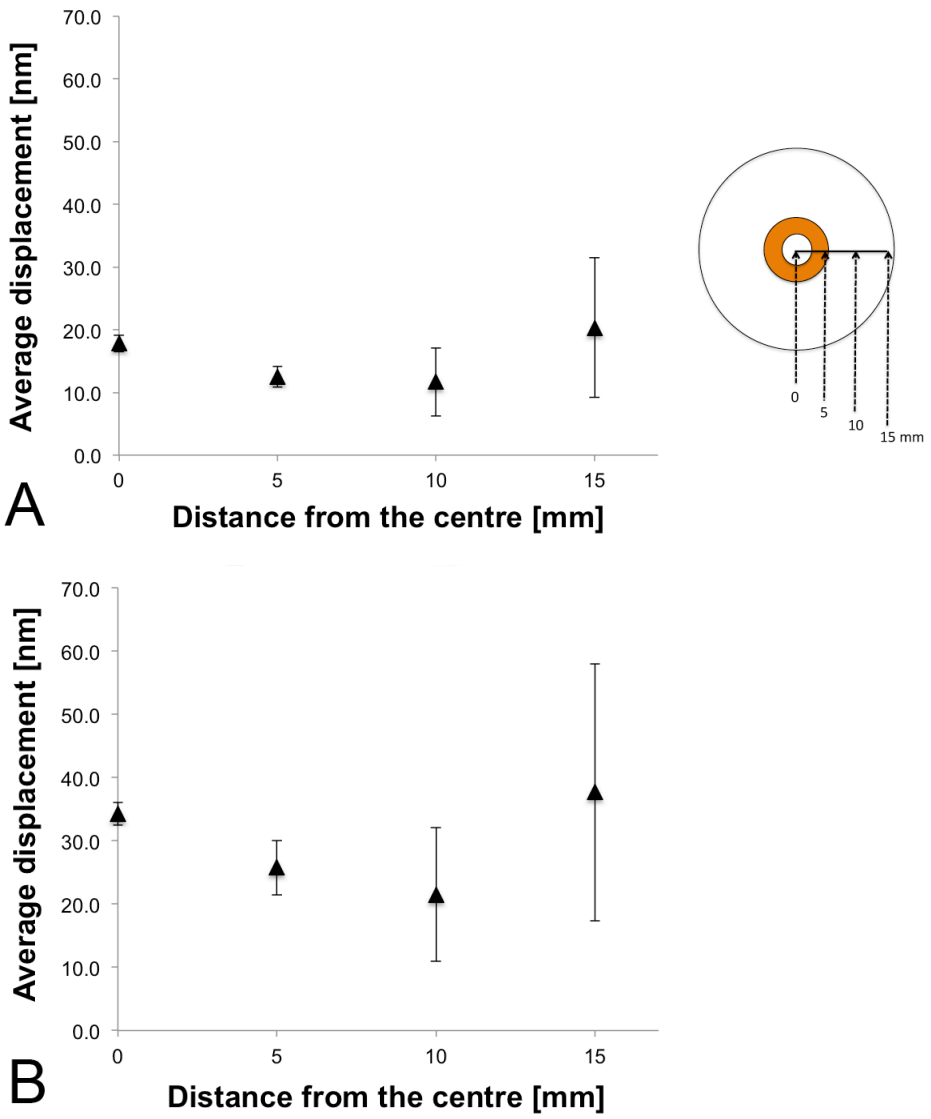

Figure 3-11- Laser vibrometer results showing the nanoscale displacements across 35 mm Petri dishes attached to a piezo actuator. A) By 10 V × 1 kHz, mean values showed decrease in displacement from the centre to the top of piezo actuator (5 mm from centre). Then disproportionate increases in displacement were observed in the majority of measurements when moving towards the periphery. B) Increasing the sinusoidal voltage to 19 V without change in frequency (1 kHz), the average displacement was observed to increase approximately two-fold as expected but inappropriate displacement increase toward the dish border was apparent. N=45.

Table 3-2 shows the measurement summary for typical displacements on the small (35mm) Petri dishes. Again, the approximately two-fold increase is observed for the higher voltage. Big variances indicative of high deviations from the mean displacements are noted. It showed that the range of displacements on the Petri dish surface is far from mean displacements.

Vpp × Hz	No	Min (nm)	Max (nm)	Mean (nm)	Med (nm)	Var	SD
10 × 1000	45	1	34	15.956	16	52.41	7.239
19 × 1000	47	3	65	30.830	31	172.88	13.149

Table 3-2- Initial measurements on 35 mm Petri dish base at four marked points as described in figure 3-10 for two voltages (Vpp) and a constant frequency (1 kHz); No: the number of measurements, Min: minimum measured displacement in nanometre (nm), Max: maximum measured displacement, Med: median, Var: Variance of measurements, SD: standard deviation.

The large variation in displacement of Petri dish base from the centre to periphery could be explained by the flexible nature of the plastic dishes. It was therefore essential to make changes to the vibration setup in order to supply a repeatable and quantifiable displacement across the entire culture. This was achieved by using glass Petri dishes, or plastic dishes reinforced with an aluminium base, both resulting in a higher rigidity of the base, and were used for the next generation stimulation experiments. The glue used to attach the additional aluminium support needed to be both hard, and easy to remove after use in order to recycle the Piezo actuators. A double bubble epoxy adhesive from Loctite® (Henkel Ltd, Hemel Hempstead, HP2 4RQ, UK) which hardens in 3-5 minutes was used. For the best connection i.e. the thinnest and hardest attachment, after application of glue the disk and the dish were pushed together firmly. After attaching the piezo actuators, the displacement measurements were repeated with multiple samples. When a glass disk (1.35mm glass disk PYREX® brand or Borosilicate 3.3 mm float glass sheet by Jencons LTD) or an aluminium support layer of 1.6 mm thickness was attached, the results showed a reverse trend for the propagation of displacement across the dish base (Figure 3-12).

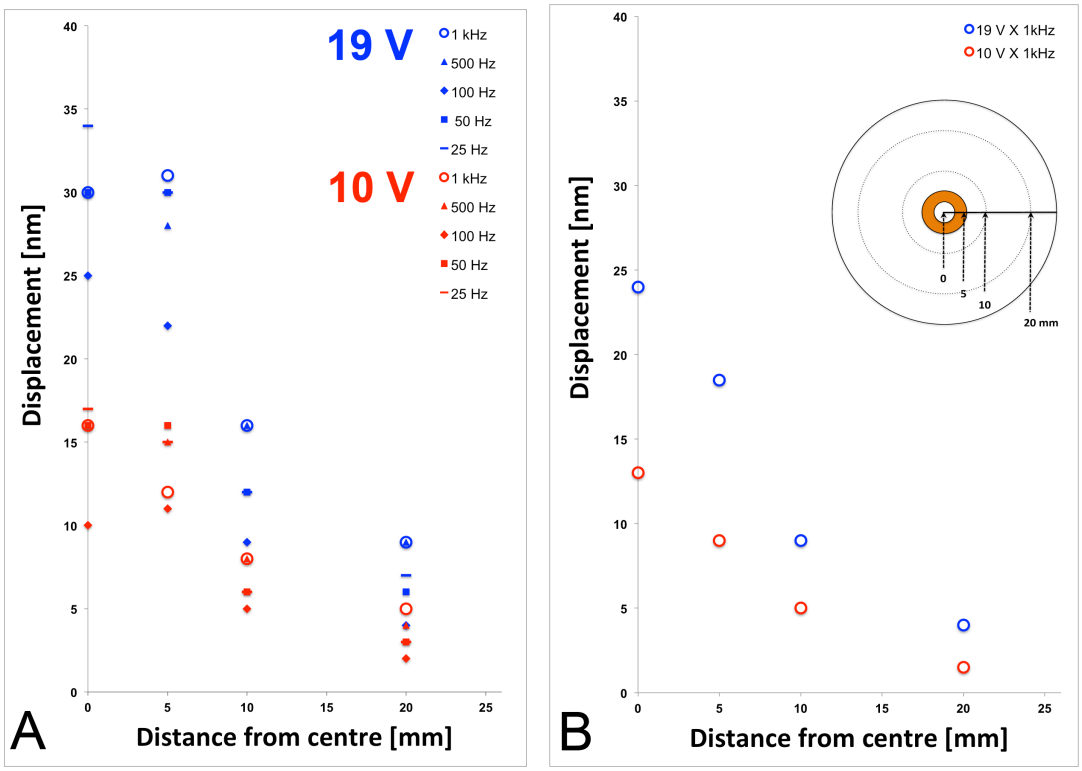

Figure 3-12- Plots of Z-axis displacement in dependence on position, amplitudes and frequencies on Petri dishes attached to hard disks, A) Glass disk: the plot shows gradual decreases in measured displacements for the glass disk when two voltages (19 volts and 10 volts coded by blue and red colours respectively) and five different frequencies (symbol coded) were applied. B) Aluminium disk (1.6 mm thickness) attached to the dish showed the same decreasing pattern of displacement for two different amplitudes at the same frequency.

After noting this pattern of displacement across the Petri dish, the aluminium disk was replaced by a thicker aluminium disk (3.4 mm). The measurements for 35 mm and 60 mm Petri dishes showed a relatively repeatable displacement over their bases measured on several locations, without significant variations (Figure 3-13, 3-14).

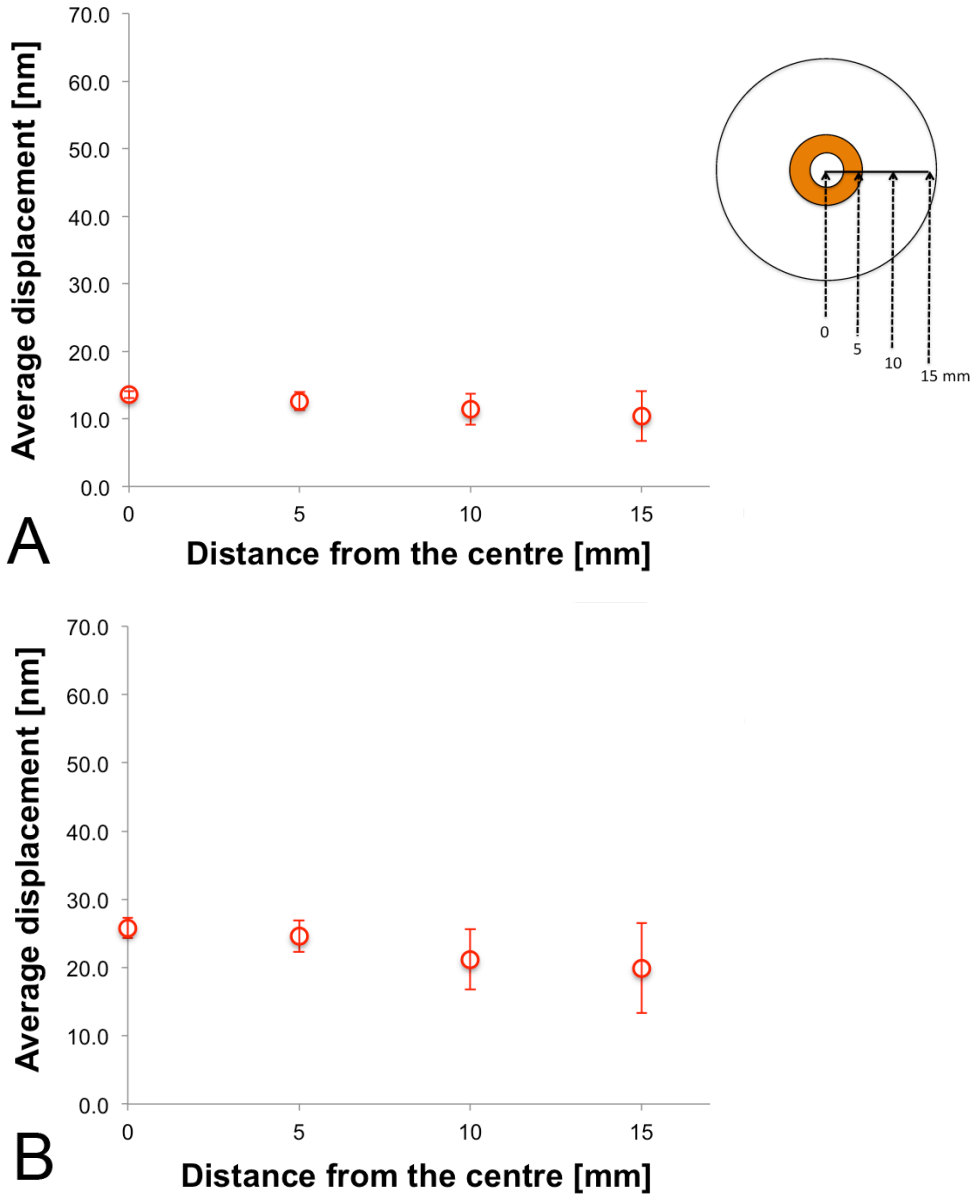

Figure 3-13- Laser vibrometer results showing the nanoscale displacement of 35 mm Petri dishes attached to a 3.4 mm aluminium disk across 4 marked points. A slight downward slow trend was observed when moving towards the periphery of the disk. Increasing the voltage from 10 V (A) to 19 V (B), at a constant frequency (1 kHz), made the observed average displacements double, as expected, but deviations also increased.

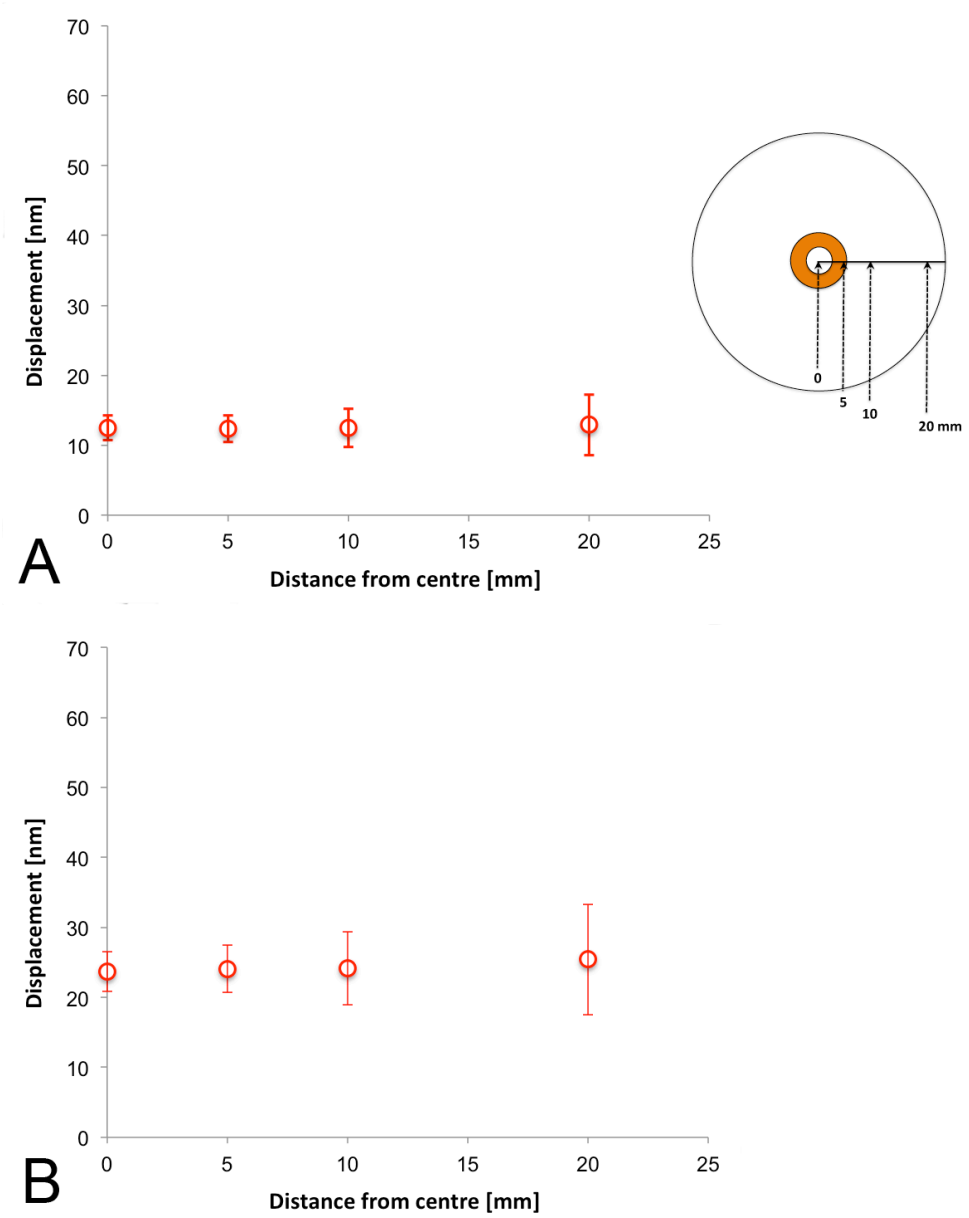

Figure 3-14- Laser vibrometer measurements on 52 mm base diameter Petri dishes attached to a 3.4 mm aluminium disk. In A) a gradual dispersion of average measurements toward the periphery of the dish was seen. Here 10 V as driving potential and 1 kHz frequency was used. In B) average measurements at the same points when the voltage increased to 19 V at the same frequency (1 kHz), showed about two times increases. The dispersion of measured numbers increased in this group.

A comparison of average displacements on 35 mm and 52 mm base dishes, with and without aluminium disk, after induction of two different driving potentials (10 V and 19 V) at 1 kHz frequency is shown in Figure 3-15.

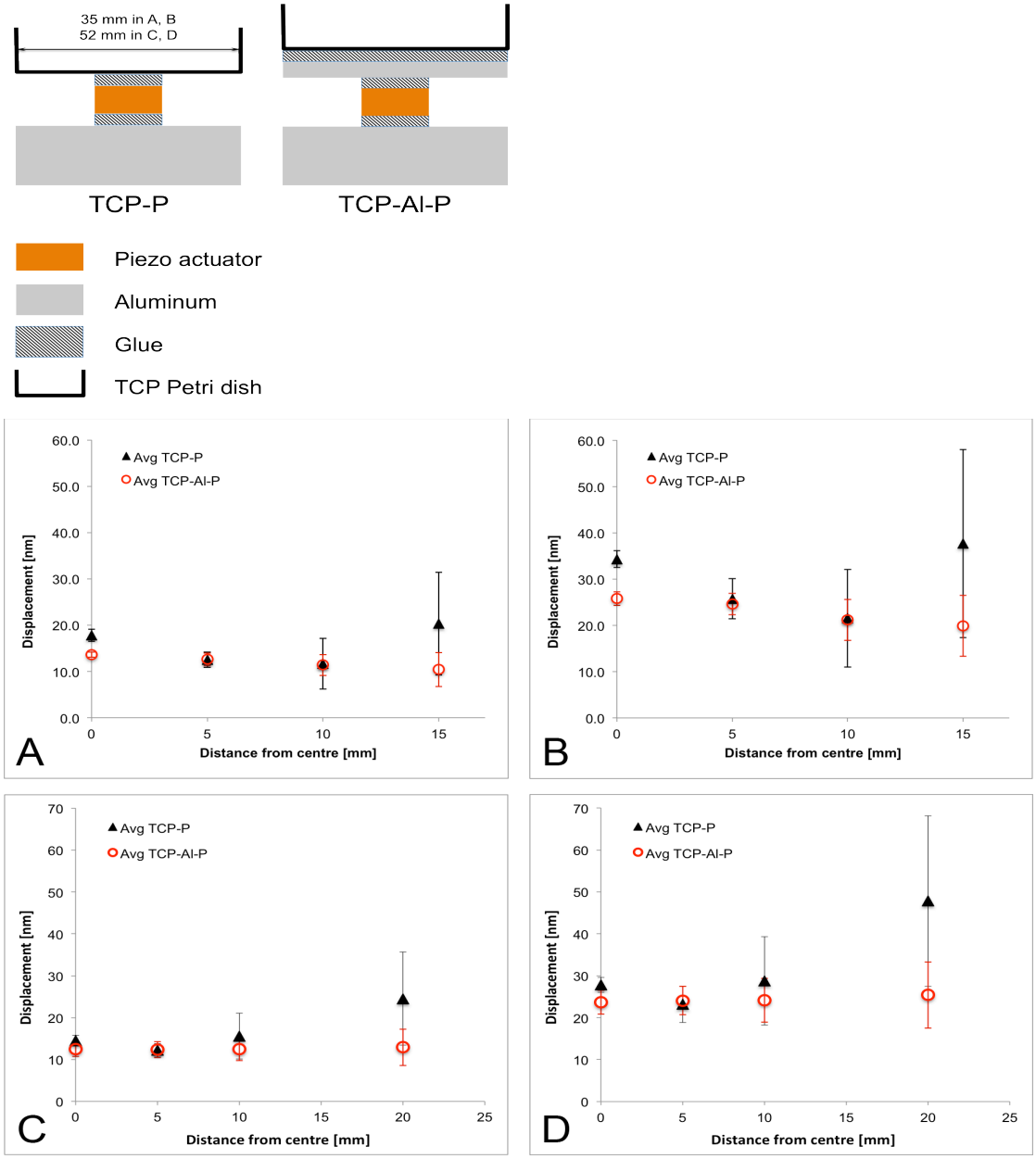

Figure 3-15- Interferometric measurement summaries, Top) Schematic pictures as key pictures for two setups show the arrangement of piezo actuator, glue layers, aluminium disk, and Petri dishes. The plots (A-D) are describing average variations that occurred in two types of Petri dishes (35 mm in plots A & B and 52 mm base in C & D) after attachment of aluminium disks. Introduction of 10 V × 1 kHz (A, C) made displacement of the base with less deviation when aluminium disk was added (red circles). Increase in voltage to 19 V with the same frequency (B, D) made higher displacement on both types of dish that showed less fluctuation when aluminium disks were attached to them. Avg: average, TCP-P: tissue culture plastic dish attached to the piezo actuator, TCP-Al-P: tissue culture plastic dish attached to the aluminium disk and piezo actuator underneath. Both setups settled on aluminium block.

Measurements for 100 mm petri dishes (86 mm base diameter) showed a larger variation with and without a 3.4 mm thick aluminium disk. The high fluctuation near the external circumference of the dish at 95 Hz indicated that the frequency of vibration might have been close to a resonant condition of the setup (Figure 3-16-A).

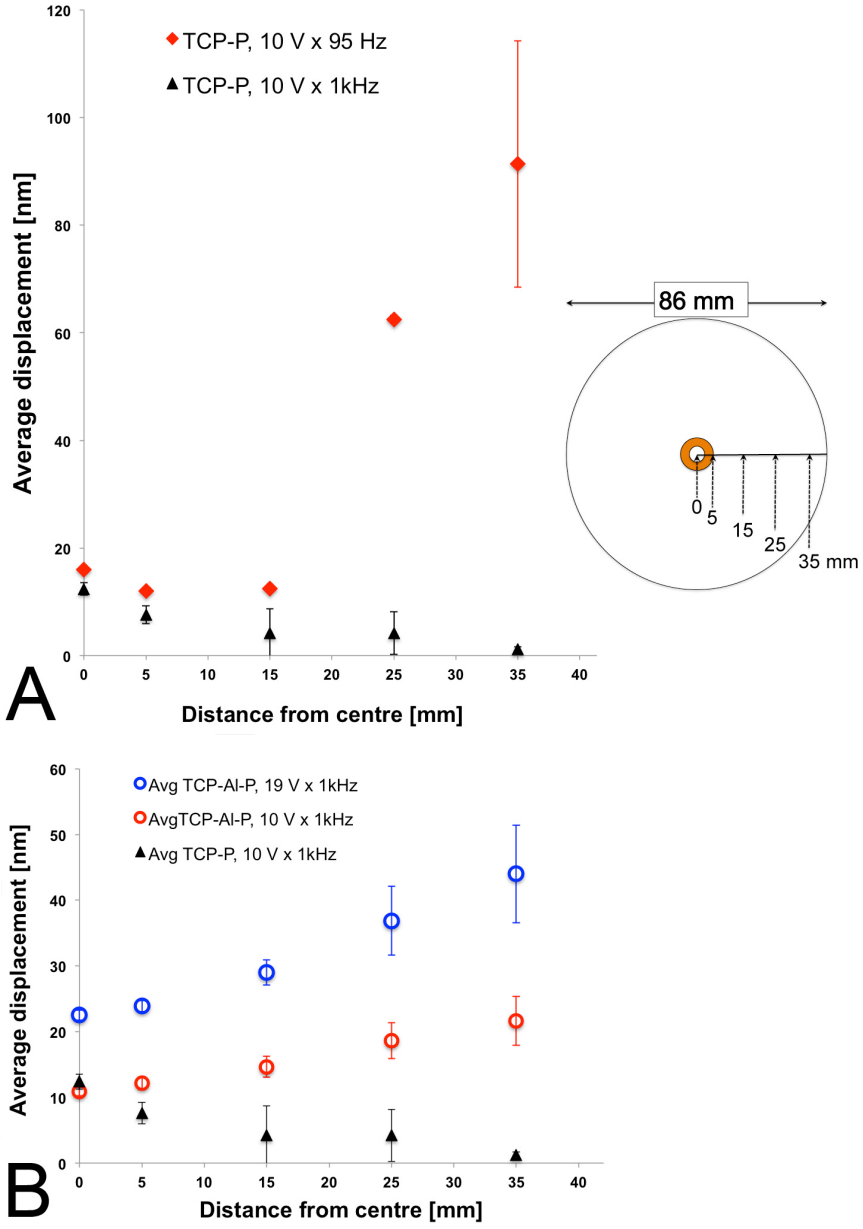

Figure 3-16- A) Laser vibrometer measurements on 86 mm Petri dish base showed a large variation of displacement without an aluminium disk attached at 10 V × 95 Hz. A gradual increase in vibration amplitude could be seen when the point at which the measurement was taken moved from the centre toward the periphery. It seems likely this frequency was near to the resonance frequency of this type of dish. Measured displacement at the same

voltage and 1 kHz showed a gradual decrease toward the periphery (black triangles). B) After attachment of an aluminium disk, the displacements showed a gradual increasing pattern toward the periphery but with higher deviation than other dish types. By increasing applied voltage to 19 V (blue circles) displacement increased accordingly. Avg: average, TCP-P: tissue culture plastic dish attached to the piezo actuator, TCP-Al-P: tissue culture plastic dish attached to the aluminium disk and piezo actuator underneath. N= 18.

Table 3-3 shows the statistical analysis of the measurements on all the types of dishes with or without aluminium disks attached. According to these records by attaching aluminium disk the mean value of displacements reduced but the reduction in variances were more prominent. This decrease was influenced by increase in induced voltage i.e. higher voltage for the same dish showed higher displacement with significant higher variances when aluminium disks were not used. Measured displacements were relatively the same for two kinds of Petri dishes (small= 35 mm and medium= 60 mm) but variances were different especially for small sized dishes with higher driving potential that showed large differences in variance when compared with aluminium-attached dishes. Large Petri dishes (100 mm) with and without 3.4 mm thick aluminium disk attached showed variable inconsistent displacements from nano- to micrometres at 95 Hz that could be a frequency close to the dish resonance. At 1 kHz, attachment of an aluminium disk made the displacement more similar over this type of Petri dishes (Table 3-3).

Setup	Voltage × Frequency	No	Min (nm)	Max (nm)	Mean (nm)	Med (nm)	Var	SD
SP	10 V × 1 kHz	45	1	34	16	16	52.41	7
SPA	10 V × 1 kHz	35	4	15	12	12	6.71	3
SP	19 V × 1 kHz	47	3	65	31	31	172.88	13
SPA	19 V × 1 kHz	39	8	29	22	24	22.72	5
MPA	10 V × 1 kHz	42	7	22	13	12	8.54	3
MPA	10 V × 500 Hz	12	11	16	14	14	2.44	2
MPA	10 V × 100 Hz	12	8	15	11	11	4.15	2
MPA	10 V × 50 Hz	12	10	14	13	13	2.27	2
MPA	10 V × 25 Hz	12	11	20	14	13.5	8.75	3
MPA	19 V × 1 kHz	42	14	42	24	24	28.54	5
MPA	19 V × 500 Hz	12	21	32	26	25.5	14.97	4
MPA	19 V × 100 Hz	12	15	28	21	21	14.08	4
MPA	19 V × 50 Hz	12	17	40	24	22	36.20	6
MPA	19 V × 25 Hz	12	20	40	25	23	37.45	6
LP	10 V × 1 kHz	25	1	14	6	4	21.9	4.7
LPA	10 V × 1 kHz	40	10	26	15.6	14	21	4.6
LP	19 V × 1 kHz	25	1	29	12	7	95.5	9.8
LPA	19 V × 1 kHz	40	22	52	31.3	29	83.5	9.1

Table 3-3- Statistical analysis of displacements measured by laser interferometric vibrometry on various types of Petri dishes and with different frequencies and voltages for supplying vibration to cell cultures. No: number of measurements, Min: minimal displacement in nm, Max: Maximum displacement in nm, Med: median, Var: Variance of measurements, SD: standard deviation.

SP= **S**mall (35 mm base diameter) standard cell culture dish connected to **P**iezo actuator

SPA= **S**mall (35 mm base diameter) standard cell culture dish connected to **P**iezo actuator + **A**luminium disk

MPA= **M**edium (52 mm base diameter) standard cell culture dish connected to **P**iezo actuator + **A**luminium disk

LPA= **L**arge (86 mm base diameter) standard cell culture dish connected to **P**iezo actuator

LPA= **L**arge (86 mm base diameter) standard cell culture dish connected to **P**iezo actuator + **A**luminium disk

When considering thermal effects, after comparing thermal images, as described previously, neither significant temperature change were observed, nor heat transfer

towards the space where cells would sit. Figures 3-17 and 3-18 show exemplary images. Significant heating of the individual piezo transducers was not observed using this technique. This is in agreement with calculations using the parameters available from the manufacturer that would estimate the heat generated in each piezo actuator to be around 20-30 μW, which would be insufficient to create an observable heat rise.

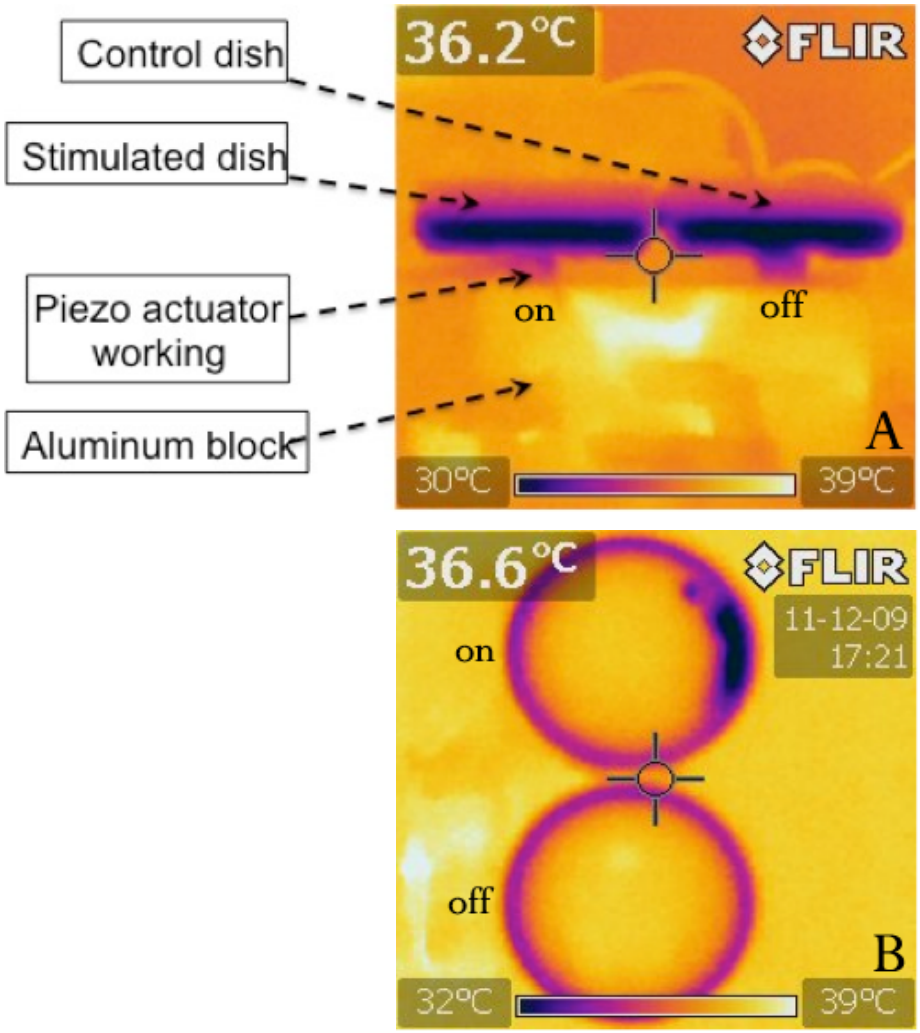

Figure 3-17- Thermal pictures of piezo actuator attached to the Petri dishes in two situations (turning on and off the actuator): A) from lateral view and B) top view. The dark blue colour in A is indicator of evaporating liquid media inside the dishes. In B the dishes are empty except some remained media around the corners. The temperature showed at the left upper corner of each picture is the recorded temperature from the central (target sign) area and the colour bar below is the indicator of the temperature scale. In lateral view a little change in colour (increased heat production) was seen in the working piezo actuator. This difference is not apparent in the top view picture (B).

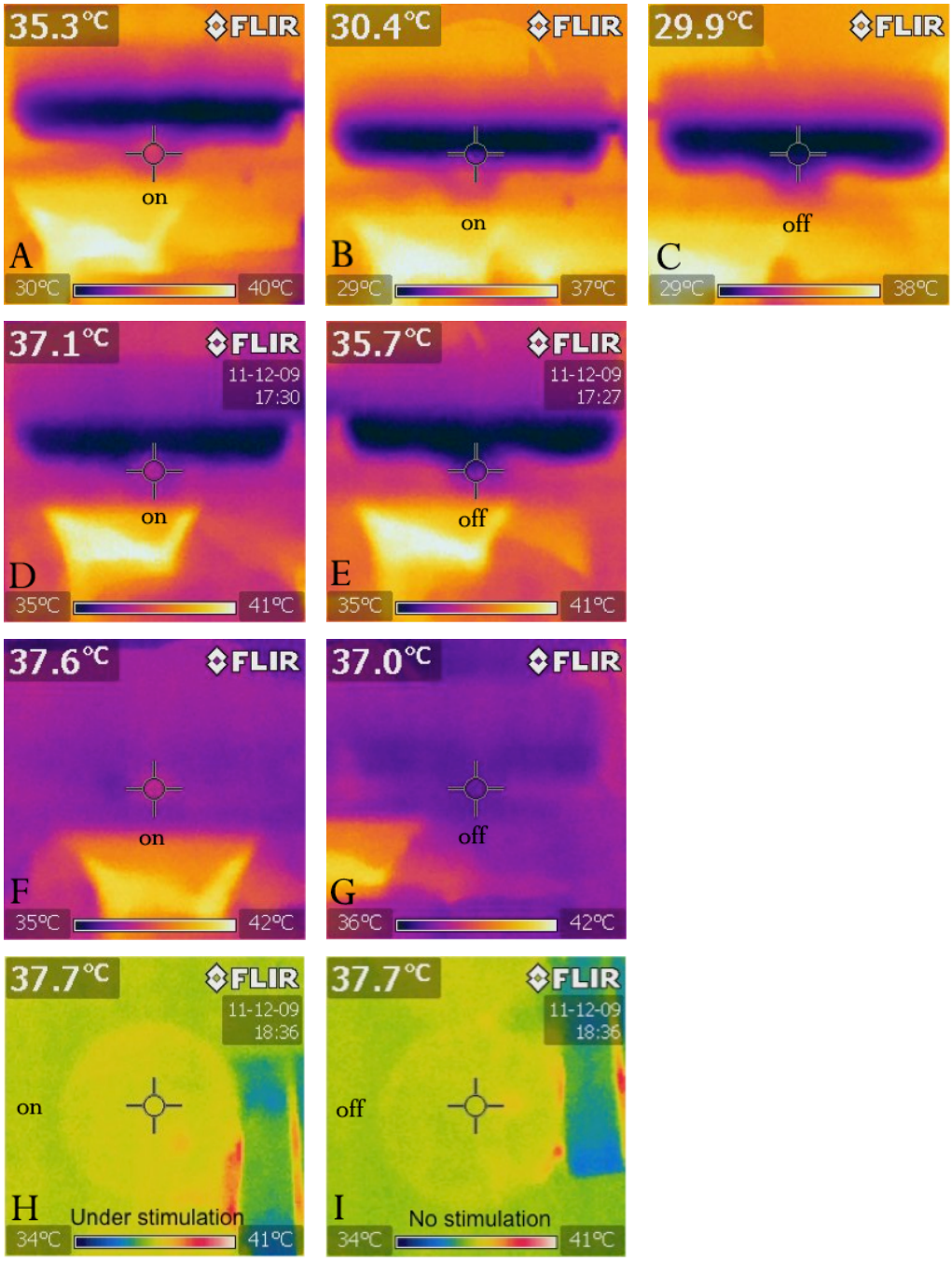

Figure 3-18- Comparison of thermal images: Selection of infrared (thermal) images of the Petri dishes, both from the side (A to G) and from the top (H, I) showed instead of 1°C increase in piezo ceramic temperature minutes after connection to the generator (A), the difference in temperature was not more than 0.5°C at the Petri dish surface (B, C). After an hour (or more) this difference reached to maximum 1.4°C between the piezo actuators (D, E). This difference was constant without any recognisable heat conduction upwards to the cell culture region (H, I). Change in the colour in H and I pictures is due to mode change of the camera. F and G are the pictures from the same dishes with closed cap and reduced media evaporation with a warm point over the working piezo actuator seen at F.

In considering shear stress, comparisons of the microscope images for macro beads and video recordings for the fluorescent micro beads before, during and after stimulation did not reveal any unintended motions and/or fluid (shear) waves or "footprint" patterns of the particulates across the Petri dishes. It was concluded that the piezoelectric stimulation did not generate any specific shear motion in this setup (data not shown).

3.5 Discussion

After verifying the repeatability of the displacements that can be induced using a piezo transducer, it was important to check that these very tiny motions can be reliably applied across the entire surface of a culture dish. Great care was taken at this stage, through direct measurement at the nanoscale, to ensure that motions were being applied without any unwanted damping or amplification due to resonances from the final set up. This will enable any biological response of the cell cultures to be associated with the simple vertical nanoscale motion and not due to other variables or forces. Accurate measurement by laser interferometry confirmed these displacements on the Petri dish surface. After initial measurements of vibration on the surface of Petri dishes-directly connected to piezo actuators, it was shown that due to plastic nature of the dishes a wavy motion with variable increasing displacement would travel from the centre to the periphery of the dish and a hard surface could conduct these motions more faithfully. By attaching glass and aluminium surfaces under the dishes, the measurements showed that the best fidelity was achieved using aluminium disks. Other aim of changes in the setup was to reduce the number of layers between vibration source and the cells. Thus the influential response of the cells could be reflection of responses to these tiny vibrations. After removing unnecessary surfaces and use of the thinnest layers of glue that were possible between the layers, measurements showed large fluctuation of the dish base that this problem was solved by attachment of aluminium disk (Figure 3-19).

Attaching an aluminium disk resulted in the magnitude of the displacement being reduced by 25% on some points however the overall variation decreased significantly. Changes in frequencies did not have a significant effect on the displacement. However, with increased voltage displacement the standard deviation increased as well. These findings are consistent with the previous investigations by Curtis and Reid (Figure 3-1) (Curtis et al., 2013).

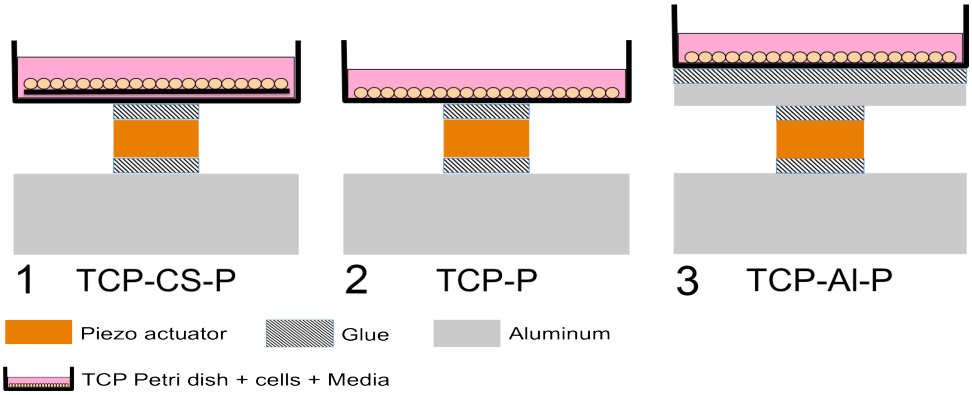

Figure 3-19- the stage changes in setup: 1) The cells lied on cover slip inside the Petri dish that connected to piezo actuator by glue. 2) The cells are resting on the Petri dish base and the dish is connected to the piezo actuator. 3) The same position of cells as in 2 but an aluminium disk is attached between piezo actuator and Petri dish by hard epoxy glue. TCP-CS-P: tissue culture plastic dish- coverslip- piezo actuator attached to each other, TCP-P: Petri dish connected directly to piezo actuator, TCP-Al-P: Aluminium disk connecting the Petri dish base on its top to piezo actuator below.

In comparison, using 3.4 mm aluminium disks between the piezo actuator and the Petri dish enabled the supplied displacements to be provided repeatedly across the entire surface of the Petri dish base. The 60 mm Petri dishes can culture more cells for analysis than the 35 mm dishes, thus representing an advantage for these studies. However the 100 mm Petri dishes were not suitable because of the large variation observed in the peripheral displacements (Figure 3-16, Table 3-3). The thickness of aluminium disk was important. By choosing an aluminium disk with 3.4 mm thickness and providing a firm attachment to the Petri dish base, the piezo actuator made nanoscale displacements faithfully across the entire surface of the dishes with 35 and 52 mm base diameter. Displacements on the large dish bases (86 mm base diameter) were not consistent. It could be the result of uncoordinated proportional diameters of the piezo actuator and the 10 mm dish (1/10) that made the vibration fluctuant when the distance between source of the motion and the point of measurement increased. On the dishes directly connected to the piezo actuators (without aluminium disk) the possibility of wave reflection when they reached to the dish borders and build-up higher waves with other wave is probable.

Between two smaller dishes, 60 mm Petri dish (52 mm base diameter) was used for the cell growth and stimulation due to higher capacity for cellular growth and feasible biological evaluation.

Chapter IV- Protocol optimization for mechanical stimulation and result analysis

4.1 Introduction

Imparting very small impulses to cells should stimulate mechanotransductory pathways (Tay et al., 2013, Brown et al., 2002). It has been shown that micro scale physical stimulation has some effects on cell morphology and behaviour (Kshitiz et al., 2012, McNamara et al., 2012). Recent evidence suggests nanoscale stimulation should also have effects on cells (Curtis et al., 2013). A stimulator with such precision as to impart nanoscale mechanical stimuli similarly to all the cells (in order to enable large experiments with multiple Petri dishes) must be tested and calibrated fully. In Chapter 3 the steps toward definition of this nanomechanical stimulator and its calibration were described. In order to evaluate cellular responses to the stimuli the phenotypical and genetic aspects should be assessed (Dalby et al., 2003, Tschumperlin et al., 2013, Tsimbouri et al., 2013). In this thesis, in order to assess changes in cell shape and cytoskeleton, various staining and microscopy techniques have been used. As well as protein level investigation, transcript level investigations were performed using PCR and DNA microarray methods.

This chapter will discuss the application of these methods to understanding MSC response to nanoscale mechanostimulation. Analysis of cell adhesion and cytoskeleton were performed in order to assess changes in contractility and intracellular tension, which are important in MSC fate (as discussed in Chapter 1). Testing on a range of phenotypes was also undertaken to link these two strands of information – cytoskeleton and differentiation.

4.2 Materials and methods

The definitive stimulation setup (Figure 4-1), as described in Chapter 2, has been used throughout this chapter. As discussed previously, addition of a hard plate (3.4 mm aluminium disk) under the Petri dish allows for uniform transfer of piezo actuator impulses across the dish base and finally to the cells (Figure 4-2). Aluminium disks prevent large changes in vertical displacement. The generation of these nanoscale vibrations was possible on 35 mm and 52 mm base diameter Petri dishes. Petri dishes with diameters of 86 mm, however, did not show coordinated motion, so were not used. Of the two smaller dish types, the 60 mm petri dish (52 mm base diameter) was chosen to allow greater numbers of cells to be grown for assessment.

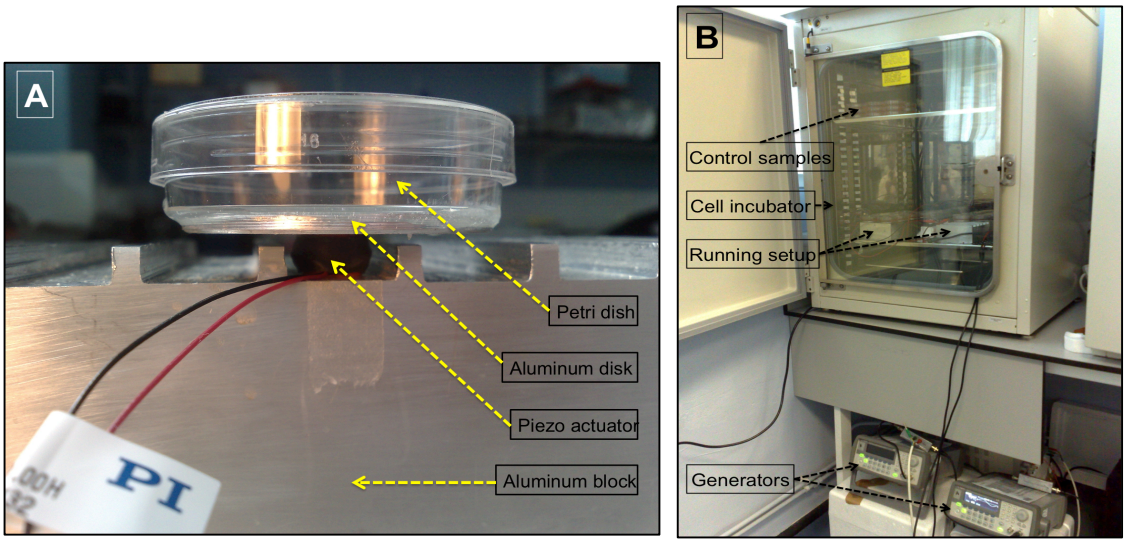

Figure 4-1- the optimal setup for nanoscale stimulation: A) A 60 mm Petri dish attached hardly to an aluminium disk and piezo actuator placed on top of an aluminium block. B) An experiment running inside the standard cell incubator where every aluminium block could carry 10 piezo attached dishes. Static controls are cultured in the same incubator.

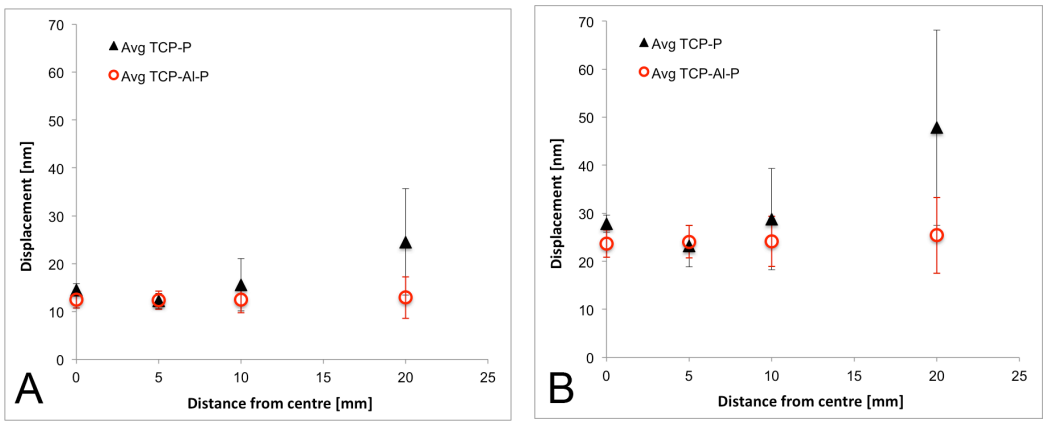

Figure 4-2- Vertical displacement differences as a result of application of nanoscale impulses across the base of 52 mm diameter Petri dishes with and without aluminium disks in place at two applied voltages and constant frequency. A) With 10 V × 1kHz induction, displacements are between 7- 25 nm and higher fluctuation when the dish is attached directly to the piezo actuator (TCP-P). B) With 19 V × 1kHz the displacements were in the range of 15- 70 nm with less fluctuation in the presence of aluminium disk attached to the piezoactuator and Petri dish (TCP-Al-P).

It is noted that changes in frequency had only very minor effects on displacements (Figure 4-3); a wide range of frequencies were used in the optimisation experiments to determine their effects on the cells as will be described shortly.

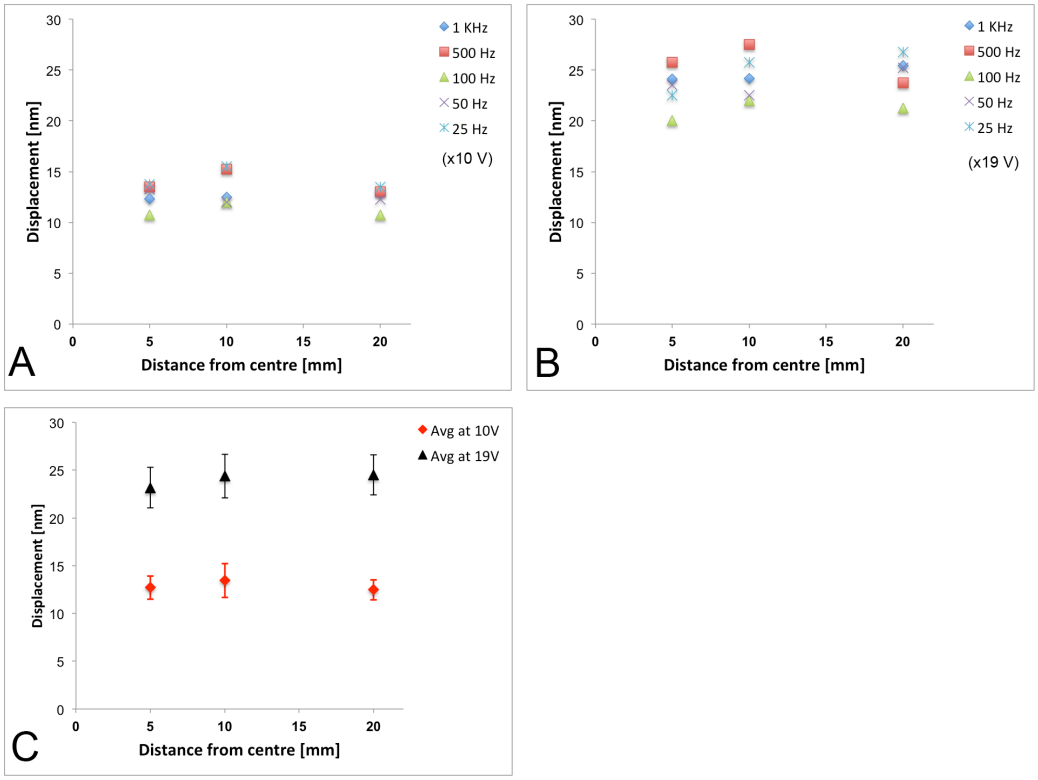

Figure 4-3- changes in amplitude of displacements following frequency changes at two different voltages: A) At 10 V induction the displacement differences were between 10- 15 nm for all frequencies tested. B) At 19 V the differences in displacement were from less than 20 nm to about 27 nm. C) Average displacement changes (Avg) showed minor fluctuations for both voltages; the fluctuation was higher in 19 V induction potential.

As a result of these measurements, the 60 mm Petri dishes (52 mm base diameter) were chosen to build the setup and to make reliably uniform nanoscale impulses. Calibration of this type of Petri dish did not show any interfering variable such as heat or shear stress (Chapter 3). In order to prevent introduction of other variables with cell culture, 5 ml media was used for every dish and the constant number of 10,000 cells per dish was used for all experiments. At this density the cells were mainly individual, which helps with cell adhesion to the substrate and cytoskeletal analysis because cell-cell contact and influence is minimised but there are enough cells to allow cells to reach confluence over a few weeks of culture. The volume of media causes a vertical pressure on the cells, thus by using the same volume this pressure would be constant for all cells. Running the experiments in the standard cell incubator under constant environmental conditions made the effects of temperature, evaporation and other physical forces the same and could be disregarded (Figure 4-1-B).

Due to the novelty of the stimulation method, pilot studies using various types of cells such as fibroblasts (hTERT), osteosarcoma cells (MG-63), and mouse epithelial progenitors (Le2) were employed. Primary human MSCs from bone marrow were used to evaluate any changes in cell fate or differentiation. As discussed in Chapter 2, for all kind of cells 10,000 cells per dish were used and after seeding they were left for four hours to settle and attach to the base. Then nanoscale stimulation was induced for the time intervals described.

4.3 Results

4.3.1 Cell responses

4.3.1.1 Staining and Microscopy

Initial staining (as described in part 2.3.1) of epithelial progenitors (Le2) showed morphological responses in spreading and actin cytoskeleton (Figure 4-4). Generally the stimulated cells showed thicker, dense actin stress fibres compared to control samples. These changes increased when stimulation time and amplitude was increased.

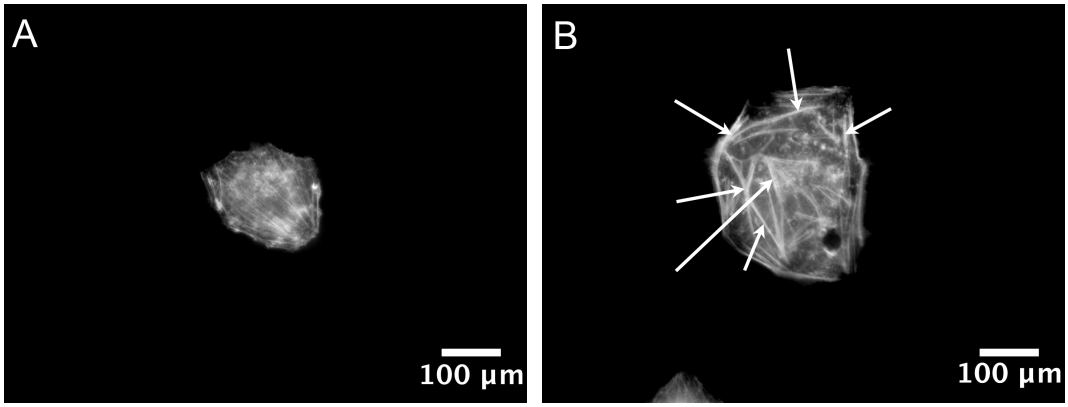

Figure 4-4- Mouse epithelial stem cells (Le2) stained for actin cytoskeleton: A) Typical control cell after 16 hours, B) Stimulated cell after 16 hours with 6 V × 1Hz (~ 7- 9 nm displacement). The prominent observation after nanoscale stimulation was increased organisation of the actin cytoskeletal stress fibres (arrows).

These responses indicated perception of nanoscale vibration by the cells and it was sufficient for us to progress in search of effects on stem cell fate and differentiation. Initial attempts during 24 hour stimulation with 10 V × 1Hz (~12-14 nm displacement) to find stem cell differentiation with STRO1^{+} MSCs (provided by Professor Richard Oreffo, Southampton, UK) showed minor changes in Runx2 (osteogenic transcription factor) expression. MyoD (the major regulatory transcription factor for myogenesis) and PPARγ

(Peroxisome proliferator-activated receptor gamma, a regulatory transcription factor for lipogenesis) were also checked but with little effect noted (Figure 4-5). Staining protocol is described in part 2.3.1.

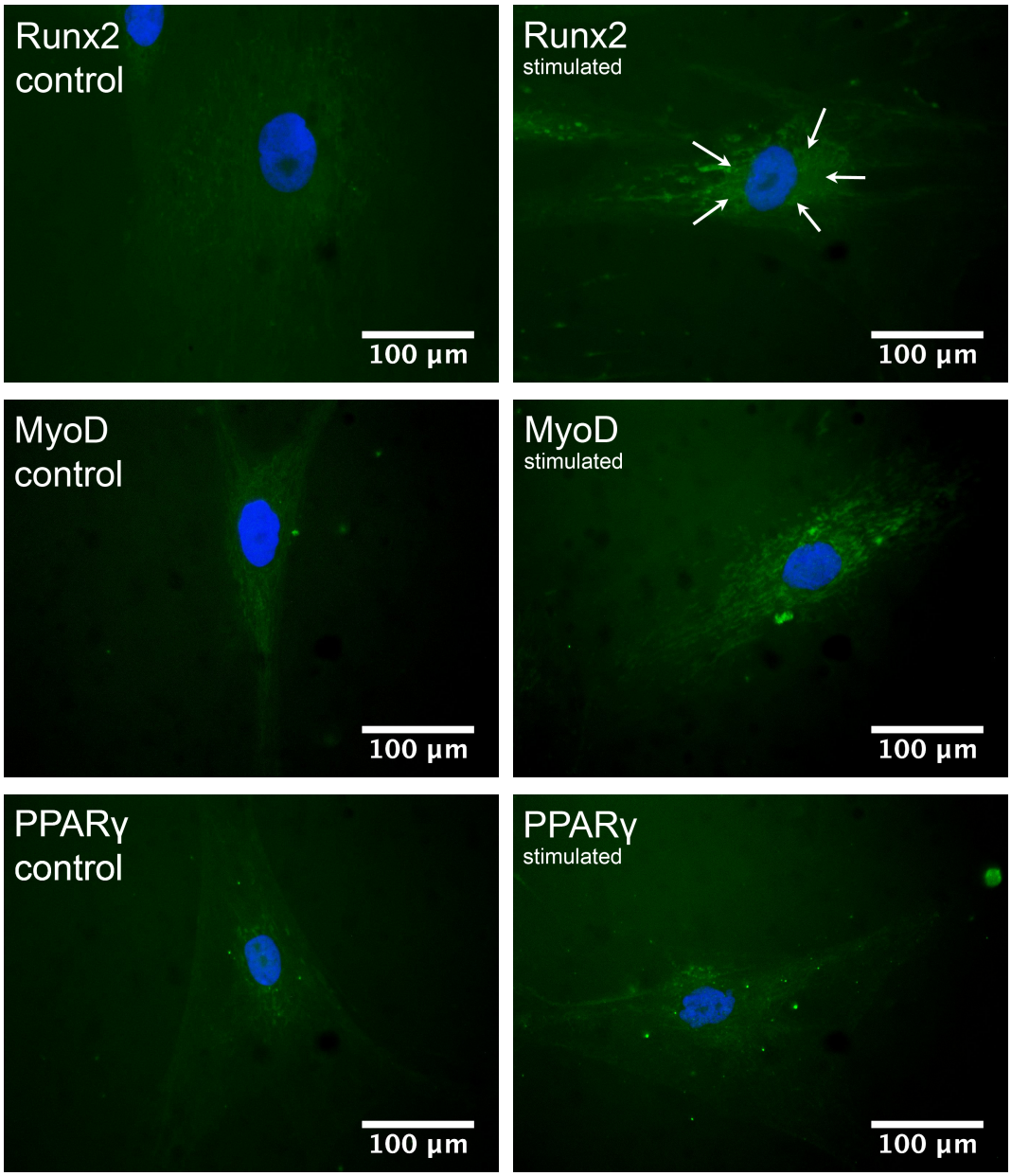

Figure 4-5- MSCs ($STRO1^{+}$) stained for Runx2, MyoD, and PPARγ after 24-hour stimulation at 10 V × 1Hz (~ 12-13 nm displacement). There was an evident increase in Runx2 presentation in most of the cells (arrows) compared to the control cells. Differences in muscle and fat indicators were not obvious, ×40 magnification.

This result indicates that MSCs are potentially nanomechano-responsive after 24 hours in culture. Now that this clue was in place, a series of rapid optimisation experiments were

required to pinpoint the voltage and frequency that would be applied to the piezo actuators to maximise effects on MSCs.

4.3.1.2 gel Polymerase Chain Reaction (gel PCR)

To achieve this, MSCs were cultured for one-week in triplicate samples with multiple choices in frequency and voltage (eight groups, table 4-1).

	Voltages	
Frequencies	10 volts	19 volts
1 Hz		
50 Hz		
500 Hz		
1000 Hz		

Table 4-1- Selection of frequencies spanning the range 1- 1000 Hz with two voltages used made a blank table with eight groups. Note that while our aim was 20V, the signal generator only produces up to 19V.

RNA was extracted and used for cDNA synthesis and gene exploration as explained in Chapter 2. Then gel PCR for Runx2, MyoD, PPARγ, nestin (an intermediate filament protein indicator of early neural differentiation), osteonectin (an osteoblast extracellular matrix component), Sox-9 (a transcription factor indicator of chondrogenesis) and GAPDH (as a housekeeping gene) was performed. The results were analysed using densitometry by ImageJ and Excel software for the eight groups (Table 4-2). In each group triplicates of unstimulated control were compared with triplicates of stimulated cells for expression of various genes.

Frequency (Hz) × Voltage (V)		**1 × 10**	**1 × 19**	**50 × 10**	**50 × 19**	**500 × 10**	**500 × 19**	**1000 × 10**	**1000 × 19**
Runx2 (Bone)	C	1.84	3.60	5.36	2.52	1.92	1.67	1.18	1.09
	S	2.24	3.85	5.64	2.59	2.01	2.05	**1.67 ↑****	1.20
Osteonectin (Bone)	C	8.47	6.97	7.43	2.99	8.16	8.17	7.05	3.97
	S	8.54	7.03	7.54	3.03	**8.44 ↑***	8.40	**7.44 ↑****	4.08
Sox9 (Cartilage)	C	3.03	4.62	6.30	3.12	4.01	5.57	2.63	2.12
	S	2.60	**3.68 ↓***	**5.27 ↓***	**2.79 ↓***	**3.41 ↓***	5.15	2.85	1.77
MyoD (Muscle)	C	1.04	0.98	0.94	1.29	1.03	1.15	1.07	1.13
	S	1.05	**1.14 ↑***	**1.02 ↑***	1.33	**1.17 ↑***	**1.30 ↑***	1.16	1.36
Nestin (Nerve)	C	1.55	3.00	1.39	3.59	1.24	1.81	1.74	1.49
	S	1.64	2.97	1.41	3.75	1.24	1.72	**2.13 ↑***	1.73
PPARγ (Fat)	C	1.00	3.62	1.44	4.61	1.35	1.47	3.23	1.73
	S	1.07	3.34	1.26	4.90	1.20	**1.23 ↓***	**2.40 ↓****	1.32

Table 4-2- gel PCR result analysis by densitometry: Evaluation of control (C) and stimulated (S) samples after introduction of four various frequencies and two voltages were showed. Samples were tested for six transcription factors representing bone, cartilage, muscle, nerve, and fat transformation of MSCs. GAPDH was used as a housekeeping gene. Small arrows (↓↑) show decreased or increased presentation that was statistically significant (*= p value≤ 0.05, **=p value≤ 0.001, two-tailed t-test for equal variance was used, n=3).

In general an increase in presentation of Runx2, osteonectin, nestin and MyoD was observed and a decrease for Sox-9 and PPARγ. Most of the changes, however, were not significant. Nestin and PPARγ showed the same trend for all experiments except for 1kHz frequency whereby nestin expression increased in stimulated groups while PPARγ expression decreased. MyoD expression was always higher than control samples after stimulation and its increase was significant in some groups. Sox-9 presented lower

transcription in stimulated groups until higher frequencies where it showed no significant changes. A significant increase in Runx2, osteonectin, and nestin expression was observed with induction using 10 volts peak-to-peak variation in amplitude and 1 kHz in frequency. In this group it is notable that a reduction in PPARγ was also statistically significant. In hard tissue formation, an increase in bone markers production (Runx2 and osteonectin) accompanied by a decrease in the fat marker presentation (PPARγ) would be expected (Sadie-Van Gijsen et al., 2013) as shown in these results and Figure 4-6.

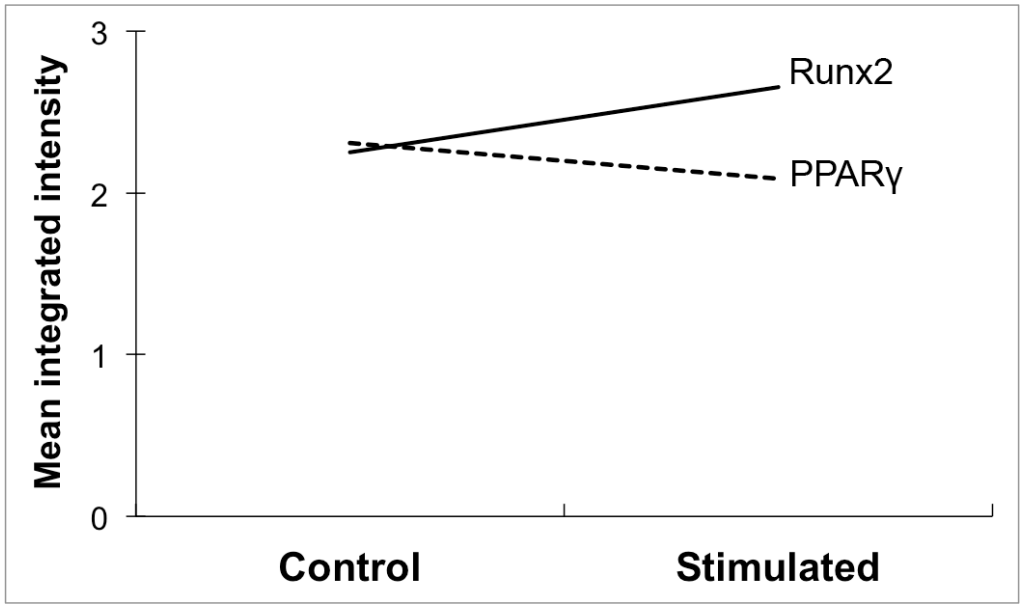

Figure 4-6- General trends for Runx2 and PPARγ expression after stimulations: Densitometry results of gel PCR showed an average increase in Runx2 (continuous line) compared to control and a decrease in PPARγ (dashed line).

This hypothesis free approach led to the use of 1000 Hz at 10 V as the optimum nanoscale mechanotransductive cue. In the rest of the thesis, 500 Hz at 10 V was also studied to allow for the dissection of close stimuli that were either successful or unsuccessful at gaining a strong MSC response. In both groups the measured displacement was the same in the vertical axis.

4.3.2 MSCs

4.3.2.1 Cell morphology

With the optimum stimulation parameters attained, continuation of stimulation for two weeks showed morphological changes in MSC perimeter, surface area, cell count and cellular projections. These changes were statistically significant compared to static control

cells, especially after 1-week stimulation. Counting results showed that after induction of stimulation, a cell growth delay for more than a week was observed then cells showed a rapid increase in numbers in both groups; i.e. they appeared to have a lag phase as the stimulation was applied. This increase was more prominent in 500 Hz × 10 V group but the same trend was observed in the 1 kHz × 10 V group (Figure 4-7).

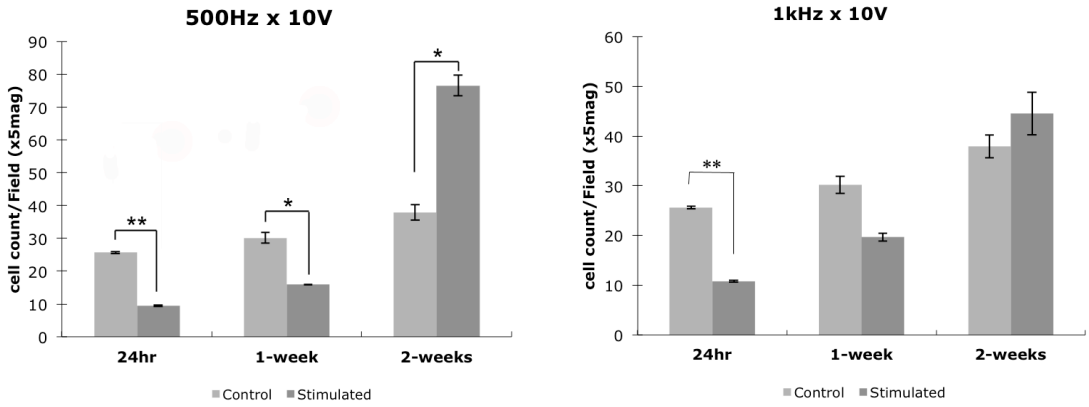

Figure 4-7- MSCs count after stimulation: these graphs show cell counts after application of the two selected frequencies for three time intervals. For every stimulated sample a static control group was counted. The total fields for cell count were more than 40 (*= p value≤ 0.05, **= p value≤ 0.001, two-tailed t-test for equal variance was used).

Calculation of other measured variables is shown in Figures 4-8. In order to work out the deviation of cellular outlines from usual round or oval cell shapes, an index of roundness, called arboration, was calculated. Because cell arboration shows the deviation in cell shape from elliptical it indirectly reflects the increase in the number of cell projections. Arboration was calculated from the ratio of measured perimeter divided by a theoretical perimeter. The theoretical perimeter is calculated according to the formula below:

Theoretical Perimeter = 2π [(A+B)/4]

A =major cell axis, B = minor cell axis, π =3.14

Arboration = Measured perimeter / Theoretical perimeter

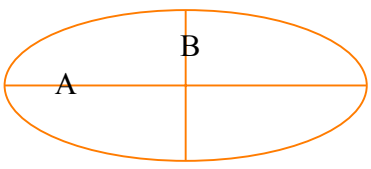

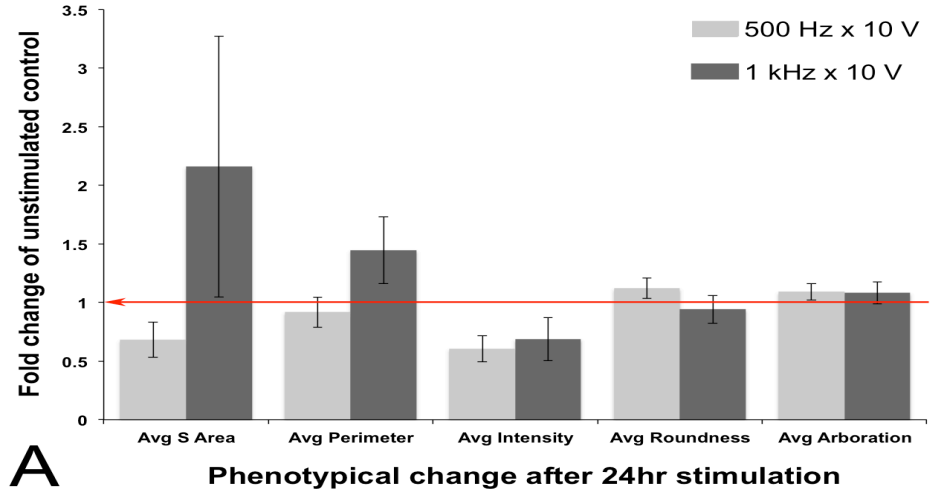

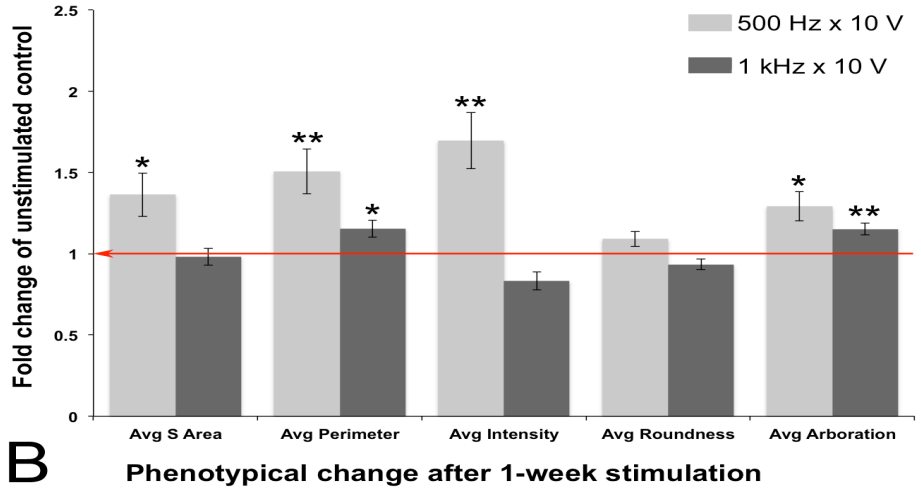

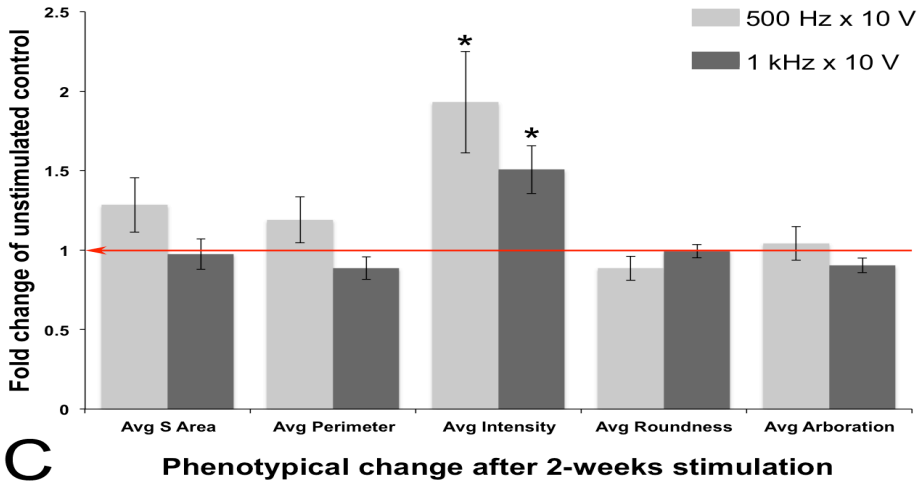

Figure 4-8- Comparisons of cell morphology at three stimulation time intervals (after 24 hours (A), 1-week (B), and 2-week (C)) showed that major differences in cellular dimensions were observed after 1-week stimulation. The variables were compared to the controls (red arrows). Avg= average, S Area= surface area (*= p value≤ 0.05, **= p value≤ 0.001, two-tailed t-test was used, N>40).

As the plots show, after 24 hours of continuous stimulation, cell shape and characteristics remain constant between stimulated and control groups. Integrated intensity in both stimulated groups decreased but that was not significant. Cellular surface area and perimeter were increased in 1 kHz × 10 V group and these two variables were decreased in 500 Hz × 10 V. Again, these changes were not statistically significant. After 1-week stimulation, morphological changes had become significant especially in the 500 Hz × 10 V group. In this group the cells showed themselves to be well spread with increased intensity and many projections. At this time interval, cells in the 1 kHz × 10 V group were larger than control with more cytoplasmic projections (higher difference in arboration) but their integrated intensity decreased. All the shape changes had returned to being relatively similar to the control group after 2-weeks stimulation except for significant increases in cellular intensity in both groups. The cell dimensions (perimeter and surface area) also showed non-significant increase in the 500 Hz × 10 V group at this time.

4.3.2.2 Electron microscopy:

To study the morphological changes in more detail, scanning electron microscopy (SEM) was used after one week of MSC stimulation. Comparison of cell shape showed that, after stimulation, MSCs were larger in size with many elongated projections. The cells in static control groups were more rounded with less projection, well attached to the surface. More ventral projections were also noted at the borders of cells that were stimulated (Figure 4-12).

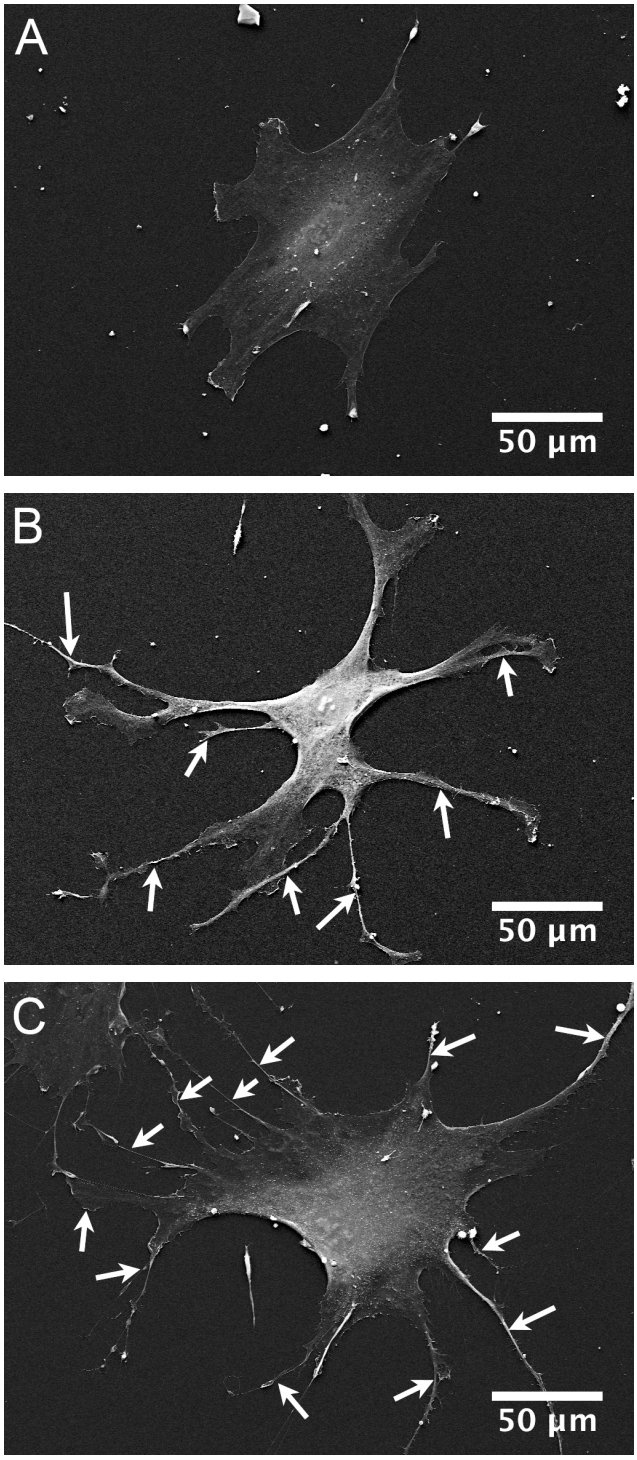

Figure 4-9- Electron microscopy changes after nanostimulation: SEM pictures showed differences in shape and projections between control cells (A), and two stimulated groups after 1-week continuous stimulation with 500 Hz × 10 V (B) and 1kHz × 10 V (C). Stimulated cells tended to be larger with many more projections (arrows) and filopodia (×1000 magnification).

4.3.2.3 Fluorescent microscopy:

After selection of frequencies and voltage, fluorescent microscopy was done and compared with control, static, samples at the same time periods (24hr, 1-week, and 2-week).

In order to assess various possible differentiation profiles of MSCs after stimulation, different immunostaining was performed (as shown in Table 4-3). Results are summarised in the table and select results are expanded upon in the following individual figures.

Marker	Primary antibody	Time period	Visible change
Cytoskeleton	Actin / Vinculin, Vinculin	24 hours	✔
		1-week	✔
		2-week	✔
	Vimentin	2-week	✔
Osteogenic indices	Osteocalcin	1-week	✔
		2-week	✖
	Osteopontin	1-week	✔
		2-week	✔
	Runx-2	1-week	✖
		2-week	✖
	MEPE-4	1-week	✔
Cartilage index	Sox-9	1-week	✖
		2-week	✖
Muscle index	MyoD	1-week	✖
Neurogenic indices	β3- Tubulin	2-week	✖
	S-100	2-week	✖

Table 4-3- various indicators of differentiation that were tested after nanostimulation: this table shows proteins chosen for phenotypical immunostaining at three time points. Cytoskeletal and osteogenic changes were most obvious. Visible findings indicated by check signs and cross means no finding.

Actin cytoskeletal changes showed many more, better organised stress fibres with stimulation especially after the 1-week period. Concomitantly, the size of the cells increased as expected with many projections visible (Figure 4-13).

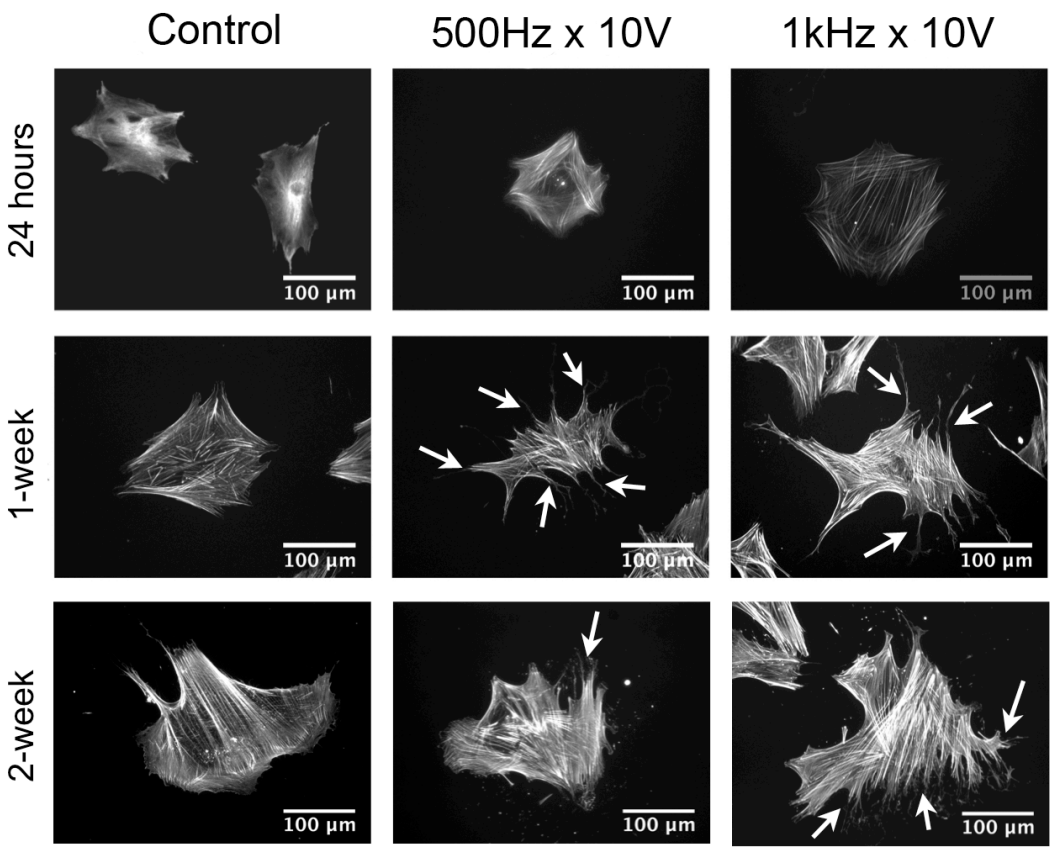

Figure 4-10- Actin cytoskeletal staining for MSCs showed significant increases in cell size (perimeter and surface area) and arboration (arrows) especially after 1-week stimulation.

Vinculin staining for focal adhesion sites showed mature FAs to be present in all control and test groups. It appeared that the spread of FAs in control groups was mostly at the cell periphery while in stimulated groups the adhesions were better distributed under the cells and along the projections, even at their ends (Figure 4-14). This finding is parallel with the electron microscopy observations that showed many projections over the entire surface of cells after stimulation.

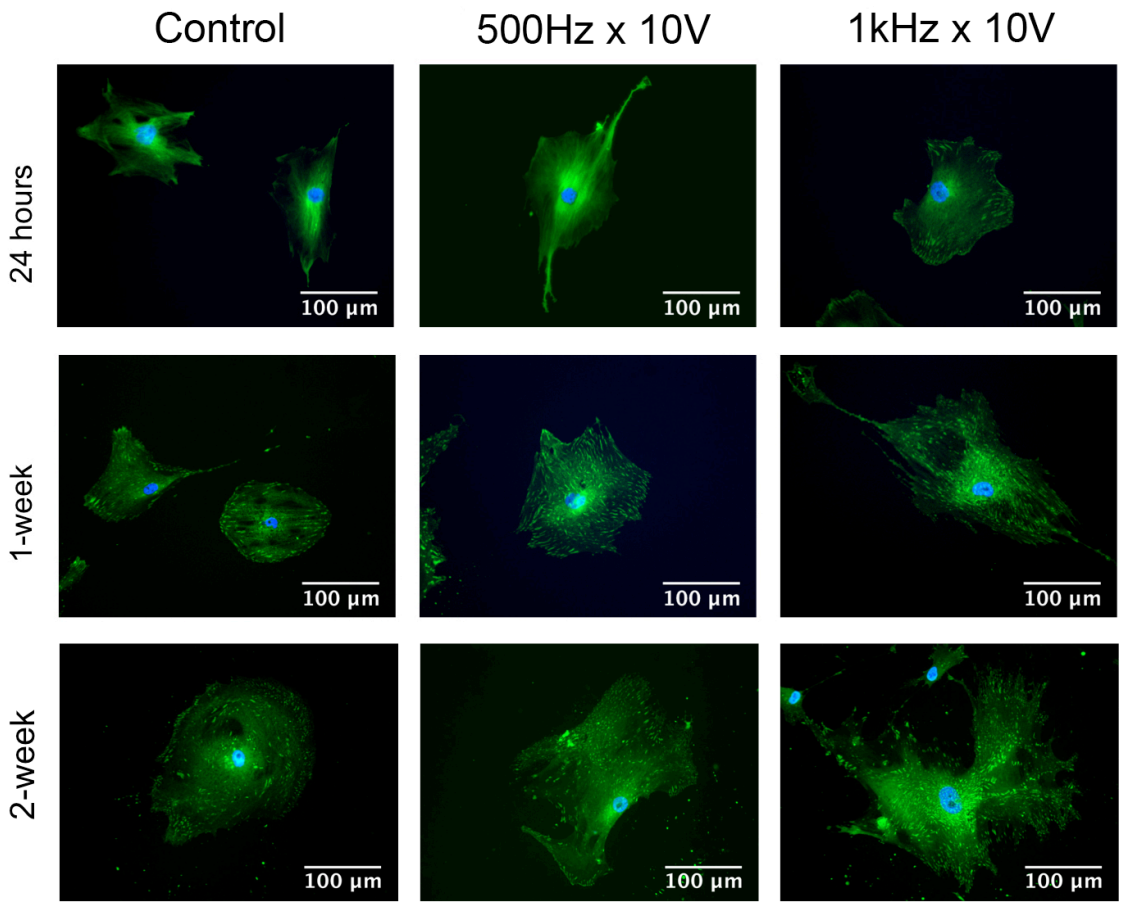

Figure 4-11- Vinculin staining for MSCs: the distribution of FAs after stimulation changed from peripheral to throughout the base of the cells. Vinculin=green, nucleus=blue.

Among the osteogenic markers, osteocalcin showed the largest increase after 1-week stimulation in the 1 kHz × 10 V group (Figure 4-15). The same was observed for osteopontin expression but to a lower degree (Figure 4-16). MEPE (matrix extracellular phosphoglycoprotein) staining after 1-week stimulation was strongly positive for both stimulated groups, especially 1kHz × 10V (Figure 4-17). MEPE is an extracellular matrix protein, regulator of bone metabolism (control of mineralization) and an indicator of osteoblastic activity.

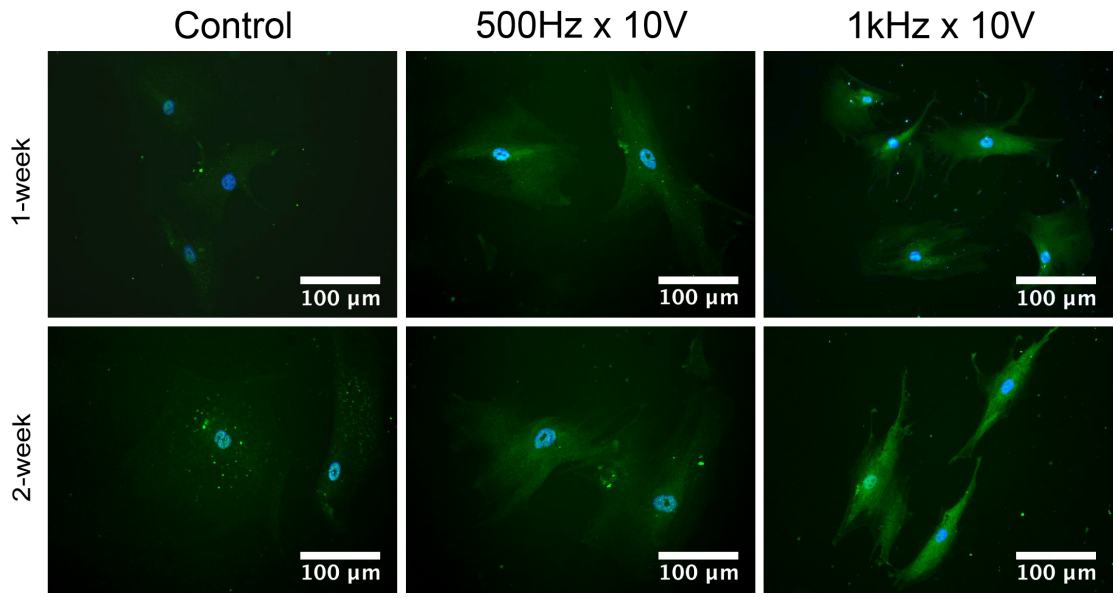

Figure 4-12- Osteocalcin staining for MSCs: Changes in osteocalcin expression was observed after stimulation. This was most obvious after one-week stimulation at 1 kHz. Osteocalcin=green, nucleus=blue, ×20 magnification.

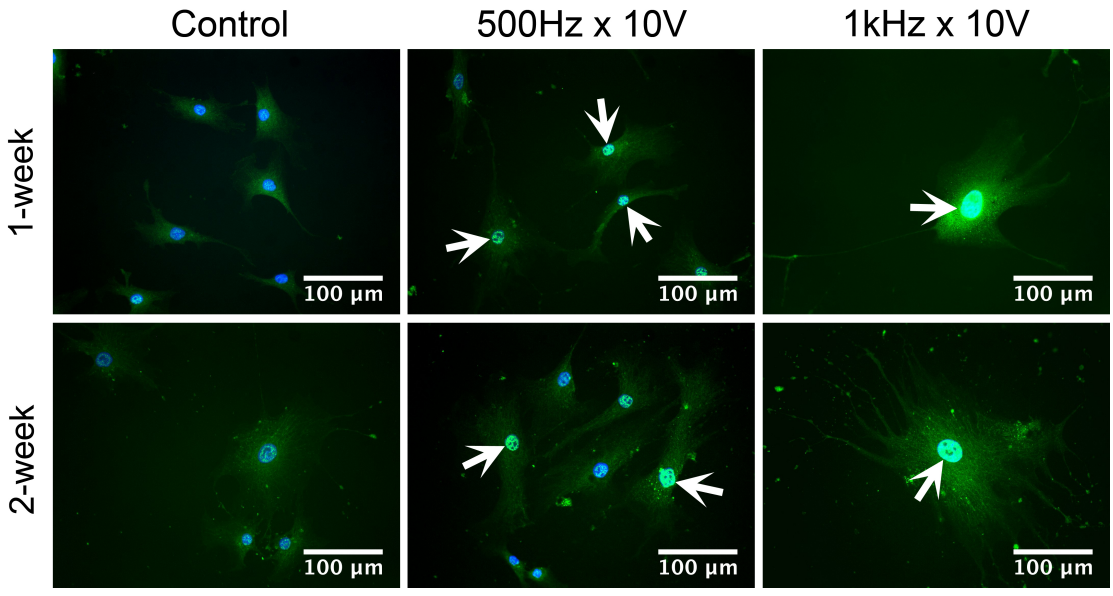

Figure 4-13- Osteopontin staining for MSCs: Changes in osteopontin expression were seen after stimulation at both 500Hz and 1 kHz (arrows). OPN= bright green, nucleus=blue.

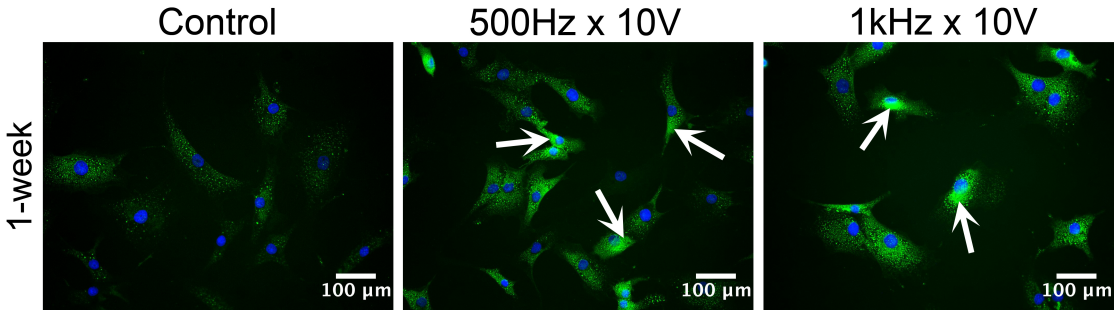

Figure 4-14- MEPE staining for MSCs: Changes in MEPE expression (arrows) was observed after stimulation at both 500Hz and 1 kHz for one week. MEPE=green, nucleus=blue, scale bar=100 µm, × 10 magnification.

4.3.2.4 Real Time quantitative PCR (RT- qPCR)

RT- qPCR was used to access BMP2 and Runx2 transcript expression from the MSCs after stimulation. Data agreed with immunofluorescence results of osteogenic markers that while expression was significantly increased at 1 kHz compared to control, there was only a trend of up-regulation at 500 Hz after 24hr stimulation (Figure 4-18-A&B).

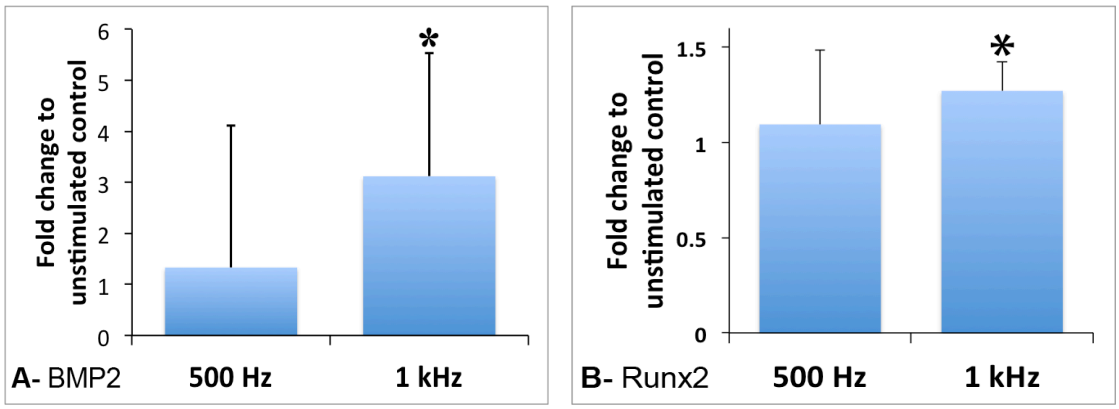

Figure 4-15- Osteogenic markers expression after MSCs stimulation: A) BMP2 transcript expression for stimulation at 500 and 1 kHz (×10 V) after 24hr stimulation showed significant up-regulation with 1kHz stimulation compared to control. B) Runx2 expression after 1-week stimulation showed significant increase with 1 kHz stimulation (Results = mean±SD, n=3, *=$p<0.05$ by ANOVA).

4.3.2.5 DNA microarray – pathway analysis

Analysis of microarray data after 1-week nanostimulation of MSCs (10^4 cells per dish) and in two test groups, 500Hz × 10 V and 1kHz × 10V (3 material replicas) was performed. Both canonical and functional analyses showed alteration in signalling for stimulated

groups compared to the static control group (3 material replicas). Figure 4-19 shows the functional changes for both stimulated groups. Cellular growth and proliferation showed the highest alterations after stimulation compared to controls and this tallies with the observation of changed cell growth profiles as observed by cell counting. Alteration in skeletal and muscular system development and cell signalling were similarly highlighted and appear logical in the context of enhanced osteogenesis after stimulation. Also highlighted are various metabolic signalling pathways – small molecule biochemistry, amino acid, lipid and carbohydrate metabolism. These are sensible in the light of enhanced differentiation as energy demand (lipid, carbohydrate) will change as will protein formation (amino acid) (Figure 4-19). It is notable that the 500 and 1000 Hz groups appear very similar in terms of global functional signalling. It is further noteworthy that these results do not show up or down regulation – just significant changes in that pathway. A complete list of functional changes is shown in Figure 4-20.

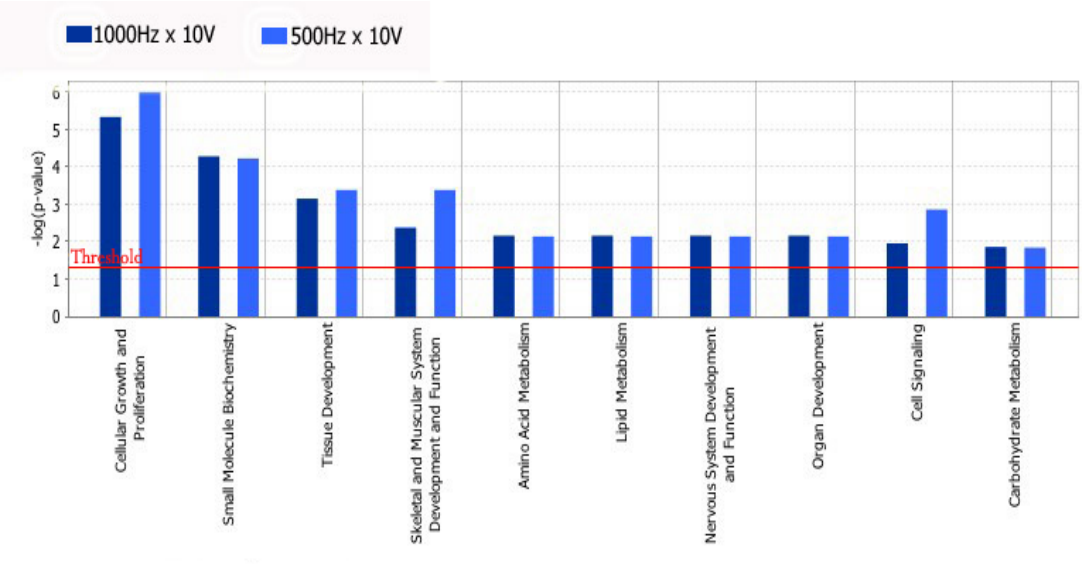

Figure 4-16- Functional pathway analysis of microarray shows changes in a number of cellular and tissue pathways. The threshold is significant at $p < 0.05$ by Fischer's exact test. The graph shows significance as –log (p value) to show the significance as positive values over a functional scale. n=3.

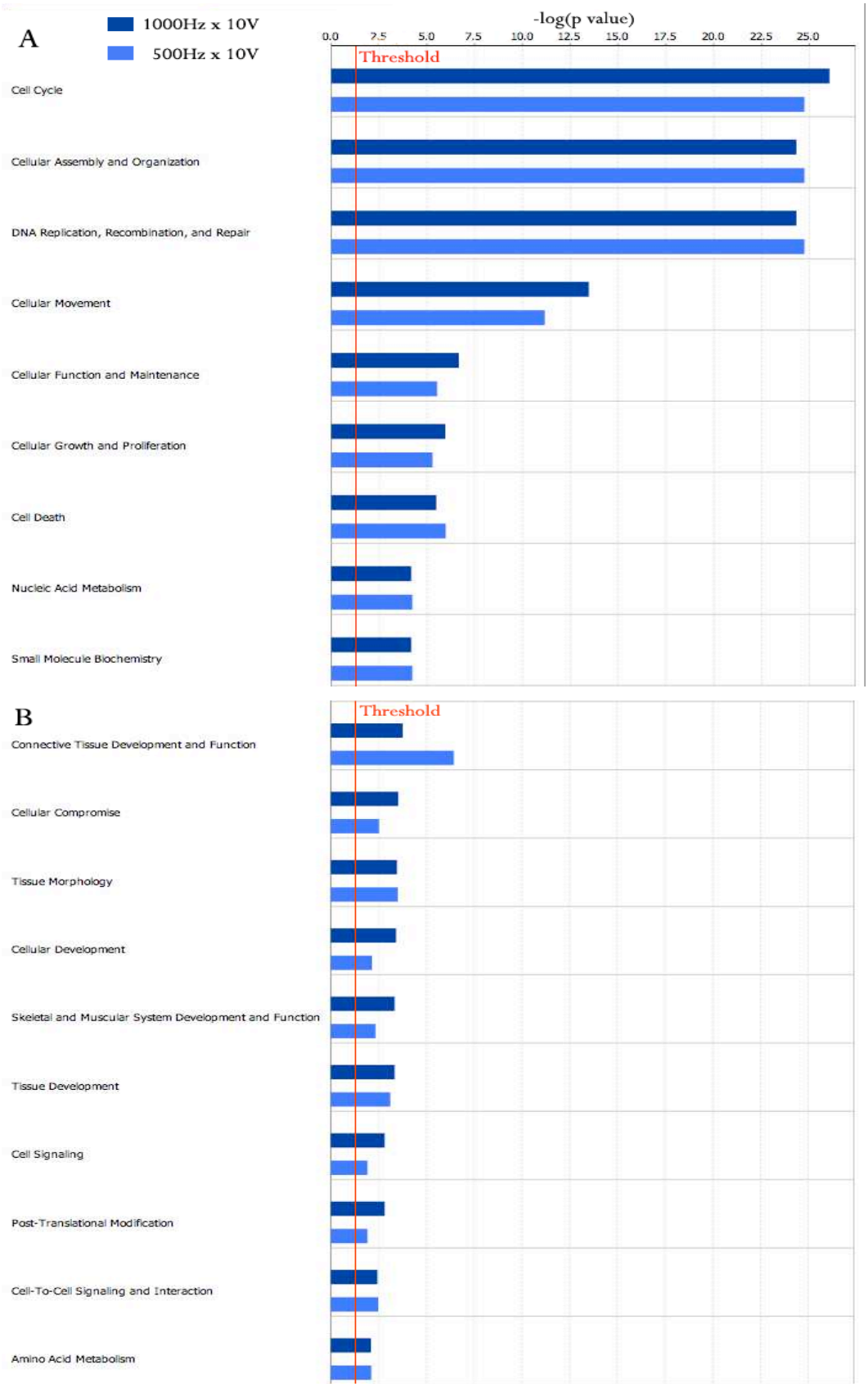
A
1000Hz x 10V
500Hz x 10V
-log(p value)
0.0
2.5
5.0
7.5
10.0
12.5
15.0
17.5
20.0
22.5
25.0
Threshold
Cell Cycle
Cellular Assembly and Organization
DNA Replication, Recombination, and Repair
Cellular Movement
Cellular Function and Maintenance
Cellular Growth and Proliferation
Cell Death
Nucleic Acid Metabolism
Small Molecule Biochemistry
B
Threshold
Connective Tissue Development and Function
Cellular Compromise
Tissue Morphology
Cellular Development
Skeletal and Muscular System Development and Function
Tissue Development
Cell Signaling
Post-Translational Modification
Cell-To-Cell Signaling and Interaction
Amino Acid Metabolism

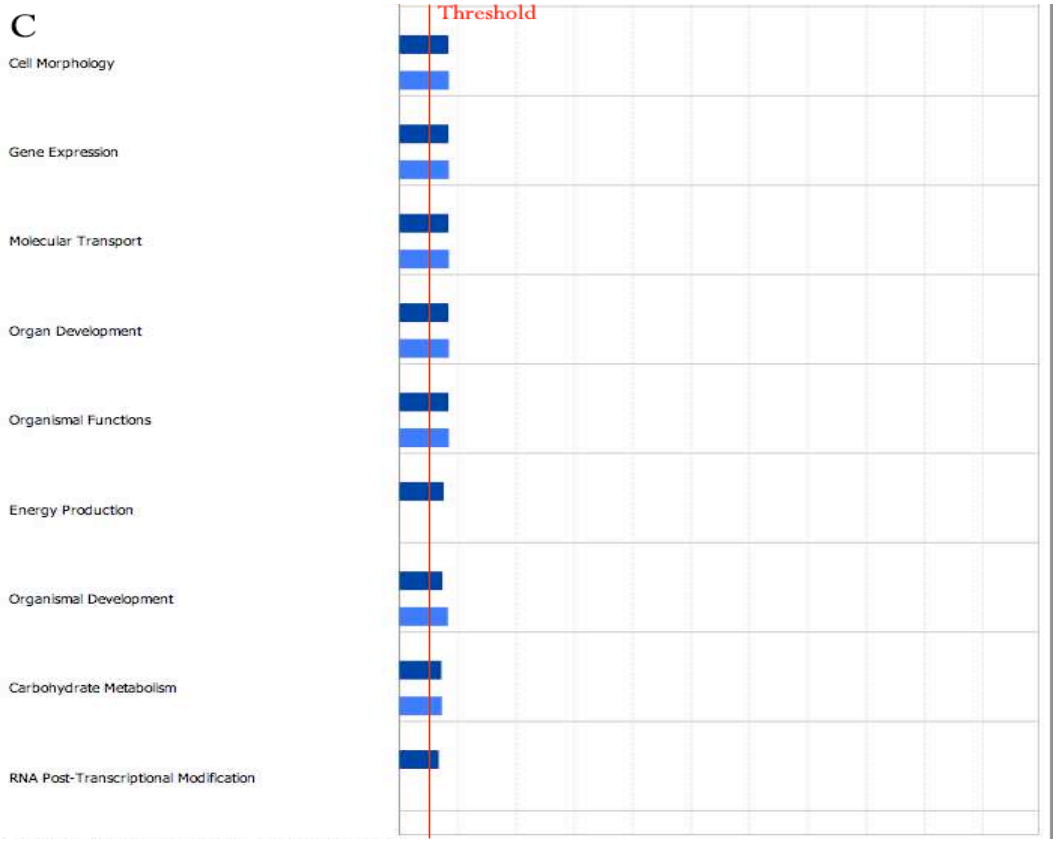

Figure 4-17- Further exploration of functional pathway analysis in three segments (A-C). For most pathways, similar responses were seen at 500 and 1000 Hz. The threshold is significant at $p < 0.05$ by Fischer's exact test. The graph shows significance as –log (p value) to show the significance as positive values over a functional scale. n=3.

By using separate analysis, it was demonstrable that the amplitude order of functional change for the two stimulations was different with cellular growth and proliferation being the highest change at 500Hz × 10 V and connective tissue development and function being the most differentially regulated at 1kHz × 10V (Figure 4-21).

Comparison of canonical signalling in both groups showed relatively similar up (mainly) and down-regulations in similar pathways (Figure 4-22). Significantly altered pathways included RhoA and FAK that have been implicated in osteogenesis (Etienne-Manneville and Hall, 2002, McBeath et al., 2004) and a wide range of cell cycle control pathways.

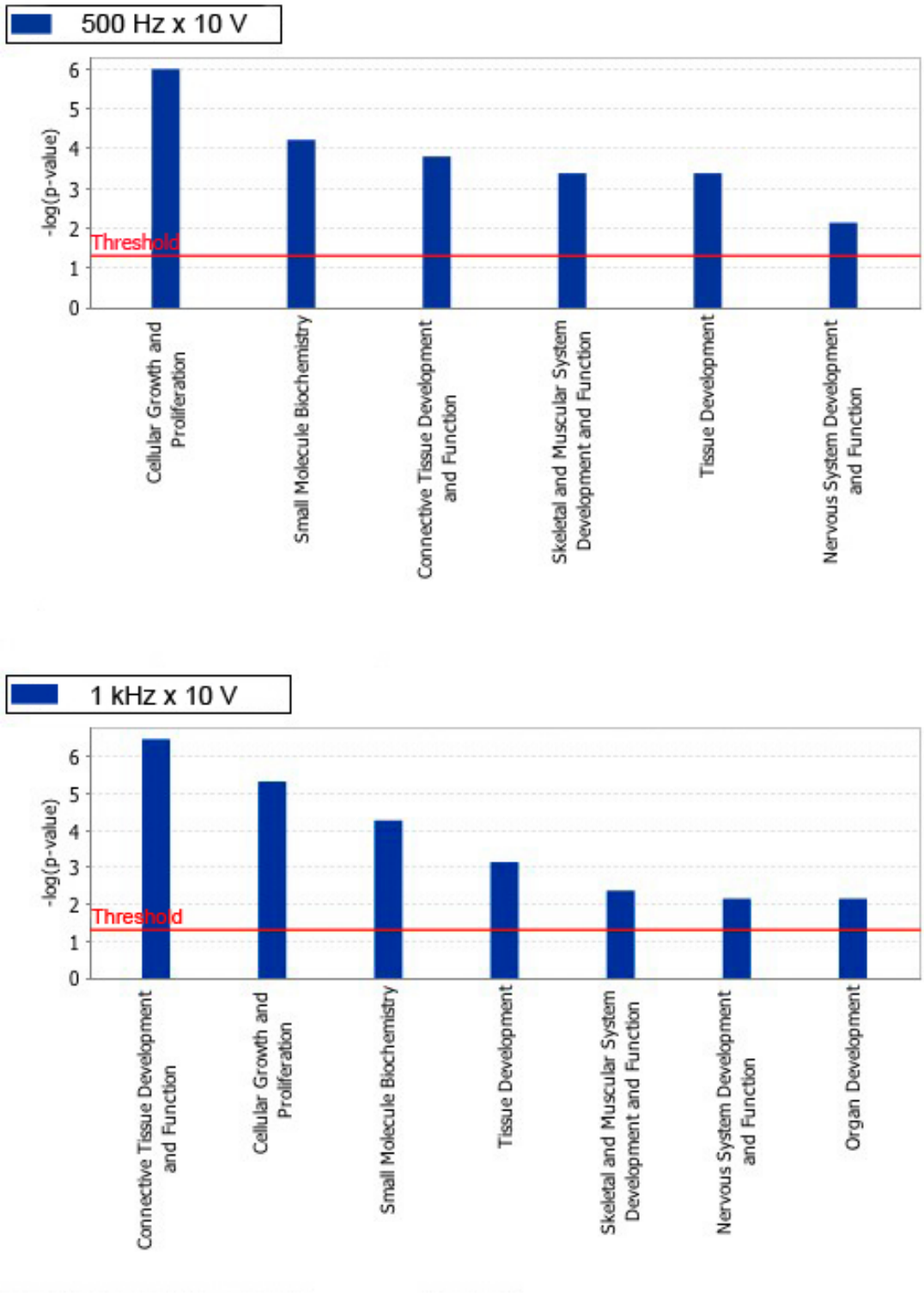

Figure 4-18- Functional pathway analysis for comparison of two stimulated groups unconnected, showed connective tissue development and function is affected earlier than other changes in the 1 kHz × 10 V group. The threshold is significant at $p < 0.05$ by Fischer's exact test. The graph shows significance as –log (p value) to show the significance as positive values over a functional scale. n=3.

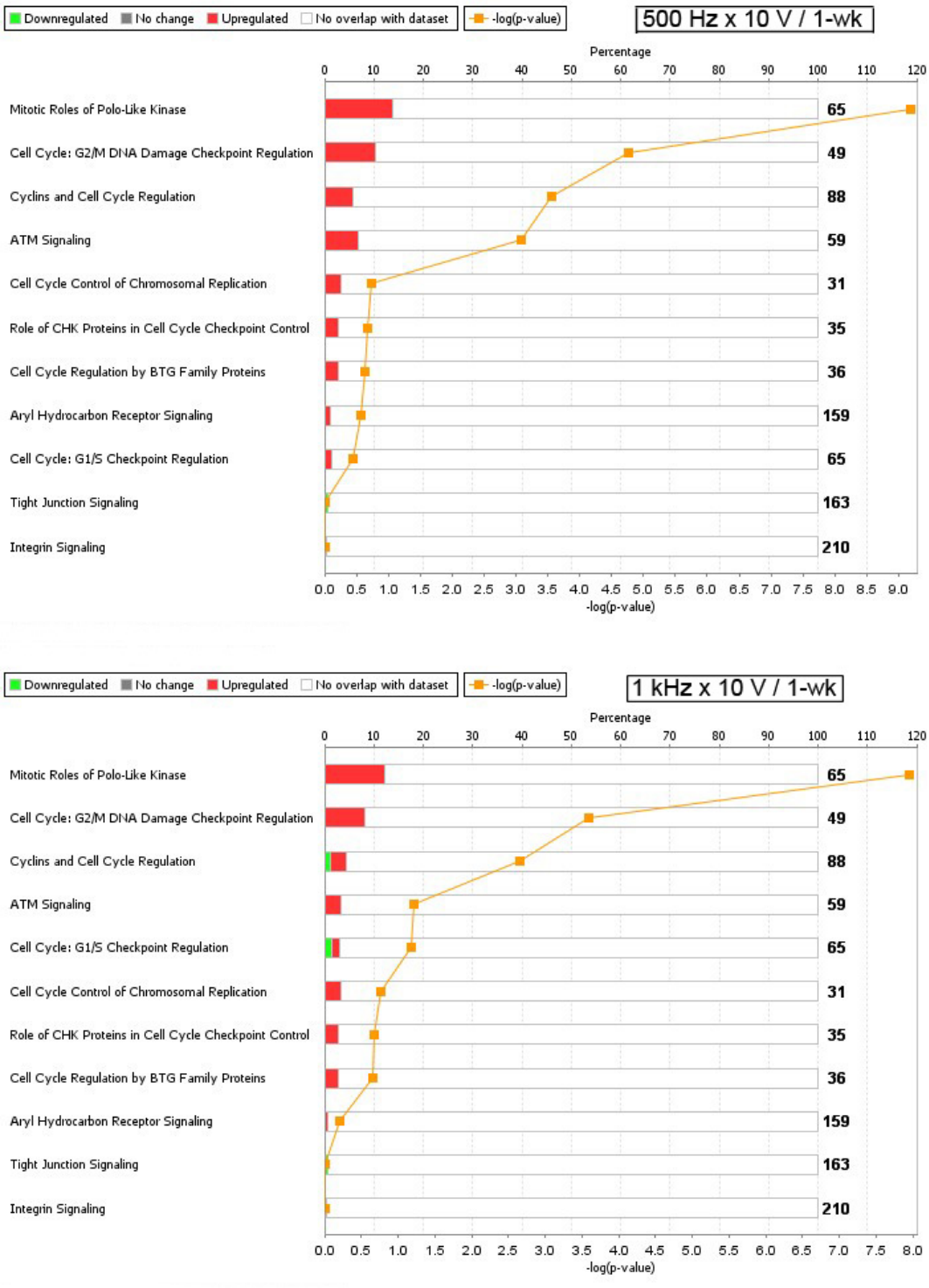

Figure 4-19- Canonical signalling pathways in stimulated MSCs compared to the planar control. Similar changes in RhoA, FAK and a wide number of cell cycle related pathways were observed. The graph shows significance as –log (p value) to show the significance as positive values over a functional scale by Fischer's exact test. n=3.

As RhoA had been highlighted as important, a specific ROCK inhibitor (Y-27632) was applied to cultures with the hypothesis it would block osteogenesis by nanomechanotransduction. This was shown to be correct as when Runx2 (1 week of culture) and osteocalcin (2 weeks of culture) staining was compared in stimulated groups (1 kHz) with Y-27632, little difference was observed (Figure 4-23).

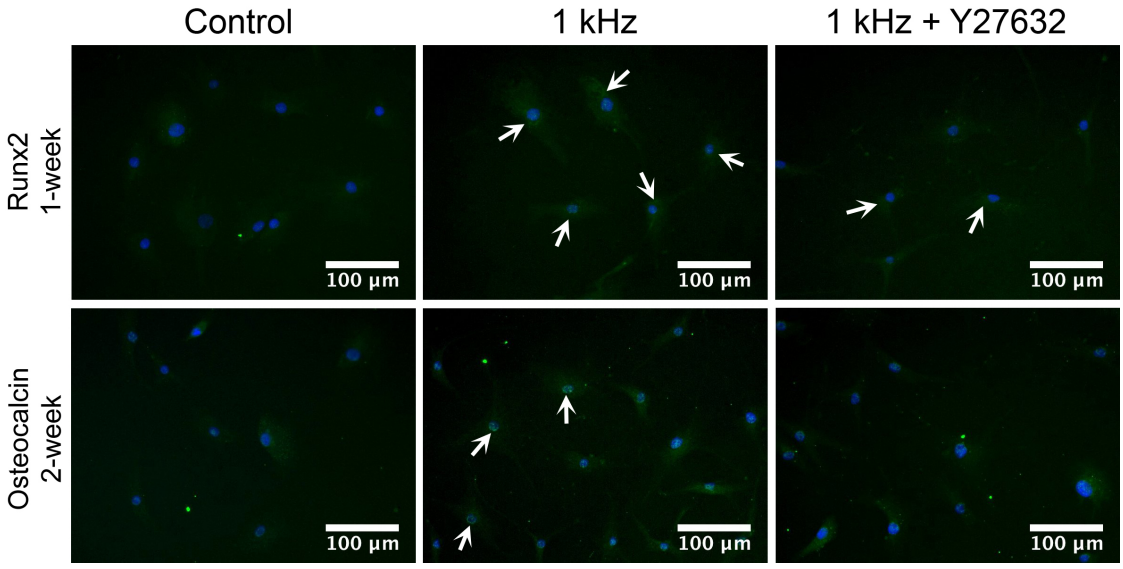

Figure 4-20- Runx2 and osteocalcin staining after using ROCK inhibition at 1 kHz × 10 V stimulation showed that the cells had similar levels of osteogenesis to the control substrates. However, if the cells were stimulated without the inhibitor, increased osteogenesis was noted. Runx2/ Osteocalcin = green, Nucleus=blue. Arrows show Runx2 and osteocalcin positive nuclei.

Microarray principle component analysis (PCA) mapping provided some clues for the apparent variation between control and stimulated groups in gene regulation (Figure 4-24). PCA mapping is one of the mathematical methods that make a visual 2D or 3D inspection of interrelationship between multidimensional variables such as genetic expression after a type of stimulation. So, by reduction of dimensionality of large groups of data, PCA could make the main groups of the data visible in two or three main dimensions or principal components (PC). Here the experiments contained three samples in three conditions (three controls, three replicates stimulated for every two defined stimulation variables) for a 1-week period. Analysis of gene expression after this period was multidimensional and PCA made it visible as three PCs (Figure 4-24). Three similar dishes were showed as spheres bounded by an ovoid network with the same colour that shows the dimension of variables

on a common surface. Gene networks showed that the genomic profiles of the MSCs after 1-week stimulation were discrete but similar. However, both varied greatly from control, unstimulated, cells. There was close proximity between the stimulated groups and some overlapping results were noted.

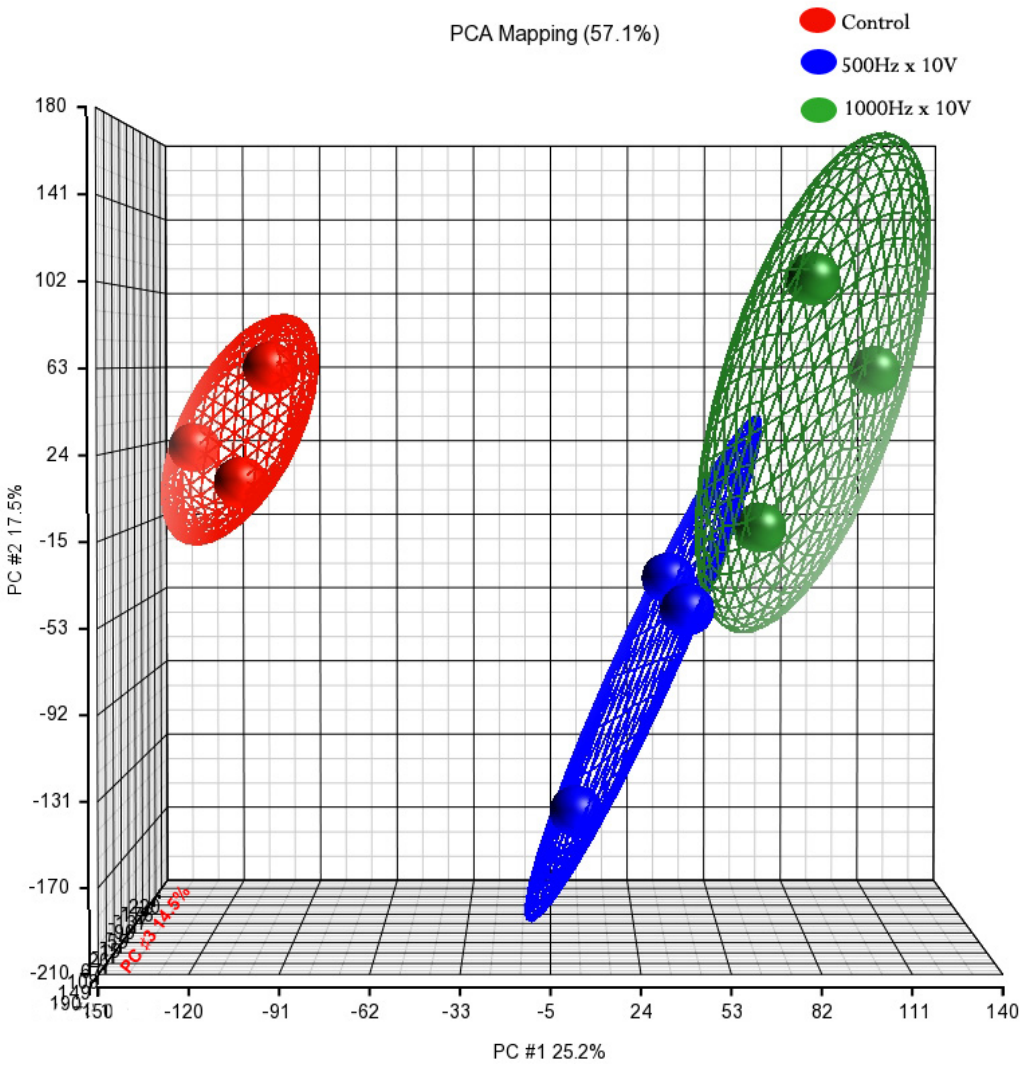

Figure 4-21- PCA mapping of genetic changes in 3D projection shows complete separation of control (red spheres) and stimulated groups (blue and green spheres). The graph shows that the main component (PC1) accounts for 25.7% of differences, the secondary component (PC2) accounts for 17.5%, and the tertiary component (PC3) accounts for 14.5% of differences (cumulative percent= 57.1%). There is some overlapping between two stimulated groups. The smaller red network around the control samples could explain less variation in genetic expression of static unstimulated cells. The changes were greater for MSCs stimulated at 1 kHz (green) than 500 Hz (blue). n= 3.

PCA mapping summarizes that this type of stimulation could make significant gene regulations in MSCs. This effect would be discussed in details in Chapter V.

4.4 Discussion

MSCs are responsive to vertical nanoscale mechanical excursions. Furthermore, it was demonstrated that this osteoblastogenic response was ROCK-dependent, in agreement with previous materials-based strategies for osteoinduction (Engler et al., 2006, McBeath et al., 2004, Gao et al., 2010, Kilian et al., 2010). That ROCK inhibition blocked osteoblastogenesis demonstrates that the stimulation is a real effect. Furthermore, that BMP2 is activated after 24 hours and RUNX2 by 7 days is logical, as RUNX2 activity is mediated by BMP2 signaling (Jang et al., 2012), this would be followed by increased osteocalcin expression by day 14 according to the Stein and Lian osteoblastogenesis timelines (Stein and Lian, 1993). Ingenuity canonical analysis also highlighted purine and nicotinamide metabolism (involved in energy demand) and sonic hedgehog signalling (involved is stem cell differentiation) (Kim et al., 2010) as well as adhesion, FAK, ERK, and actin-mediated biochemical signalling (all known to be implicated in RUNX2 activation) (Biggs et al., 2009, Biggs et al., 2008, Ge et al., 2007, Xiao et al., 2002) being central to nanomechanotransduction (James et al., 2010, Day and Yang, 2008).

Use of an open hypothesis for input frequency led to use of 1 kHz. Although cell responses appeared to be starting to be initiated at 500 Hz (as phenotypical changes), significant gene and protein expression responses were seen only at 1 kHz. It seemed that 500 Hz did not supply sufficient stimulus for mechanotransduction driven osteoblastogenesis but was enough for architectural change as well as cell shape and some cell pathway alterations. With 1kHz frequency, however, the MSCs demonstrated strong osteoblastic differentiation. It is noted that this appears high for the time scale of many cell actions. Interestingly, however, erythrocyte membranes display high-frequency undulations - as high as 1 kHz - in the tens of nanometers range called flickering (Rappaz et al., 2009, Evans et al., 2008); this is a very similar scale to the stimulation we supply the cells with in this report. However, it is noted that such movements have been noted as being slower in nucleated cells such as lymphocytes and monocytes from blood displaying 20- 30 nm undulations at up to 30 Hz and fibroblasts (descendants of MSCs) displaying 1- 4 nm displacements at up to 0.5 Hz (Pelling et al., 2007a, Szabo et al., 2002).

In addition to describing the details of the applied motion in terms of frequency and amplitude, it may also be of interest to consider the forces being applied to each cell. During the MSC stimulation presented here, a periodic force is imposed on each cell through the Petri dish substrate. Since the cells are adherent to the substrate surface prior to stimulation, this force is transmitted through each cell as it supports the column of aqueous solution directly above (Figure 4-25). Taking approximations for the cell shape (adhered surface area typically a few tens of micrometer × a few tens of micrometers) and height of solution (3 to 5 mm), the accelerative force on each cell can be calculated to be in the range of 1 to 10 pN. This can be calculated from Newton's second law: $F_{acc} = ma$, where the accelerative force (F_{acc}), driving the motion of the column of water with acceleration (a) and with mass (m) must be transmitted through the cell to the oscillating substrate surface.

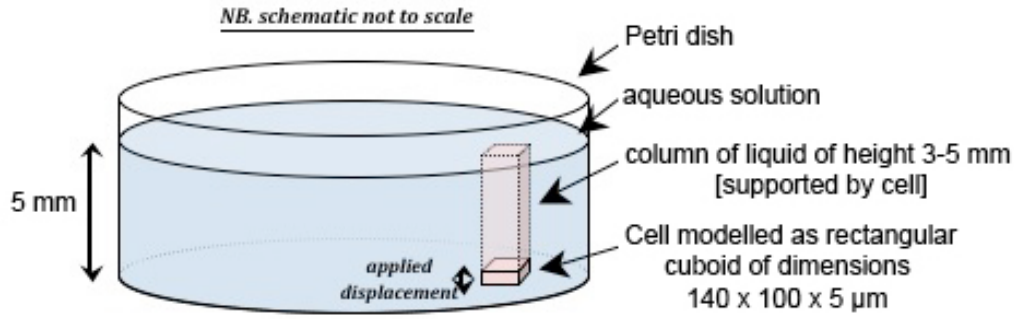

Figure 4-22- Schematic representations of applied forces on a single cell from the top by the weight of a media column.

Note that these forces are of a similar order of magnitude to the forces exerted by fibroblast undulations, observed in the range of 20 to 80 pN (Pelling et al., 2007b). Further investigations are required to evaluate the precise mechanisms responsible for how MSCs sense these applied mechanical forces.

Chapter V- Nuclear morphology following nanomechanotransduction of stem cells

5.1 Introduction

Nanoscale stimulation could influence MSC behaviour via direct or indirect mechanotransduction (Curtis et al., 2013). The evidence in favour of a direct effect (alterations in nuclear morphology following cytoskeletal rearrangement) can be observed in cytoskeletal changes such as alterations in microfilament architecture and FA rearrangement and also structural nuclear changes. Various mechanical forces could also influence the cell responses by the activation of intracellular pathways, especially MAP kinase and Rho GTPases (Boccafoschi et al., 2013, Martins et al., 2012). The complexity of indirect (biochemical) mechanotransduction is illustrated by a combination of cytoskeletal rearrangement and intracellular cascade activation effecting gene transcription.

The cell nucleus is a large organelle and has to respond to mechanical stimulation for mechanotransduction to occur. The nucleus has a continuous connection with the cytoplasm, with highly organised pores and links between the cytoskeleton and nucleoskeleton (LINC) (Crisp et al., 2006, Dahl et al., 2010). The nucleoskeleton provides a resistant and supportive layer around the nucleus that is important in maintaining nuclear shape and structure. Nuclear lamins are type V intermediate filaments and there are various lamin (A, C, and AΔ10, B1, B2) positioned between the internal nuclear membrane and the chromosomes. Lamins can act as shock absorbers and also transfer mechanical stimuli from the periphery of the cell into the nucleus (Dahl et al., 2004, Lammerding et al., 2005). Lamin A/C is only expressed around the lamina in differentiated cells (hence stem cells have more deformable nuclei than differentiated cells, a feature stem cells have in common with cancerous cells) but lamin B is found in all eukaryotic cell nuclei and lamina.

In eukaryotic cells the genetic material occupies the main component of the intranuclear volume. Deoxyribonucleic acid (DNA) and ribonucleic acid (RNA) are two well-known nucleic acids in eukaryotes. DNA, the major compartment of chromosomes, alongside carbohydrates and proteins is organised as a compact architecture, chromatin. A small circular DNA is present in human mitochondria that contains 37 genes, coding for some mitochondrial proteins (Chan, 2006). Inside the nucleus, active genes that are transcribed

frequently tend to be positioned more centrally in the nucleus and these can be seen as lighter area, euchromatin under the microscope. Other parts of each chromatin with lower activity tend to be arranged peripherally- adjacent to the nuclear membrane. They appear denser and darker by microscopy (heterochromatin). These two parts are in a dynamic situation and according to gene transcription needs can change their position. In the interphase nucleus, each chromosome occupies a relatively defined position called a chromosome territory. It has been shown that chromosome territories have constant localization in various species during interphase (Croft et al., 1999, Cremer and Cremer, 2001). It is considered that the position of the territories is important for gene activity; the lamina has more heterochromatic DNA and is predisposed to gene silencing while the central nucleus has more euchromatic, and more transcription factories (foci of transcriptional activity containing RNA polymerase) (Osborne et al., 2004).

Ribonucleic acid (RNA) is another essential macromolecule in the body made from nucleotides (Adenine, Guanine, Cytosine, and Uracil) and usually is found as a single strand. Most of the RNA is made by enzymatic activity (RNA polymerase) inside the nucleus (transcription) being template from DNA and there are many types of RNA named according to their actions. Their main activity is transferring coding gene messages outside the nucleus for protein synthesis (messenger, mRNA). Ribosomes contain ribosomal RNA (rRNA) and special proteins. They are the centres of cytoplasmic protein synthesis from mRNA (translation process). Transfer RNA (tRNA) is found mostly in cell cytoplasm and bonds to amino acids helping transfer them for protein synthesis on the ribosomes. A group of RNA shows enzyme activity (ribozymes or riboswitches) such as RNAse P, a ribonuclease that is involved in tRNA synthesis. MicroRNAs (miRNA) and small interfering RNAs (siRNA) are non-coding RNAs that have an inhibitory effect on translation of some genes by making complementary strands to specific mRNAs and hence preventing translation (Higgs, 2000).

Repositioning of chromosomes through mechanotransduction could thus directly affect gene expression. The nucleoli are the non-membrane bound centres of ribosomal RNA production inside the nucleus and appear rounded and phase-dense. In the response to some kinds of stimuli directing to the cellular hyperactivity the number and size of nucleoli could be changed (Neuburger et al., 1998). In addition, shifts in nucleolar positioning could give an indirect measure of changes in chromosomal positioning. In this chapter we

examine gene-level responses using microarray results. Then, two main nuclear structures were analysed after stimulation.

5.2 Materials and methods

Please refer to Chapter 2 for the materials and methods.

5.3 Results

5.3.1 DNA microarray

After treating MSCs at 500 and 1000 Hz (×10 V) for a week, RNA was extracted as described before in part 2.5.1. Nanodrop® (Agilent Technologies), was used to quantify the RNA concentration, the cDNA was reverse transcribed and microarray performed. The results showed significant changes (p value≤ 0.001) in transcript abundance levels in more than 900 known genes in each stimulated group compared to the static control group. The number of regulations were slightly higher in the 1000 Hz × 10 V group (994 vs. 933 as the total regulations) (Table 5-1, Figure 5-1).

	500 Hz x 10 V		**1 kHz x 10 V**	
Chromosome number	**No of up regulated genes**	**No of down regulated genes**	**No of up regulated genes**	**No of down regulated genes**
1	69	44	73	35
2	35	25	38	22
3	33	11	34	9
4	27	18	29	16
5	34	14	32	13
6	52	22	57	19
7	30	13	27	15
8	24	17	22	10
9	26	12	20	18
10	33	11	29	8
11	38	15	35	11
12	49	17	49	13
13	11	4	8	4
14	16	11	19	12
15	27	8	25	11

	500 Hz x 10 V		1 kHz x 10 V	
Chromosome number	**No of up regulated genes**	**No of down regulated genes**	**No of up regulated genes**	**No of down regulated genes**
16	27	11	26	8
17	53	14	43	16
18	10	4	9	2
19	23	16	22	15
20	18	8	18	7
21	6	2	7	0
22	12	7	10	6
X	26	11	21	10
Y	0	0	0	0
Total	679	315	658	280
	994		933	

Table 5-1- The number (No) of gene regulations after nanoscale stimulation. These changes were significant compared to control static groups ($p \leq 0.001$) and are presented as up- or down regulated groups.

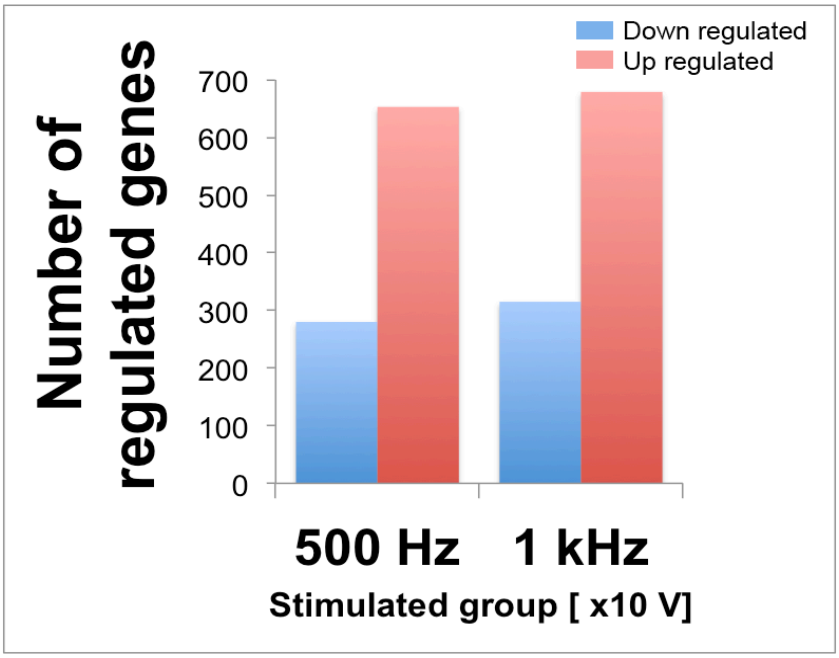

Figure 5-1- Distribution of gene regulations after nanostimulation of MSCs: This graph shows the number of up and down regulated genes in both stimulated groups are relatively equal. Most of the genes are up regulated (two-tailed t-test for equal variance was used, $p \leq 0.001$).

Linking the gene changes to the chromosome number the gene is found on, showed chromosomal differences in response to nanoscale stimulation. The most significant changes were linked to genes positioned on chromosome 1 (108-113 changes). Chromosome Y (no changes when thresholds were applied) and then chromosome 21 (7-8 changes) showed the least number of alterations Plotting the data appeared to link changes to chromosomal length. Chromosome 1, the largest chromosome has the highest and chromosome 21, the shortest autosomal chromosome has the lowest number of gene expression changes amongst autosomal chromosomes (Figure 5-2).

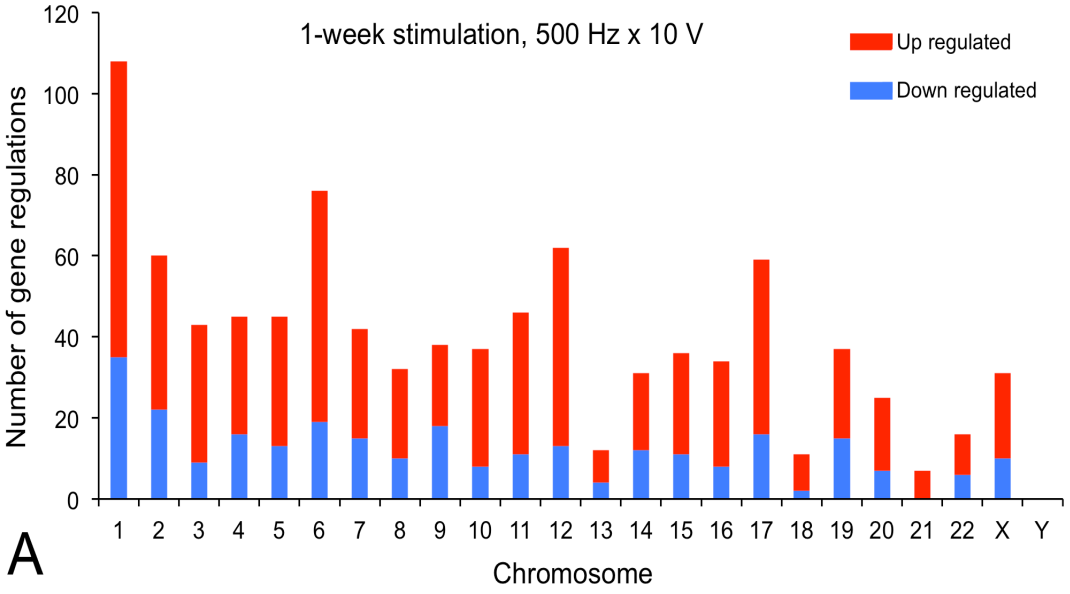

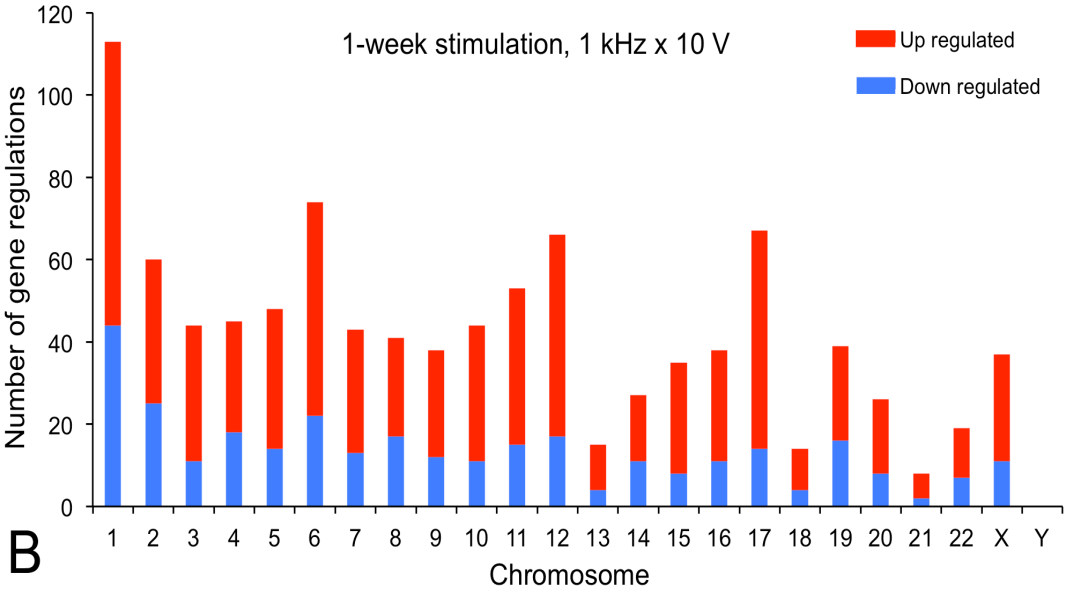

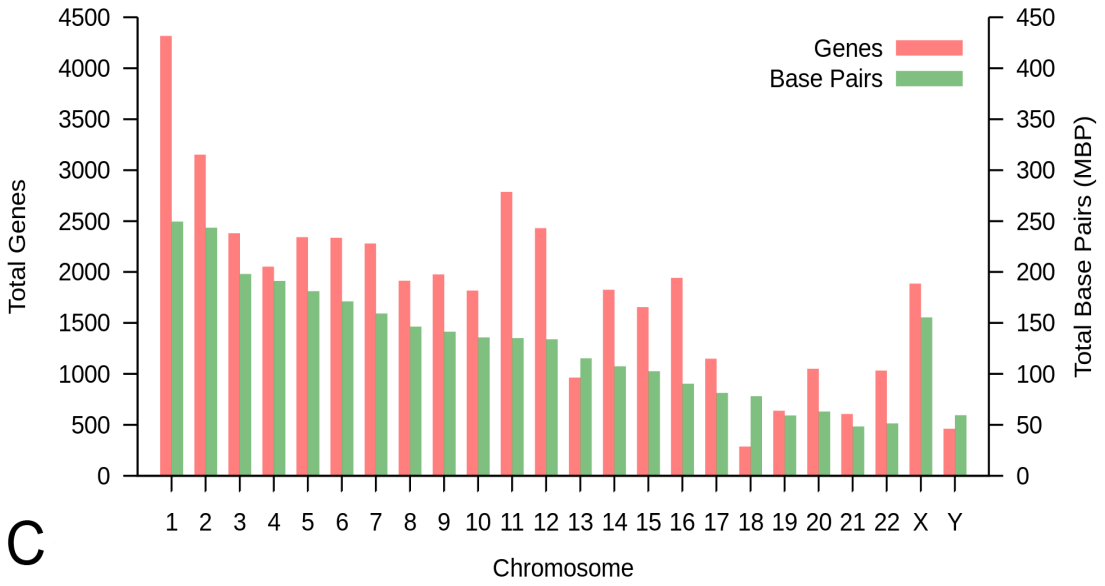

Figure 5-2- Gene regulations on chromosomes after nanostimulation of MSCs for 1-week at 500 (A) and 1kHz (B) with the same induced potential (×10 V) showed significant up and down-regulations compared to control ($p \leq 0.001$, n=3). Comparison to the length and number of known coding genes (C) shows a relative direct relation between the number of regulations and the known genes on chromosomes (graph C is taken from Wikimedia commons, Genes and base pairs on chromosomes).

Based on dividing the number of gene regulation changes to the number of known coding genes on every chromosome (chromosome map based on Ensembl: http://www.ensembl.org) the overall picture of changes altered and chromosome 6 is then shown to have the highest percentage of gene changes (Figure 5-3).

It is noted that chromosomal maps and the number of genes on each chromosome are controversial issues in many references; so the genotypic interpretation of changes only according to this map is presently suggestive. It is noted that there is still a large to small chromosome trend in terms of highest to lowest number of changes per chromosome, even after normalisation.

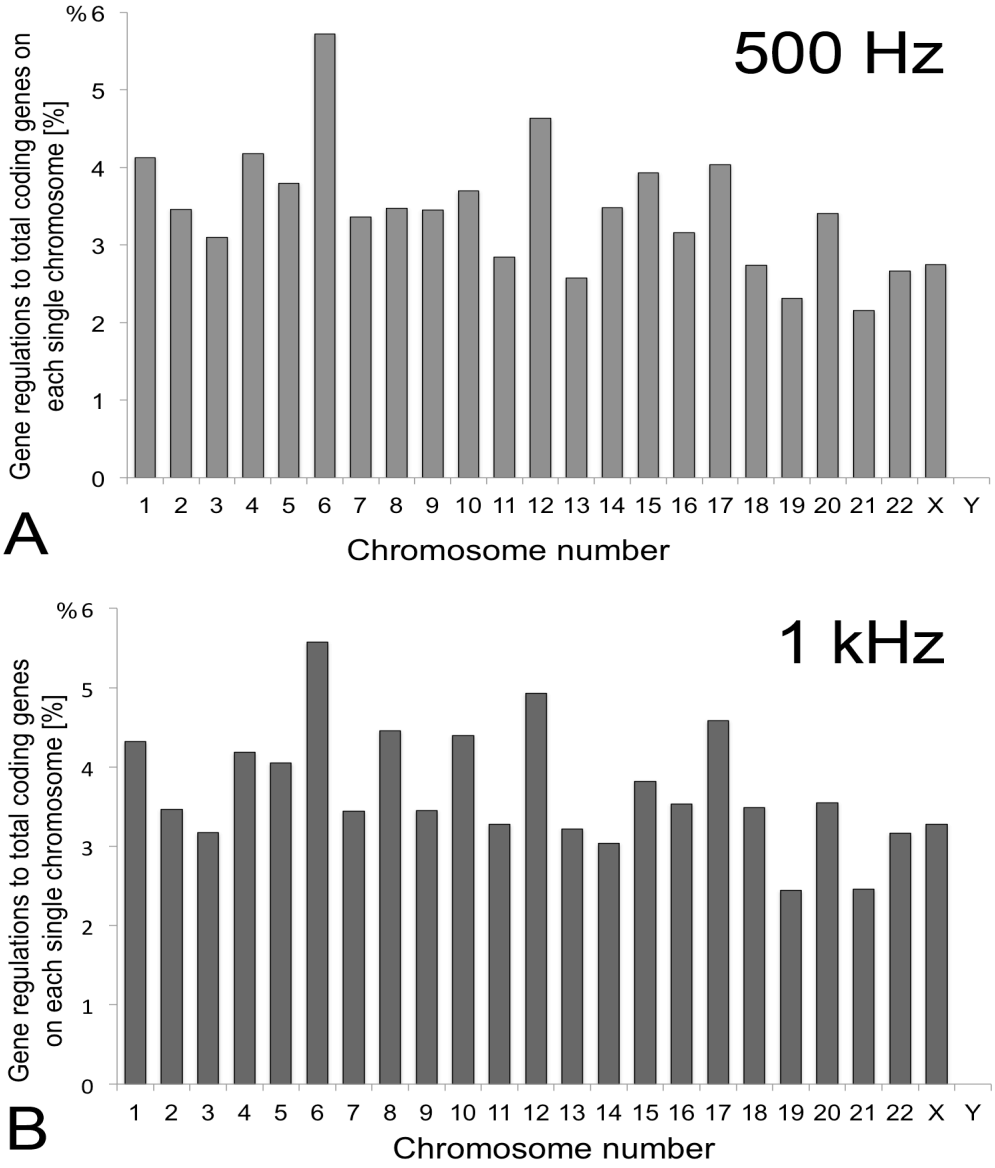

Figure 5-3- The ratio of gene regulations to the number of coding genes on each chromosome showed chromosome 6 was the most affected chromosome in both stimulated groups. Chromosome 21 remained the least affected.

As discussed in Chapter 4, both canonical and functional pathway analysis showed mainly increases (and in some cases decreases) in cellular activities. Here, a slightly different approach is taken by using IPA® (Ingeuity® pathway analysis) to generate common networks for 500 and 1000 Hz stimulation compared to control. IPA® is a software provided by Ingenuity® Systems (www.ingenuity.com, California, USA) for analysis of complex biological data such as genomic or proteomic datasets. It is one of the most popular tools in life science for data analyses such as biomarker analysis, molecular toxicology analysis, and interactive signalling and metabolic pathways. It allows results to

be presented in networks, graphs, pathways, and figures with multipurpose ability to combine and compare them with each other.

Microarray pathway analysis gave clues for activity changes in some important intracellular pathways those are strongly are connected to mechanosensing and mechanotransduction. Some of these pathways are positively activated and most of them may be attributed to direct mechanotransduction. It is especially noteworthy, in the context of this chapter, that RhoA and actin cytoskeletal signalling are linked to main networks. Before evaluation of these changes, a brief introduction of these pathways is needed (Thompson et al., 2012).

Rho family GTPases (Etienne-Manneville and Hall, 2002): are a group of molecular switches that use Guanosine-5'-triphosphate (GTP) for activation. They are small proteins (about 21 kDa) with their roles in cytoskeletal (actin) dynamics, cell division and cell motility. RhoA, Rac1, and Cdc 42 (cell division control 42), the three members of this family are tightly controlled inside the cells. The role of Rho is in acto-myosin complex formation (stress fibres), Rac is involved in lamellopodial formation and Cdc 42 is involved in filopodial formation. All of these actions make a connection between cell mechanoreceptors and intracellular architectures during cell response. Overactivation of many members of this family has been shown in various types of cancer (Ellenbroek and Collard, 2007). Rho-A kinase (ROCK) was the first known effector of Rho family with its main function in stress fibres dynamics and FA reinforcement. Specific chemical inhibition of ROCK can prevent stress fibre formation and F-actin assembly (Schofield and Bernard, 2013, Ishizaki et al., 1997).

Actin cytoskeleton signalling (Schmidt and Hall, 1998): Signalling through actin cytoskeleton dynamics is mainly through small the aforementioned GTPases. FA formation, stress fibre formation, filopodia and lamellopodail formation involved F-actin organisation to provide architecture and contraction. Integrin activation and signalling have a close relationship to activation of this pathway (DeMali et al., 2003). Presence or absence of focal adhesion kinase (FAK, the main non receptor tyrosine kinase found in adhesions) has an inhibitory or activating stimulation on Rho activity (Ren et al., 2000). Also, FAK inhibition has been shown to decrease mechanotransductive osteogenesis (Leucht et al.,

2007). These relations are indicative of mechanotransduction from integrins to control cytoskeletal rearrangement.

Sonic Hedgehog signalling (Villavicencio et al., 2000): One of the main pathways in human cell development and differentiation is Hedgehog signalling. Hedgehog proteins (Sonic, Indian, and Desert) control various aspect of development. Adult stem cell division, differentiation (James et al., 2010), neurogenesis (Faigle and Song, 2013) and carcinogenesis (Karamboulas and Ailles, 2013) are amongst the main functions of this pathway. This signalling pathway has a key role in vertebrate organogenesis especially in osteogenesis. For example, oxidative stress showed a suppressive effect on osteogenesis by inhibition of this pathway (Kim et al., 2010).

Protein kinase A signalling (Meinkoth et al., 1993): This kinase is a cAMP-dependent protein kinase that phosphorylates serine and threonine residues. It is a widely used signalling pathway in cell response. This pathway can stimulate enzymes and transcription factors that both are necessary in cell growth and differentiation.

ERK/MAPK signalling (Shaul and Seger, 2007): Extracellular signal-regulated kinases (ERK) also called mitogen-activated protein kinases (MAPK) and the Ras-Raf- MEK-ERK pathway are another kinase group that couple cytoplasmic receptors to nuclear transcription and have roles in survival, proliferation (Meloche and Pouyssegur, 2007), differentiation, and apoptosis. It has been shown, for example, that ERK activation had a major role in mechanotransductive osteogenesis after cyclic hydrostatic pressure (Kim et al., 2007).

Figure 5-4 shows a common network illustrated in 1000 Hz stimulated samples.

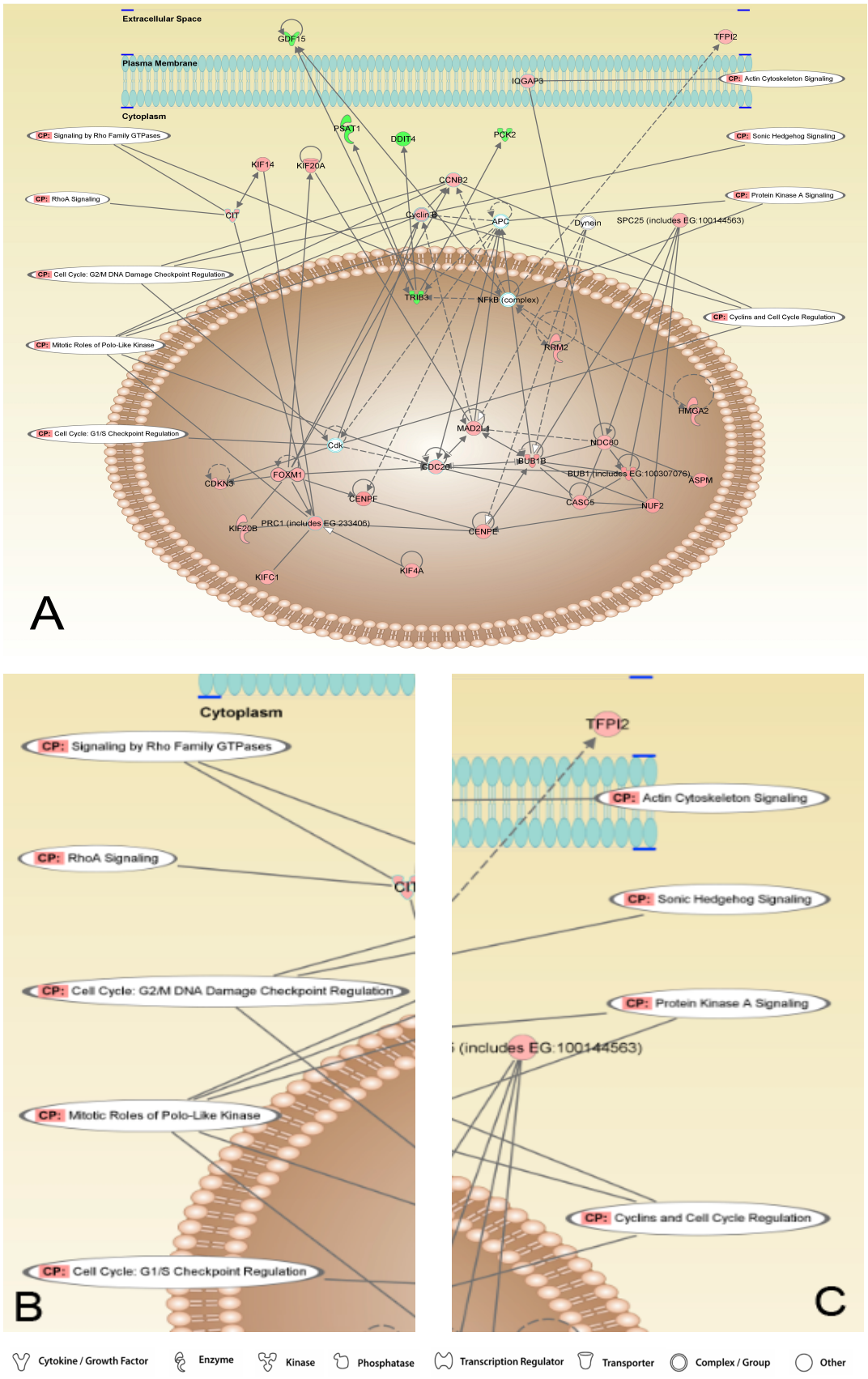

Figure 5-4- Microarray pathway analysis: A) this schematic picture is presenting some major intracellular pathways that were affected after nanostimulation at 1000 Hz in various

intracellular locations. The affected pathways are similar in both groups. B and C) magnified pictures to show the affected pathways in more detail. The network shows where gene activity is linked to major canonical biochemical pathways. Red: increased activity, Green: decreased activity.

Further IPA® network analysis showed common variation between two stimulated groups. Some of the major cellular pathways are shown in the common networks (both data sets overlapped – note that orange lines denote matching pathway links) as illustrated in Figure 5-5 and again include RhoA, Rho GTPase, actin cytoskeleton and ERK/MAPK. Both actin cytoskeleton and ERK/MAPK signalling showed increased activity through MAPK, ERK, Raf, and Sos genes, all of which are involved in adhesion and contractility.

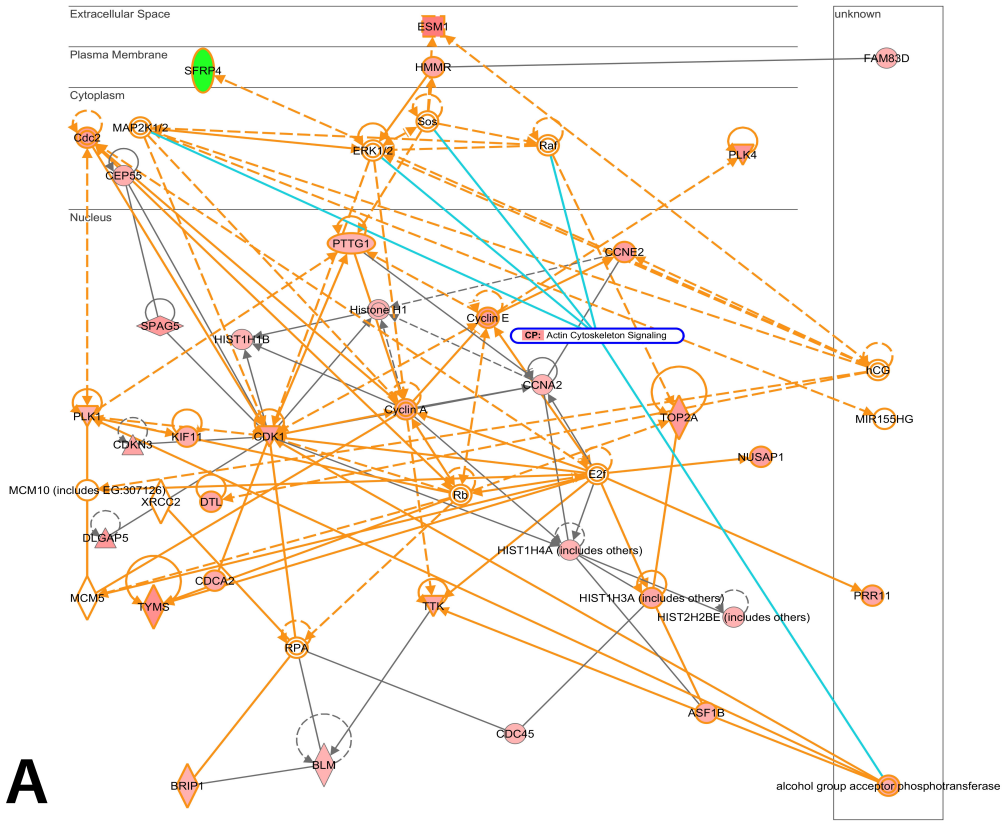

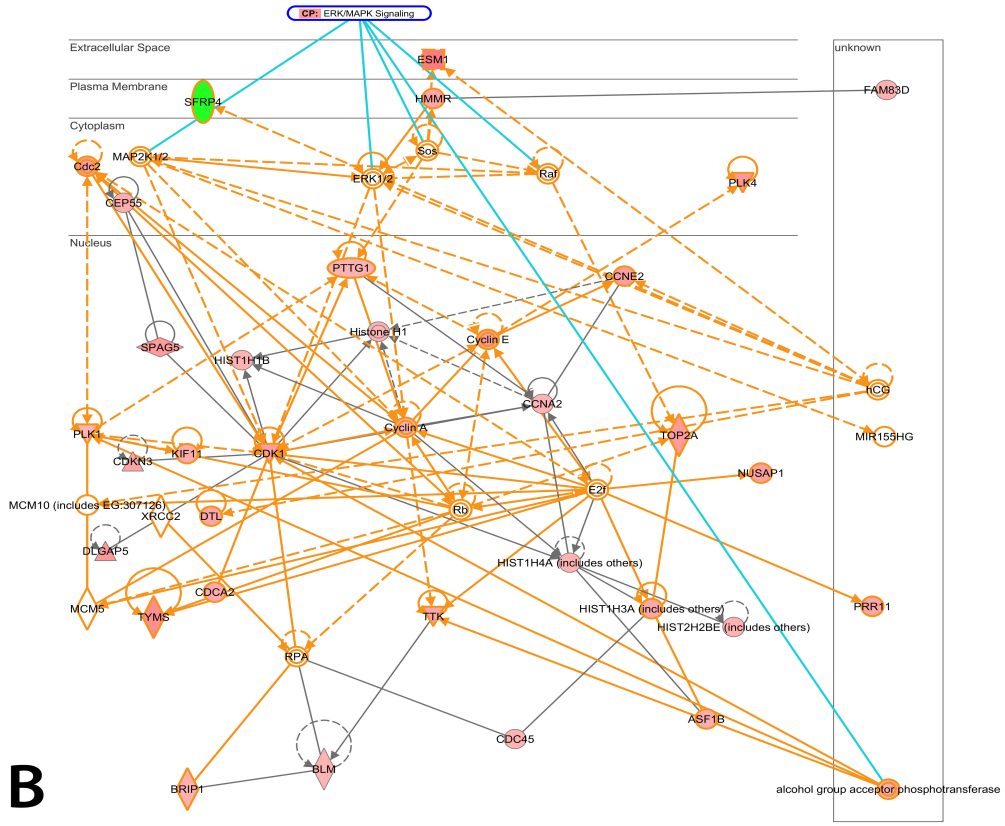
CP: ERK/MAPK Signaling
Extracellular Space
Plasma Membrane
Cytoplasm
Nucleus
unknown
ESM1
SFRP4
HMMR
FAM83D
Sos
MAP2K1/2
Cdc2
ERK1/2
Raf
PLK4
CEP55
PTTG1
CCNE2
Histone h1
Cyclin E
SPAG5
HIST1H1B
HCG
CCNA2
PLK1
Cyclin A
TOP2A
MIR155HG
CDKN3
KIF11
CDK1
NUSAP1
E2f
MCM10 (includes EG:307126)
XRCC2
DTL
Rb
DLGAP5
HIST1H4A (includes others)
CDCA2
PRR11
MCM5
TYMS
TTK
HIST1H3A (includes others)
HIST2H2BE (includes others)
RPA
ASF1B
CDC45
BLM
BRIP1
alcohol group acceptor phosphotransferase
B

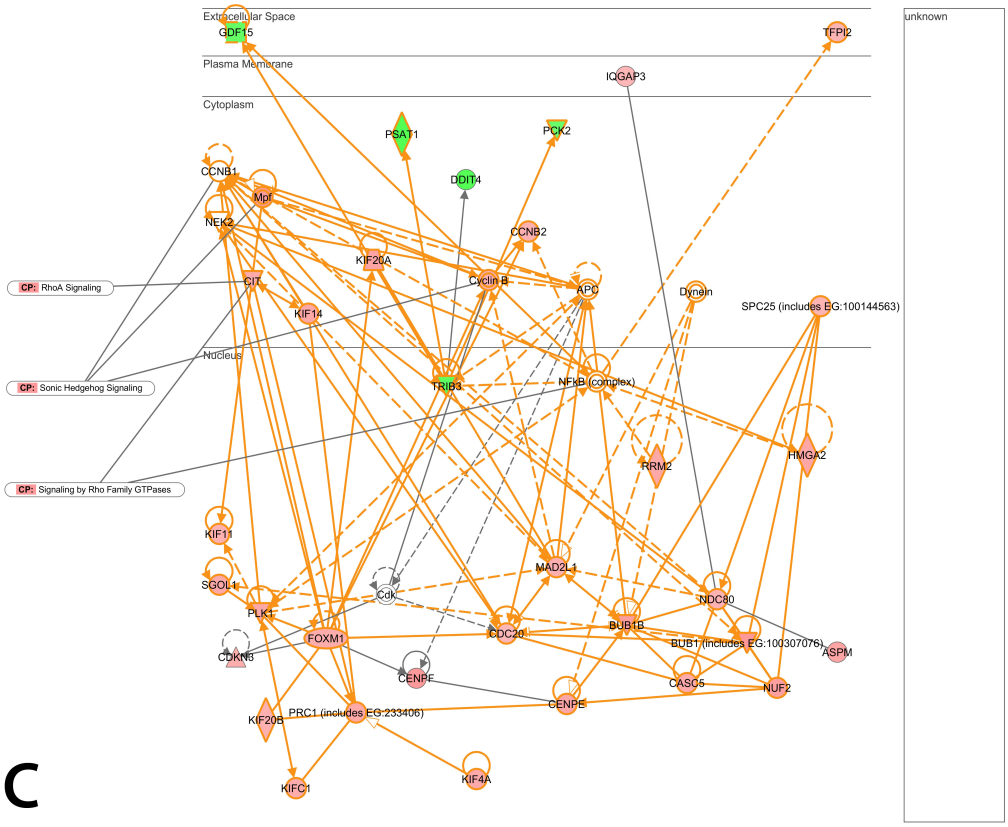
Extracellular Space
Plasma Membrane
Cytoplasm
Nucleus
unknown
GDF15
TFPI2
IQGAP3
PSAT1
PCK2
CCNB1
DDIT4
Mpf
NEK2
CCNB2
KIF20A
CP: RhoA Signaling
CIT
Cyclin B
APC
Dynein
SPC25 (includes EG:100144563)
KIF14
CP: Sonic Hedgehog Signaling
TRIB3
NFkB (complex)
HMGA2
RRM2
CP: Signaling by Rho Family GTPases
KIF11
MAD2L1
SGOL1
Cdk
NDC80
PLK1
BUB1B
FOXM1
CDC20
BUB1 (includes EG:100307076)
ASPM
CDKN3
CENPF
CASC5
NUF2
CENPE
KIF20B
PRC1 (includes EG:233406)
KIFC1
KIF4A
C

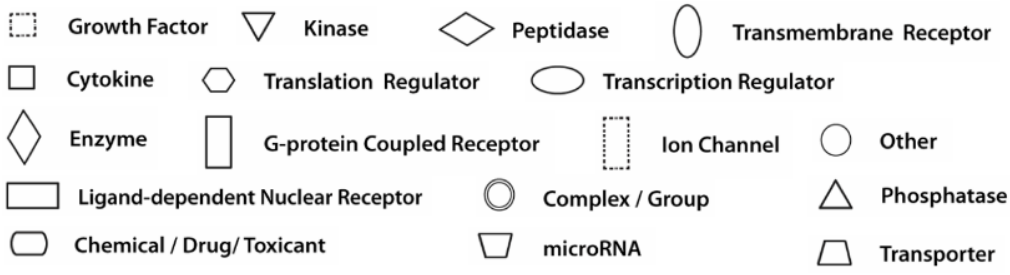

Figure 5-5- Microarray networks linked to five major canonical signalling pathways after 500 Hz and 1000 Hz (×10 V) nanostimulation. A) Actin cytoskeleton signalling (blue lines), B) ERK/MAPK signalling (blue lines), C) RhoA, Sonic Hedgehog, and Rho family GTPase signalling. Arrows are indicators of possible effects: orange arrows are common in both groups, black arrows: solitary effects. Red: increased, Green: decreased activity.

5.3.2 Lamin morphology

After 1-week treatment (500 Hz × 10 V, 1 kHz × 10 V), the cells were fixed and stained for lamin as described in Chapter 2. The samples were viewed at x100 magnification and the results were analysed by ImageJ and Microsoft Excel software. Lamin staining exhibited a decrease in intensity with concomitant increase in nuclear sizes and changes in lamin rearrangements with stimulation (Figures 5-6, 5-7). Nuclei after stimulation tended to show a more abundant and dispersive pattern of lamin speckles notably for lamin A/C. A positional change in the localisation of these speckles, from a central gathering (around the nucleoli) to the peripheries was noted particularly after 1-week of stimulation. The speckles also looked more prominent after stimulation. It is notable that after a week even the control cells exhibited a lamin A/C lamina, suggestive that they were also differentiating away from stem cell state – probably to fibroblasts.

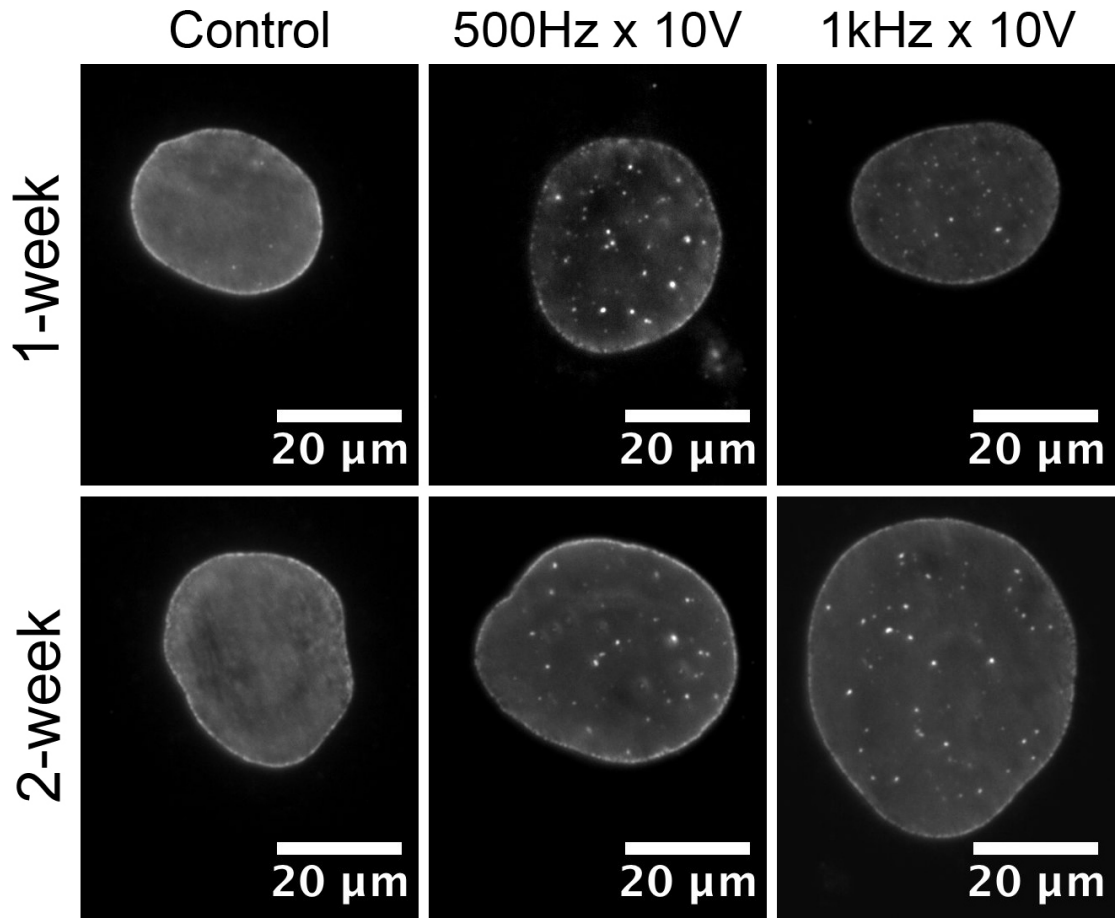

Figure 5-6- Lamin A/C presentation after 1-week and 2-week in two stimulated groups of MSCs showed increase in nuclear size, less intense staining and appearance of lamin speckles, N≥ 40.

After a week of stimulation, in many of the nuclei, there was an increased presence of putative tubular lamin B structures, thought to be important for nuclear structure and transport (McNamara et al., 2012, Broers et al., 1999) (Figure 5-7- B, C).

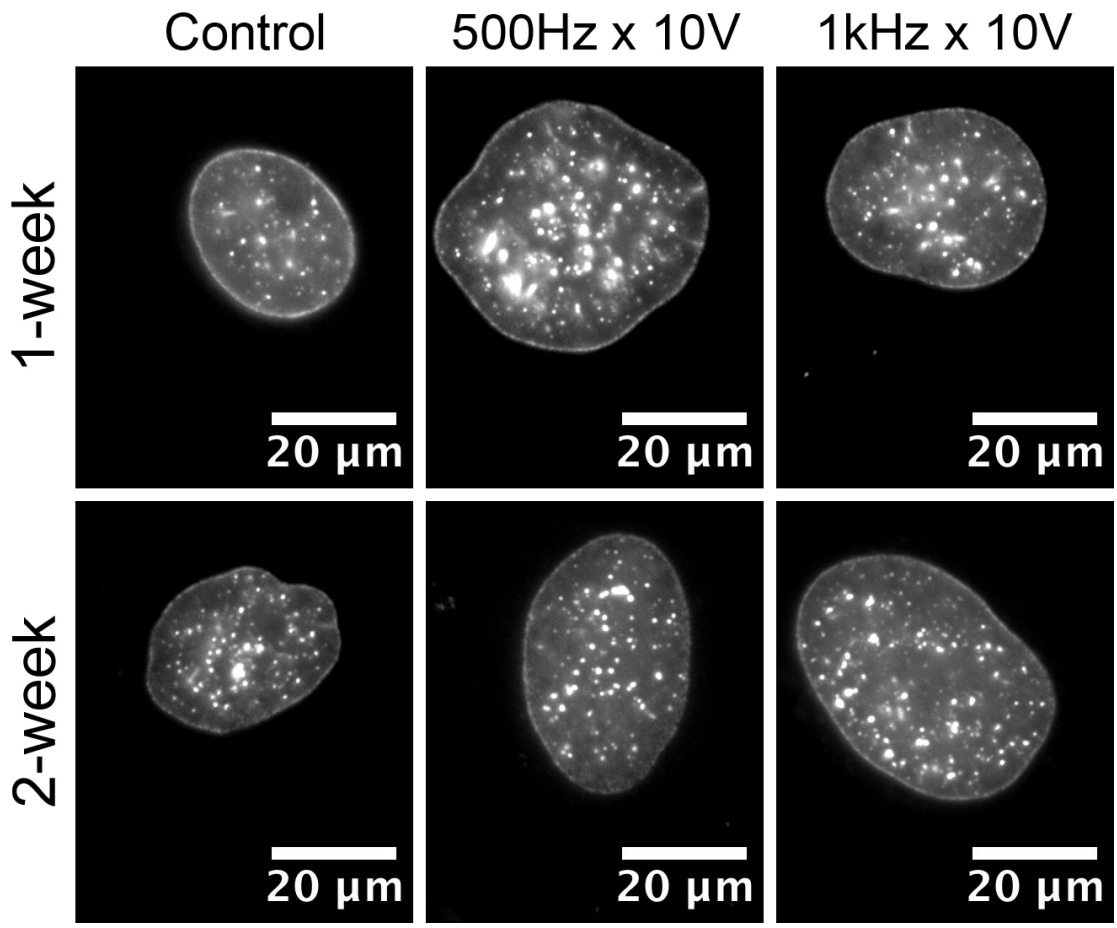

Figure 5-7- Lamin B presentation after 1-week and 2-week stimulation in two stimulated groups showed a more disperse pattern with more prominent speckles. N≥ 40.

To quantify the changes in nuclear size, image analysis was performed. This demonstrated increased nuclear perimeter and cut area (nuclear cross sectional area) after stimulation that was significant after 1-week and 2-week stimulation and with 1 kHz frequency. After 1-week only 500 Hz showed a significant increase in the nuclear perimeter (Figure 5-8).

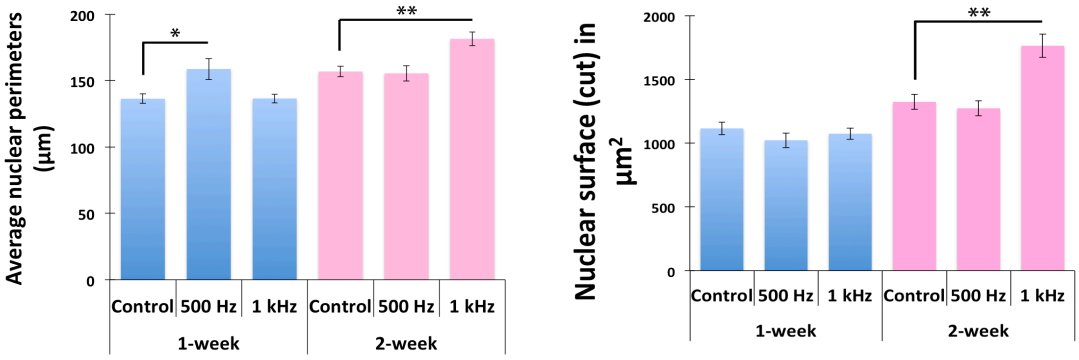

Figure 5-8- Average measurements for nuclear perimeter and nuclear surface area (as seen under the microscope) showed initial changes in 500 Hz × 10 V after 1-week (blue bars). After 2-week stimulation (pink bars), the changes were significant in the 1 kHz × 10 V group (two-tailed t-test for equal variance was used, *= p value ≤ 0.05, **= p value ≤ 0.001, N>40).

Image analysis also showed a significant decrease in the lamin A/C intensity after 1-week stimulation in both defined groups compared to the control that instead of decreasing pattern it was not significant after the 2-week period. Intensity measurements for lamin B showed a significant increasing pattern in two groups (Figure 5-9).

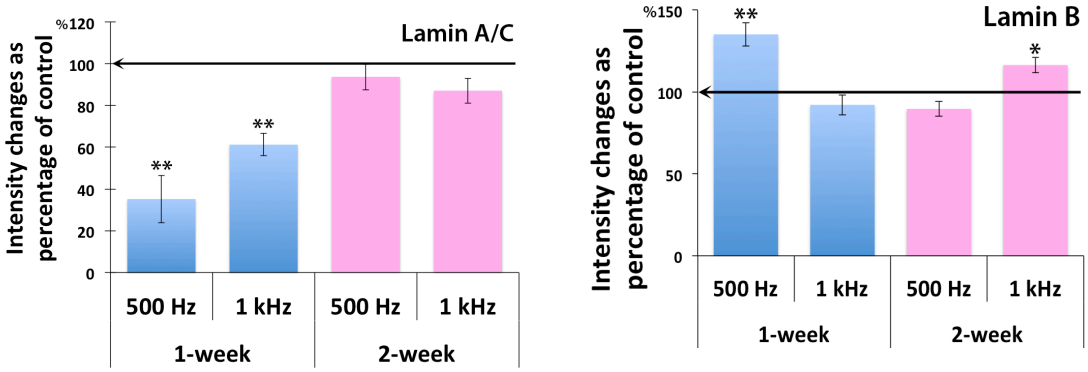

Figure 5-9- Lamins intensity analyses (expressing the results from the stimulated groups as a percentage of the control groups) showed significant decreases in lamin A/C intensity after one week. The results for lamin B intensity were more variable possibly due to speckle effects (two-tailed t-test for equal variance was used, *= p value ≤ 0.05, **= p value ≤ 0.001, N>40).

5.3.3 Nucleolar staining

As a major described nuclear organelle, the nucleolus is the largest and densest compartment in the nucleus. In addition to its role in ribosomal biogenesis, the nucleolus has a role in nuclear protein sequestration (Raska et al., 2006). Also, then nucleoli showed changes in response to various types of stress (Boulon et al., 2010). Looking for any possible effect by this nanoscale vibration on intranuclear structures, the nucleolus, as a dynamic structure, was stained and analysed for morphological modification. It was found that increases in cellular activity could generate increased numbers of nucleoli (Neuburger et al., 1998). After 1-week stimulation with 500 Hz and 1 kHz frequencies at 10 V, MSCs were fixed and stained for nucleoli and actin microfilaments as described in Chapter 2. The stimulated cells showed increases in the number of nucleoli (Figure 5-10) but they did not show significant differences in size, shape or their spatial position in the nucleus.

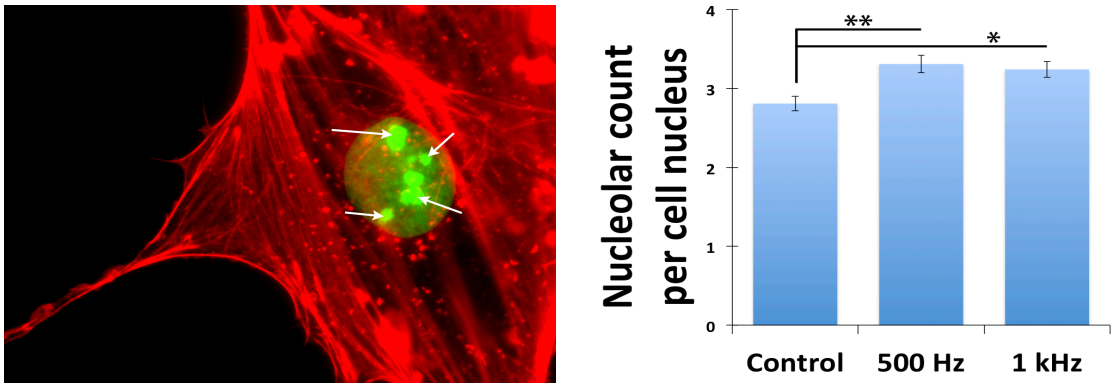

Figure 5-10- nucleolar count analyses after 1-week stimulation in both groups (500 and 1 kHz × 10 V) showed significant increases in the number of nucleoli (arrows). Red: F-actin microfilaments, light green: nucleus, green: nucleoli. (*= p value ≤ 0.05, **= p value ≤ 0.001, N>40).

5.4 Discussion

The microarray results are indicators of the influence of nanoscale vibration on genetic transcription. The longest chromosome with the largest occupied space in the nucleus (chromosome 1) was the most affected by this nanoscale vibration. The transcripts that were up or down regulated mostly encoded regulators of cell adhesion, the cell cycle and motility, and cellular interactions. The interactions of β1, α1β1, and α2β1 integrins with collagen have been previously shown to be important in osteoblastic differentiation (Takeuchi et al., 1997), all showed changes after nanostimulation.

The most notable functional effects of nanoscale stimulation were in the connective tissue and musculoskeletal development. These pathways were more significant than those for soft tissues, such as neural tissue. It seems that nanostimulation stimulated intracellular tension and activation of FAs and associated genes. The data presented also indicates roles for the cytoskeleton and alterations in nuclear morphology. The role of RhoA family GTPase activation is notable and will be key to both, for example, MAPK signalling and application of cytoskeletal tension to the nucleus.

Lamin analysis illustrated an initial change in nuclear size (enlargement) and density after stimulation. This is indicative of the nucleus becoming stretched and the lamins expanded (Dahl et al., 2008). After two weeks the cells appeared to have re-organised the nucleoskeleton with greater intensity of staining and speckle distribution. Lamin A/C presentation after stimulation is a positive sign for MSC differentiation and rearrangement for genetic regulation (Andres and Gonzalez, 2009). According to the supportive role of lamins (especially lamin B) (Martin et al., 2009, Dahl et al., 2004) in the nucleus the increased presentation of lamin speckles, the cut surface of tubular lamin structures (confocal would be required to reassemble the tubules in 3D), was noticeable especially with stimulation. Perhaps the formation of a network containing vertical tubular structures of lamin formed perpendicular to the dish surface and in the same direction of displacements (z-axis) could be supportive for nuclear architecture and elasticity. This network may assist in the transfer the vibratory messages from the ECM, FA (integrins), and cytoskeletal filaments to the chromosomal territories (Maniotis et al., 1997, Dahl et al., 2008) or could also act to cushion the nucleus. The observed increase in the number of nucleoli is another likely indicator of nuclear stimulation and potentially of direct mechanotransductive nuclear stimulation, possibly to support increased protein production at the ribosomes.

Chapter VI- General discussion

6.1 Introduction

Cell responses to external stimuli can be used to help influence activities such as migration, adhesion, polarity, proliferation and survival. For stem cells, another important activity, differentiation may also be determined through application of external factors. All these activities are regulated by complex mechano-chemical reactions inside and outside the cell. The ECM is important in relation to cell response to materials. Collagen is the most common natural protein in mammals in the ECM and cells are in close contact with it (Abou Neel et al., 2013, Micol et al., 2011). In this case ECM initial absorption will likely be similar between sample and control (as the cells were not stimulated while they settled), but stimulation will likely result in different rates of collagen production from the cells and then different reorganisation via focal adhesion pulling on the collagen fibrils (Karamichos et al., 2007, Karamichos et al., 2008).

FA assembly and subsequent interaction with the ECM is a major cellular pathway for sensing and responding to the environment and can be a determinant of health and disease states (Seong et al., 2013, Schiller and Fassler, 2013). Integrins are the first protein that link ECM to cytoskeleton as a part of the FA that crosses the cell membrane. Their composition (α and β receptors) can vary in various cell types, in different conditions and in response to different ECM compositions and they can also present in various combinations on the surface of single cells especially stem cells (Friedland et al., 2009). As described through this thesis, the connection of FAs to the cytoskeleton, nuclear membrane, and nucleoskeleton could possibly explain some direct mechanotransductive effects as well as the better understood biochemical effects (FAK, G-protein, ERK etc.) that can be stimulated by adhesion (Kuo, 2013, Wang et al., 1993).

Multipotent cells with the ability to differentiate to other lineages are currently being intensively researched in order to establish methods of controlling their fate towards developing regenerative strategies. Mechanical stimulation of stem cells is one of these topics (Wang and Chen, 2013a). By controlling the stem cell fate without using chemicals and by just sending messages through mechanical forces it is hoped that new ways of *in vitro /ex vivo* conditioning of cells or seeded constructs can be established. It is considered

that the combination of mechanical stimulation, biomaterial scaffold, and topography could accelerate developments in tissue engineering (Brown et al., 2013). Working in nanoscale, as in this thesis, provides a new depth of understanding in this area.

Mechanical stimulation of cells has been employed in various forms such as tensile stress, shear stress, vibration in all spatial axes, magnetic field application and electrical stimulation (Wang and Chen, 2013b, Kaverina et al., 2002, Yuan et al., 2013, Lim et al., 2013, Balint et al., 2013, Tang et al., 2012, Kirkham et al., 2010, Gaston et al., 2012). In this project, the indirect piezo effect was used to make nanoscale displacements under growing stem cells and they showed significant responses to this type of stimulation.

Many natural and synthetic crystals have piezoelectric activity e.g. non-centrosymmetric crystals in response to mechanical force or strain make electrical current (direct effect) and conversely if electrical fields applied on them, they will show mechanical displacements (indirect effect). Due to molecular nature of this type of energy conversion these smart materials could make very tiny and powerful displacements and will respond mechanically to very small electrical currents. These behaviours have been used for many industrial devices such as very sensitive biomedical instruments, sensors, transformers and actuators (Fang et al., 2013, Zhu, 2010) and also in biological experiments.

Over a number of years, there has been discussion of piezoelectric effect in bone. This is because, while collagen is piezoelectric when dry, for effect to be seen in hydrated bone, kilohertz range stimulus is required, that is, beyond what is considered physiological (Reinish and Nowick, 1975). Furthermore, it is known that electricity can be used to guide cells (galvanotaxis) (Finkelstein et al., 2007, Mycielska and Djamgoz, 2004), and stimulate bone repair (Goldstein et al., 2010). It has been postulated that bones' piezoelectrical properties facilitate osteoblast activity as they are attracted by the electrical dipoles produced by piezoelectricity or deformation of the bone (Noris-Suarez et al., 2007). Modelling has been used to show that piezo effects could be important in bone homeostasis with mechanical loads leading to polarization of bone, suggesting that negative charges accumulate at sites of bone removal and positive charges at sites of bone formation (Fernandez et al., 2012).

Multipotent stem cells have showed reactions to various types of micro- mechanical stimulations (Tay et al., 2013, Dalby et al., 2007) and induction of movements or vibration as a mechanical stimulus is now being investigated by a number of research groups (Ito et al., 2011, Gaston et al., 2012, Cho et al., 2012). Many scientists also have investigated osteoblastic differentiation of stem cells by vibrational stimuli at the microscale (Zhou et al., 2011, Tirkkonen et al., 2011, Pre et al., 2011, Zhang et al., 2012). These studies tend to show that high frequency vibration (Between 30- 180 Hz) usually promotes increased osteoblastic activity and osteoblastic differentiation in stem cells. A reverse effect on adipogenesis was a common observation (Rubin et al., 2007, Sadie-Van Gijsen et al., 2013).

These points on microscale mechanical stimulation considered and taken together with observations of cellular features in the scales of micrometres or less (such as lamellipodia and filopodia) 'sensing' and responding to nanoscale stimuli and sometimes changing the whole cell behaviour to adapt the new nano situations (Curtis et al., 2004, Dalby, 2009) provided the sense in pursuing nanoscale vibration.

6.2 Technical development

Piezoelectric buzzers were used as vibrators for initial experiments developed by Curtis, A. By attachment of a glass-cloning ring on top of buzzer, a simple cell culture dish was made (Figure 6-1) but evaluation of stimulated cells was difficult. Tubular piezoelectric actuators provided by PI Ceramic® (Germany) made the same scale displacement by gluing them to the Petri dish base.

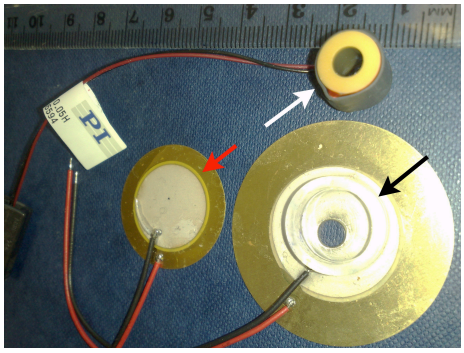

Figure 6-1- Piezo actuators: Piezo buzzers (red and black arrows) used for cell stimulation when a glass-cloning ring was attached on top (black arrow). Piezo actuator stalk from PI Ceramic® used for this project (white arrow) is a cylindrical actuator with vertical displacement when connected to an electrical current.

Z-axis displacements generated by an actuator move the cells growing on the dish up and down to allow us to evaluate cell responses by application of analytical biological methods. When initial experiments on cell culture response to nanoscale vibration were running, the first steps for measurement and calibration of displacements were prepared. The measurements were performed on three standard types of Petri dishes, 35, 60, and 100 mm (Chapter 3) with the base diameters of 35, 52, and 86 mm respectively. Using a laser interferometry-based method seated on an ophthalmologic table (fixed and stable) the preliminary measurements showed that displacements from the centre of the dish toward the periphery, although in the nanoscale range, they were not steady or consistent across the dish base. Several measurements in various types of dishes confirmed that optimisation was required. To remove the dish elasticity, several hard plates (from various materials and different thicknesses) were tested and finally, an aluminium disks with a 3.4 mm thickness when glued to Petri dish base showed faithful displacement results by vibrometry and were selected. This setup with a 52 mm base diameter Petri dish, glued to an aluminium disk and a piezo actuator was defined as our setup for this project (Figure 4-1). Various types of cells showed cytoskeletal changes with stimulation using this setup and thus I introduced nanoscale mechanical stimulation to MSCs.

6.3 Nanomechanostimulation influences human MSC function

Early manifestation of effects of nanoscale stimulation was shown in MSCs as increases in actin microfilament organisation, whole cell morphological changes with alterations in arboration, increased filopodial projections and increases in nuclear perimeters. This encouraged me to refine the stimulation system as described above.

To scan for differentiation, two different voltages and four frequencies were used. Then, by choosing three time intervals, 24 hours, a week and two weeks, twenty-four variables were defined and MSCs were stimulated to ‘fish’ for effect in this large parameter space. Happily, preliminary tests using gel qRT-PCR showed changes in phenotype marker transcript expression. Most of the significant data were seen with 500 and 1 kHz frequencies, with 10 volts amplitude and after one to two weeks’ continuous sine wave stimulation. These findings helped limit my choices for future work to two frequencies, one voltage and one time interval. Immunofluorescent studies and qRT-PCR results showed that osteoblastogenic activity was significantly increased after 1-week stimulation with 1 kHz × 10 V. This data was then supported by microarray analysis with significant up and down regulation of gene transcripts after stimulation with mRNA expression fitting

sensible canonical and functional pathways to support potential osteoblastic activity (e.g. RhoA and skeletal signalling).

6.4 Biological observations

Initial clues to cell response after the induction of nanoscale vertical vibration were found in immunofluorescent study of the cytoskeleton. Actin microfilaments appeared stronger and better organised across the cell, followed long cellular projections to the end points. Vinculin, as the indicator of FA assembly was better dispersed throughout the cells rather than being concentrated at the motile cell boarders suggestive of a less motile phenotype. Speculatively, they may have been distributed to 'sense' displacements from all parts of the cell to the nucleus through cytoskeletal fibres. At early hours of stimulation extending to a week, the cells showed a proliferation lag compared to control and then they showed a rapid growth and proliferation pattern up to two weeks. Their shape after stimulation changed to be larger.

Performing force measurements at the cellular level, Wu et al. showed that the combination of these long projections and FAs provide better mechanosensitive receptors across the cell surface (Wu et al., 2011). The size of the nucleus also increased after stimulation. Looking for nucleoskeletal changes inside the nucleus, lamins (A/C and B) exhibited expanded appearance (larger nucleus, less intense nucleoskeletal stain) with more and more dispersed speckles that could be indicators of lamin rearrangement to provide nuclear support in response to stimulation. This is in line with micropipette studies by Dahl et al (Dahl et al., 2004).

As discussed above, these morphological changes paired to observed changes in expression of bone markers and further supported by microarray all tie in with stimulation of osteogenesis. RUNX2 is BMP sensitive (Phimphilai et al., 2006, Jeon et al., 2006) and expression of this transcription factor is central to e.g. osteocalcin production and expression of mature osteoblast phenotype. That the cell response is ROCK dependant ties this new data together with data found on biomaterials (changes in topography, chemistry and stiffness) (McMurray et al., 2011, McBeath et al., 2004, Engler et al., 2006, Kilian et al., 2010) and helps to validate my observations.

Furthermore, tentative data is provided on direct mechanotransductive effects through transfer of mechanical forces direct to the nucleus. Theories such as tensegrity suggest how the cytoskeleton can provide required inhomogeneity to send signals across the cytoplasm through interconnected cytoskeletal networks working in a balance on tensile and compressive loads (Ingber, 1998, Ingber, 2008). Forces transmitted to the nuclear membrane then could cross the nucleus through LINC complexes to the nucleoskeleton then to the chromosomes via MARs. Figure 6-2 illustrates how this could work in the nanovibrational setting.

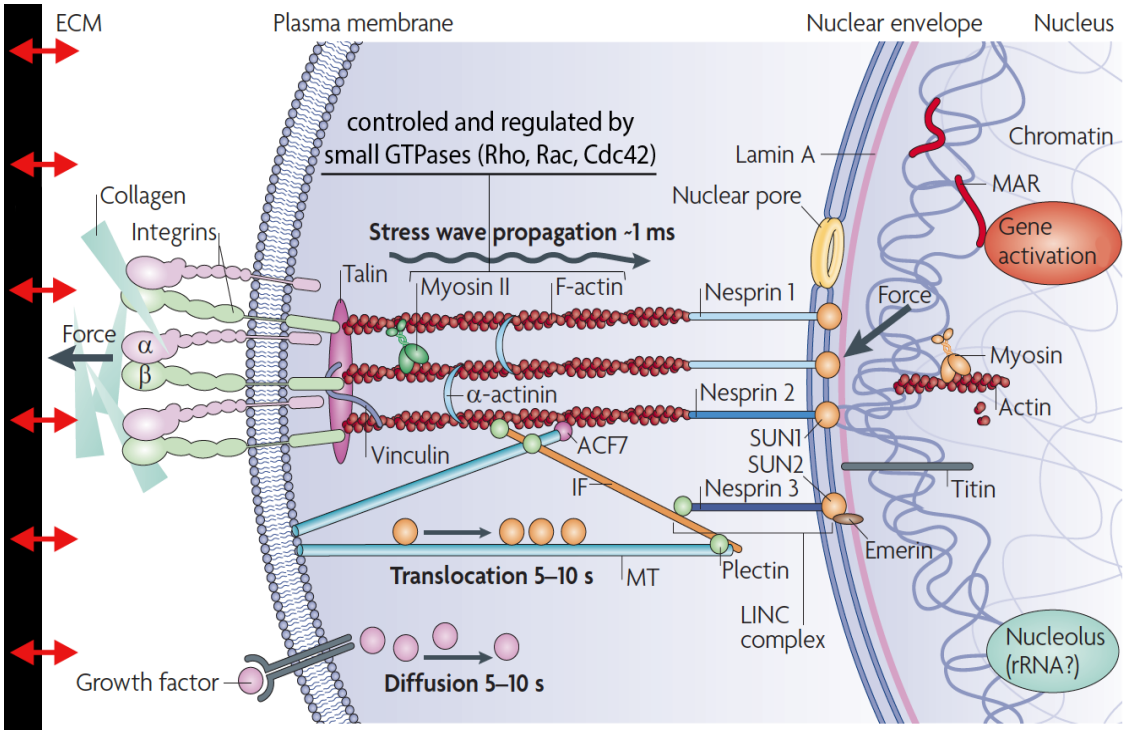

Figure 6-2- Possible mechanism for mechanotransduction after application of nanoscale displacements (red arrows) is indicated. Integrins as the cell sensors, sense and concentrate the forces through FA complexes. Actin-myosin complex could transfer the message (stress wave) to the nucleus. The contractility of acto-myosin complex is enforced and regulated by Rho GTPase activation. Transmission of force to the nucleus by LINC (linker of nucleoskeleton and cytoskeleton) and possible integration of nuclear actin and myosin might lead to chromosomal positioning and osteoblastic gene expression. ECM: extra cellular matrix, F: filamentous –actin, IF: intermediate filament, MT: microtubule, ACF7: actin-crosslinking factor 7, rRNA: ribosomal RNA, MAR: matrix attachment region. Adapted and changed from (Wang et al., 2009).

6.5 Conclusions

A new nanoscale method of MSC stimulation for targeted osteoblastogenesis was introduced. This does not rely on novel materials, complex chemistry, or electronic clean room facilities. Rather, it is based on traditional cell culture plastics with simple addition of piezo ceramics. Although I showed this change in MSCs' fate in a very limited way – on the surface of a Petri dish, up-scale to bioreactors that can prime autologous MSCs to form osteoblasts without recourse to soluble factors can be easily envisaged. Furthermore, we note that whole body vibration is becoming adopted in the clinic to help with musculoskeletal regeneration following, for example, spinal trauma, osteoporosis, and stress fracture repair (Wysocki et al., 2011, Alizadeh-Meghrazi et al., 2012, Brown et al., 2013). It could thus be envisaged that *in vitro* experiments could be used to inform therapy with the noted caveat that the modelling from cell to whole body is nontrivial and much research aimed at practical/theoretical scaling between nanoscale cell culture and the human body is required. Such techniques could be complementary to existing external stimuli for musculoskeletal regeneration such as extracorporeal shock wave treatment (Tamma et al., 2009). However, we note that while it is tempting to try and draw parallels between the values obtained for piezoelectric effect in bone, the benefit to bone of electrical stimulation, and the 1 kHz osteogenic stimulation we have used here, it is far too speculative, at this stage, to do so.

6.6 Future work

At this stage we showed that this type of nanoscale impulses could change MSCs behaviour toward osteogenesis. However, this is early stage research and many parameters have not been explored (and those that have only been looked at in a limited way). It could be expected that various type of wave types, continuity, voltages, frequencies, and time intervals might stimulate the MSCs toward other possible lineages. The preservation of these changes after discontinuation of stimuli is another question that should be investigated. Up-scaling the bioreactor with optimum potentials might create future products.

Also these experiments were performed on the dish base (in 2D) and it is expected that MSCs show different fates to this stimulus on 3D scaffold such as smart scaffolds or gel based ECM. Culture of cells in gels and coupling stiffness matching and vibrational activation could work together to improve results further and drive this research towards

tissue engineering. An excellent scaffold choice would be tissue-like compressed collagen where natural matrix conditions can be reproduced quickly (Cheema et al., 2007, Kruger et al., 2011).

Combination of this type of mechanical stimulation with other cues such as nanotopography (Dalby et al., 2007) or electrical stimulation (Kim et al., 2011) are other interesting possibilities.

To develop the platform for human use two possibilities could be considered. Firstly the development of footplates attached to an array of piezo actuators that are synchronised could provide a foot platform. The bonding between the device base, piezo actuator, footplate and the materials used would have to be considered so as not to permit dampening of such small movements. Another possibility would be to use e.g. sound waves to produce these small forces at focussed points.

All of these possibilities are now being investigated in the CCE labs.

References:

ABOU NEEL, E. A., BOZEC, L., KNOWLES, J. C., SYED, O., MUDERA, V., DAY, R. & HYUN, J. K. 2013. Collagen--emerging collagen based therapies hit the patient. *Adv Drug Deliv Rev,* 65**,** 429-56.

AKHTER, S., AHMAD, I., AHMAD, M. Z., RAMAZANI, F., SINGH, A., RAHMAN, Z., AHMAD, F. J., STORM, G. & KOK, R. J. 2013. Nanomedicines as Cancer Therapeutics: Current Status. *Current Cancer Drug Targets,* 13**,** 362-378.

ALBERTS, B., JOHNSON, A. & LEWIS, J. 2001. The Lipid Bilayer. *Molecular Biology of the Cell.* 4th ed.

ALDAHMASH, A., ZAHER, W., AL-NBAHEEN, M. & KASSEM, M. 2012. Human stromal (mesenchymal) stem cells: basic biology and current clinical use for tissue regeneration. *Annals of Saudi Medicine,* 32**,** 68-77.

ALLAMEH, A. & KAZEMNEJAD, S. 2012. Safety evaluation of stem cells used for clinical cell therapy in chronic liver diseases; with emphasize on biochemical markers. *Clin Biochem,* 45**,** 385-96.

ALLHOFF, F. 2009. The coming era of nanomedicine. *Am J Bioeth,* 9**,** 3-11.

ALON, R. & LEY, K. 2008. Cells on the run: shear-regulated integrin activation in leukocyte rolling and arrest on endothelial cells. *Curr Opin Cell Biol,* 20**,** 525-32.

AMIT, M., SHARIKI, C., MARGULETS, V. & ITSKOVITZ-ELDOR, J. 2004. Feeder layer- and serum-free culture of human embryonic stem cells. *Biol Reprod,* 70**,** 837-45.

ANDRES, V. & GONZALEZ, J. M. 2009. Role of A-type lamins in signaling, transcription, and chromatin organization. *J Cell Biol,* 187**,** 945-57.

ATALA, A., BAUER, S. B., SOKER, S., YOO, J. J. & RETIK, A. B. 2006. Tissue-engineered autologous bladders for patients needing cystoplasty. *Lancet,* 367**,** 1241-6.

BADDOUR, J. A., SOUSOUNIS, K. & TSONIS, P. A. 2012. Organ repair and regeneration: an overview. *Birth Defects Res C Embryo Today,* 96**,** 1-29.

BALINT, R., CASSIDY, N. J., HIDALGO-BASTIDA, L. A. & CARTMELL, S. 2013. Electrical Stimulation Enhanced Mesenchymal Stem Cell Gene Expression for Orthopaedic Tissue Repair. *Journal of Biomaterials and Tissue Engineering,* 3**,** 212-221.

BALLATO, A. 1998. Historical development of piezoelectric materials and applications. *Advances in Dielectric Ceramic Materials,* 88**,** 1-14.

BARILE, L., CHIMENTI, I., GAETANI, R., FORTE, E., MIRALDI, F., FRATI, G., MESSINA, E. & GIACOMELLO, A. 2007. Cardiac stem cells: isolation, expansion and experimental use for myocardial regeneration. *Nat Clin Pract Cardiovasc Med,* 4 Suppl 1**,** S9-S14.

BIGGS, M. J., RICHARDS, R. G. & DALBY, M. J. 2010. Nanotopographical modification: a regulator of cellular function through focal adhesions. *Nanomedicine,* 6**,** 619-33.

BIGGS, M. J., RICHARDS, R. G., GADEGAARD, N., WILKINSON, C. D., OREFFO, R. O. & DALBY, M. J. 2009. The use of nanoscale topography to modulate the dynamics of adhesion formation in primary osteoblasts and ERK/MAPK signalling in STRO-1+ enriched skeletal stem cells. *Biomaterials,* 30**,** 5094-103.

BIGGS, M. J., RICHARDS, R. G., MCFARLANE, S., WILKINSON, C. D., OREFFO, R. O. & DALBY, M. J. 2008a. Adhesion formation of primary human osteoblasts and the functional response of mesenchymal stem cells to 330nm deep microgrooves. *J R Soc Interface,* 5**,** 1231-42.

BIGGS, M. J., RICHARDS, R. G., WILKINSON, C. D. & DALBY, M. J. 2008b. Focal adhesion interactions with topographical structures: a novel method for immuno-SEM labelling of focal adhesions in S-phase cells. *J Microsc,* 231**,** 28-37.

BOCCAFOSCHI, F., MOSCA, C., RAMELLA, M., VALENTE, G. & CANNAS, M. 2013. The effect of mechanical strain on soft (cardiovascular) and hard (bone) tissues: common pathways for different biological outcomes. *Cell Adh Migr,* 7**,** 165-73.

BOULON, S., WESTMAN, B. J., HUTTEN, S., BOISVERT, F. M. & LAMOND, A. I. 2010. The nucleolus under stress. *Mol Cell,* 40**,** 216-27.

BROERS, J. L. V., MACHIELS, B. M., VAN EYS, G. J. J. M., KUIJPERS, H. J. H., MANDERS, E. M. M., VAN DRIEL, R. & RAMAEKERS, F. C. S. 1999. Dynamics of the nuclear lamina as monitored by GFP-tagged A-type lamins. *Journal of Cell Science,* 112**,** 3463-3475.

BROWN, P. T., HANDORF, A. M., JEON, W. B. & LI, W. J. 2013. Stem cell-based tissue engineering approaches for musculoskeletal regeneration. *Curr Pharm Des,* 19**,** 3429-45.

BROWN, R. A., SETHI, K. K., GWANMESIA, I., RAEMDONCK, D., EASTWOOD, M. & MUDERA, V. 2002. Enhanced fibroblast contraction of 3D collagen lattices and

integrin expression by TGF-beta1 and -beta3: mechanoregulatory growth factors? *Exp Cell Res,* 274**,** 310-22.

BRYANT, Z., STONE, M. D., GORE, J., SMITH, S. B., COZZARELLI, N. R. & BUSTAMANTE, C. 2003. Structural transitions and elasticity from torque measurements on DNA. *Nature,* 424**,** 338-41.

BUKORESHTLIEV, N. V., HAASE, K. & PELLING, A. E. 2013. Mechanical cues in cellular signalling and communication. *Cell Tissue Res,* 352**,** 77-94.

BUSTAMANTE, C., BRYANT, Z. & SMITH, S. B. 2003. Ten years of tension: single-molecule DNA mechanics. *Nature,* 421**,** 423-7.

CARTMELL, S. H., PORTER, B. D., GARCIA, A. J. & GULDBERG, R. E. 2003. Effects of medium perfusion rate on cell-seeded three-dimensional bone constructs in vitro. *Tissue Eng,* 9**,** 1197-203.

CARTMELL, S. H., RATHBONE, S., JONES, G. & HIDALGO-BASTIDA, L. A. 2011. 3D sample preparation for orthopaedic tissue engineering bioreactors. *Methods Mol Biol,* 695**,** 61-76.

CASAROLI-MARANO, R. P., NIETO-NICOLAU, N. & MARTINEZ-CONESA, E. M. 2013. Progenitor cells for ocular surface regenerative therapy. *Ophthalmic Res,* 49**,** 115-21.

CATERSON, E. J., NESTI, L. J., ALBERT, T., DANIELSON, K. & TUAN, R. 2001. Application of mesenchymal stem cells in the regeneration of musculoskeletal tissues. *MedGenMed***,** 1-6.

CHAN, D. C. 2006. Mitochondria: dynamic organelles in disease, aging, and development. *Cell,* 125**,** 1241-52.

CHARRAS, G. T. & HORTON, M. A. 2002. Determination of cellular strains by combined atomic force microscopy and finite element modeling. *Biophys J,* 83**,** 858-79.

CHEEMA, U., NAZHAT, S. N., ALP, B., FOROUGHI, F., ANANDAGODA, N., MUDERA, V. & BROWN, R. A. 2007. Fabricating tissues: Analysis of farming versus engineering strategies. *Biotechnology and Bioprocess Engineering,* 12**,** 9-14.

CHHABRA, P. & BRAYMAN, K. L. 2009. The use of stem cells in kidney disease. *Curr Opin Organ Transplant,* 14**,** 72-8.

CHIQUET, M., TUNC-CIVELEK, V. & SARASA-RENEDO, A. 2007. Gene regulation by mechanotransduction in fibroblasts. *Appl Physiol Nutr Metab,* 32**,** 967-73.

CHO, H., SEO, Y. K., JEON, S., YOON, H. H., CHOI, Y. K. & PARK, J. K. 2012. Neural differentiation of umbilical cord mesenchymal stem cells by sub-sonic vibration. *Life Sciences,* 90**,** 591-9.

CLAUSE, K. C., LIU, L. J. & TOBITA, K. 2010. Directed stem cell differentiation: the role of physical forces. *Cell Commun Adhes,* 17**,** 48-54.

CLOVER, J. & GOWEN, M. 1994. Are MG-63 and HOS TE85 human osteosarcoma cell lines representative models of the osteoblastic phenotype? *Bone,* 15**,** 585-91.

COLLIN, O., NA, S., CHOWDHURY, F., HONG, M., SHIN, M. E., WANG, F. & WANG, N. 2008. Self-organized podosomes are dynamic mechanosensors. *Curr Biol,* 18**,** 1288-94.

CREMER, T. & CREMER, C. 2001. Chromosome territories, nuclear architecture and gene regulation in mammalian cells. *Nat Rev Genet,* 2**,** 292-301.

CRISAN, M., YAP, S., CASTEILLA, L., CHEN, C. W., CORSELLI, M., PARK, T. S., ANDRIOLO, G., SUN, B., ZHENG, B., ZHANG, L., NOROTTE, C., TENG, P. N., TRAAS, J., SCHUGAR, R., DEASY, B. M., BADYLAK, S., BUHRING, H. J., GIACOBINO, J. P., LAZZARI, L., HUARD, J. & PEAULT, B. 2008. A perivascular origin for mesenchymal stem cells in multiple human organs. *Cell Stem Cell,* 3**,** 301-13.

CRISP, M., LIU, Q., ROUX, K., RATTNER, J. B., SHANAHAN, C., BURKE, B., STAHL, P. D. & HODZIC, D. 2006. Coupling of the nucleus and cytoplasm: role of the LINC complex. *J Cell Biol,* 172**,** 41-53.

CROFT, J. A., BRIDGER, J. M., BOYLE, S., PERRY, P., TEAGUE, P. & BICKMORE, W. A. 1999. Differences in the localization and morphology of chromosomes in the human nucleus. *J Cell Biol,* 145**,** 1119-31.

CURTIS, A. S., REID, S., MARTIN, I., VAIDYANATHAN, R., SMITH, C. A., NIKUKAR, H. & DALBY, M. J. 2013. Cell interactions at the nanoscale: piezoelectric stimulation. *IEEE Trans Nanobioscience,* 12**,** 247-54.

CURTIS, A. S. G., GADEGAARD, N., DALBY, M. J., RIEHLE, M. O., WILKINSON, C. D. W. & AITCHISON, G. 2004. Cells react to nanoscale order and symmetry in their surroundings. *IEEE Transactions on Nanobioscience,* 3**,** 61-65.

DAHL, K. N., BOOTH-GAUTHIER, E. A. & LADOUX, B. 2010. In the middle of it all: mutual mechanical regulation between the nucleus and the cytoskeleton. *J Biomech,* 43**,** 2-8.

DAHL, K. N., KAHN, S. M., WILSON, K. L. & DISCHER, D. E. 2004. The nuclear envelope lamina network has elasticity and a compressibility limit suggestive of a molecular shock absorber. *J Cell Sci,* 117**,** 4779-86.

DAHL, K. N., RIBEIRO, A. J. & LAMMERDING, J. 2008. Nuclear shape, mechanics, and mechanotransduction. *Circ Res,* 102**,** 1307-18.

DALBY, M. J. 2009. Nanostructured surfaces: cell engineering and cell biology. *Nanomedicine (Lond),* 4**,** 247-8.

DALBY, M. J., ANDAR, A., NAG, A., AFFROSSMAN, S., TARE, R., MCFARLANE, S. & OREFFO, R. O. 2008. Genomic expression of mesenchymal stem cells to altered nanoscale topographies. *J R Soc Interface,* 5**,** 1055-65.

DALBY, M. J., CHILDS, S., RIEHLE, M. O., JOHNSTONE, H. J., AFFROSSMAN, S. & CURTIS, A. S. 2003. Fibroblast reaction to island topography: changes in cytoskeleton and morphology with time. *Biomaterials,* 24**,** 927-35.

DALBY, M. J., GADEGAARD, N., TARE, R., ANDAR, A., RIEHLE, M. O., HERZYK, P., WILKINSON, C. D. W. & OREFFO, R. O. C. 2007. The control of human mesenchymal cell differentiation using nanoscale symmetry and disorder. *Nat Mater,* 6**,** 997-1003.

DAY, T. F. & YANG, Y. 2008. Wnt and hedgehog signaling pathways in bone development. *J Bone Joint Surg Am,* 90 Suppl 1**,** 19-24.

DE PEPPO, G. M., MARCOS-CAMPOS, I., KAHLER, D. J., ALSALMAN, D., SHANG, L., VUNJAK-NOVAKOVIC, G. & MAROLT, D. 2013. Engineering bone tissue substitutes from human induced pluripotent stem cells. *Proc Natl Acad Sci U S A,* 110**,** 8680-5.

DEL RIO, A., PEREZ-JIMENEZ, R., LIU, R., ROCA-CUSACHS, P., FERNANDEZ, J. M. & SHEETZ, M. P. 2009. Stretching single talin rod molecules activates vinculin binding. *Science,* 323**,** 638-41.

DEMALI, K. A., WENNERBERG, K. & BURRIDGE, K. 2003. Integrin signaling to the actin cytoskeleton. *Curr Opin Cell Biol,* 15**,** 572-82.

DISCHER, D. E., MOONEY, D. J. & ZANDSTRA, P. W. 2009. Growth factors, matrices, and forces combine and control stem cells. *Science,* 324**,** 1673-7.

DMITRIEVA, R. I., MINULLINA, I. R., BILIBINA, A. A., TARASOVA, O. V., ANISIMOV, S. V. & ZARITSKEY, A. Y. 2012. Bone marrow- and subcutaneous adipose tissue-derived mesenchymal stem cells: differences and similarities. *Cell Cycle,* 11**,** 377-83.

DOMINICI, M., LE BLANC, K., MUELLER, I., SLAPER-CORTENBACH, I., MARINI, F., KRAUSE, D., DEANS, R., KEATING, A., PROCKOP, D. & HORWITZ, E. 2006. Minimal criteria for defining multipotent mesenchymal stromal cells. The International Society for Cellular Therapy position statement. *Cytotherapy,* 8**,** 315-7.

DONZELLI, E., SALVADE, A., MIMO, P., VIGANO, M., MORRONE, M., PAPAGNA, R., CARINI, F., ZAOPO, A., MILOSO, M., BALDONI, M. & TREDICI, G. 2007. Mesenchymal stem cells cultured on a collagen scaffold: In vitro osteogenic differentiation. *Arch Oral Biol,* 52**,** 64-73.

DVIR, T., TIMKO, B. P., KOHANE, D. S. & LANGER, R. 2011. Nanotechnological strategies for engineering complex tissues. *Nat Nanotechnol,* 6**,** 13-22.

EDALAT, F., BAE, H., MANOUCHERI, S., CHA, J. M. & KHADEMHOSSEINI, A. 2012. Engineering approaches toward deconstructing and controlling the stem cell environment. *Ann Biomed Eng,* 40**,** 1301-15.

EHNERT, S., GLANEMANN, M., SCHMITT, A., VOGT, S., SHANNY, N., NUSSLER, N. C., STOCKLE, U. & NUSSLER, A. 2009. The possible use of stem cells in regenerative medicine: dream or reality? *Langenbecks Arch Surg,* 394**,** 985-97.

EL HAJ, A. J. & CARTMELL, S. H. 2010. Bioreactors for bone tissue engineering. *Proc Inst Mech Eng H,* 224**,** 1523-32.

ELLENBROEK, S. I. & COLLARD, J. G. 2007. Rho GTPases: functions and association with cancer. *Clin Exp Metastasis,* 24**,** 657-72.

ENGLER, A., CHIRASATITSIN, S., VIWANATHAN, P. & BATTAGLIA, G. 2012. Adhesive heterogeneity within the stem cell niche promotes differentiation. *Glycobiology,* 22**,** 1587-1588.

ENGLER, A. J., SEN, S., SWEENEY, H. L. & DISCHER, D. E. 2006. Matrix elasticity directs stem cell lineage specification. *Cell,* 126**,** 677-89.

ENGLER, A. J., SWEENEY, H. L., DISCHER, D. E. & SCHWARZBAUER, J. E. 2007. Extracellular matrix elasticity directs stem cell differentiation. *J Musculoskelet Neuronal Interact,* 7**,** 335.

ETHERIDGE, M. L., CAMPBELL, S. A., ERDMAN, A. G., HAYNES, C. L., WOLF, S. M. & MCCULLOUGH, J. 2013. The big picture on nanomedicine: the state of investigational and approved nanomedicine products. *Nanomedicine,* 9**,** 1-14.

ETIENNE-MANNEVILLE, S. & HALL, A. 2002. Rho GTPases in cell biology. *Nature,* 420**,** 629-35.

EVANS, C. H. 2011. Barriers to the clinical translation of orthopedic tissue engineering. *Tissue Eng Part B Rev,* 17**,** 437-41.

EVANS, J., GRATZER, W., MOHANDAS, N., PARKER, K. & SLEEP, J. 2008. Fluctuations of the red blood cell membrane: relation to mechanical properties and lack of ATP dependence. *Biophys J,* 94**,** 4134-44.

FAIGLE, R. & SONG, H. 2013. Signaling mechanisms regulating adult neural stem cells and neurogenesis. *Biochim Biophys Acta,* 1830**,** 2435-48.

FANG, X. Q., LIU, J. X. & GUPTA, V. 2013. Fundamental formulations and recent achievements in piezoelectric nano-structures: a review. *Nanoscale,* 5**,** 1716-26.

FAUSTO, N. 2004. Liver regeneration and repair: hepatocytes, progenitor cells, and stem cells. *Hepatology,* 39**,** 1477-87.

FERNANDEZ, J. R., GARCIA-AZNAR, J. M. & MARTINEZ, R. 2012. Piezoelectricity could predict sites of formation/resorption in bone remodelling and modelling. *Journal of Theoretical Biology,* 292**,** 86-92.

FERRARA, F., PALMIERI, S. & MELE, G. 2010. Peripheral blood or bone marrow as hematopoietic stem cell source for autologous transplantation in acute myeloid leukemia? *J Clin Oncol,* 28**,** e246-7; author reply e248-9.

FINKELSTEIN, E. I., CHAO, P. H., HUNG, C. T. & BULINSKI, J. C. 2007. Electric field-induced polarization of charged cell surface proteins does not determine the direction of galvanotaxis. *Cell Motil Cytoskeleton,* 64**,** 833-46.

FRIEDLAND, J. C., LEE, M. H. & BOETTIGER, D. 2009. Mechanically activated integrin switch controls alpha-5 beta-1 function. *Science,* 323**,** 642-4.

FRUMKIN, T., MALCOV, M., TELIAS, M., GOLD, V., SCHWARTZ, T., AZEM, F., AMIT, A., YARON, Y. & BEN-YOSEF, D. 2010. Human embryonic stem cells carrying mutations for severe genetic disorders. *In Vitro Cell Dev Biol Anim,* 46**,** 327-36.

GALBRAITH, C. G., YAMADA, K. M. & SHEETZ, M. P. 2002. The relationship between force and focal complex development. *J Cell Biol,* 159**,** 695-705.

GAO, L., MCBEATH, R. & CHEN, C. S. 2010. Stem cell shape regulates a chondrogenic versus myogenic fate through Rac1 and N-cadherin. *Stem Cells,* 28**,** 564-72.

GASTON, J., QUINCHIA RIOS, B., BARTLETT, R., BERCHTOLD, C. & THIBEAULT, S. L. 2012. The response of vocal fold fibroblasts and mesenchymal stromal cells to vibration. *PLoS ONE,* 7**,** e30965.

GE, C., XIAO, G., JIANG, D. & FRANCESCHI, R. T. 2007. Critical role of the extracellular signal-regulated kinase-MAPK pathway in osteoblast differentiation and skeletal development. *J Cell Biol,* 176**,** 709-18.

GEIGER, B., SPATZ, J. P. & BERSHADSKY, A. D. 2009. Environmental sensing through focal adhesions. *Nat Rev Mol Cell Biol,* 10**,** 21-33.

GIANNONE, G., DUBIN-THALER, B. J., ROSSIER, O., CAI, Y., CHAGA, O., JIANG, G., BEAVER, W., DOBEREINER, H. G., FREUND, Y., BORISY, G. & SHEETZ, M. P. 2007. Lamellipodial actin mechanically links myosin activity with adhesion-site formation. *Cell,* 128**,** 561-75.

GLENN, L. M. & BOYCE, J. S. 2012. Regenerative nanomedicine: ethical, legal, and social issues. *Methods Mol Biol,* 811**,** 303-16.

GOLDMANN, W. H., CANTIELLO, H. F. & CHASAN, B. 2005. Actomyosin II interaction modulates cell cortex stability. *Cell Biol Int,* 29**,** 245-8.

GOLDSTEIN, C., SPRAGUE, S. & PETRISOR, B. A. 2010. Electrical stimulation for fracture healing: current evidence. *J Orthop Trauma,* 24 Suppl 1**,** S62-5.

GRECO, R. S., PRINZ, F. B. & SMITH, R. L. 2005. *Nanoscale Technology in Biological Systems,* FL, USA, CRC PRESS-TAYLOR & FRANCIS GROUP, USA.

GROSSMANN, J. 2002. Molecular mechanisms of "detachment-induced apoptosis--Anoikis". *Apoptosis,* 7**,** 247-60.

GRUSKIN, E., DOLL, B. A., FUTRELL, F. W., SCHMITZ, J. P. & HOLLINGER, J. O. 2012. Demineralized bone matrix in bone repair: history and use. *Adv Drug Deliv Rev,* 64**,** 1063-77.

GUILAK, F., COHEN, D. M., ESTES, B. T., GIMBLE, J. M., LIEDTKE, W. & CHEN, C. S. 2009. Control of stem cell fate by physical interactions with the extracellular matrix. *Cell Stem Cell,* 5**,** 17-26.

HADDAD, B., PAKRAVAN, A. H., KONAN, S., ADESIDA, A. & KHAN, W. 2013. A systematic review of tissue engineered meniscus: cell-based preclinical models. *Curr Stem Cell Res Ther,* 8**,** 222-31.

HAGHIGHIPOUR, N., HEIDARIAN, S., SHOKRGOZAR, M. A. & AMIRIZADEH, N. 2012. Differential effects of cyclic uniaxial stretch on human mesenchymal stem cell into skeletal muscle cell. *Cell Biol Int,* 36**,** 669-75.

HALPERIN, C., MUTCHNIK, S., AGRONIN, A., MOLOTSKII, M., URENSKI, P., SALAI, M. & ROSENMAN, G. 2004. Piezoelectric effect in human bones studied in nanometer scale. *Nano Letters,* 4**,** 1253-1256.

HANSSON, E. M., LINDSAY, M. E. & CHIEN, K. R. 2009. Regeneration next: toward heart stem cell therapeutics. *Cell Stem Cell,* 5**,** 364-77.

HAQUE, F., LLOYD, D. J., SMALLWOOD, D. T., DENT, C. L., SHANAHAN, C. M., FRY, A. M., TREMBATH, R. C. & SHACKLETON, S. 2006. SUN1 interacts with nuclear lamin A and cytoplasmic nesprins to provide a physical connection between the nuclear lamina and the cytoskeleton. *Mol Cell Biol,* 26**,** 3738-51.

HARRIS, M. A., CRIPTON, P. A. & TESCHKE, K. 2012. Retrospective assessment of occupational exposure to whole-body vibration for a case-control study. *J Occup Environ Hyg,* 9**,** 371-80.

HE, L. & MONTELL, D. 2012. A cellular sense of touch. *Nat Cell Biol,* 14**,** 902-3.

HIGGS, P. G. 2000. RNA secondary structure: physical and computational aspects. *Quarterly Reviews of Biophysics,* 33**,** 199-253.

HOLLE, A., TANG, X. Y. & ENGLER, A. 2012. Substratum stiffness-dependent vinculin activation modulates mechanosensitive stem cell differentiation. *Glycobiology,* 22**,** 1529-1529.

HUANG DA, W., SHERMAN, B. T. & LEMPICKI, R. A. 2009. Systematic and integrative analysis of large gene lists using DAVID bioinformatics resources. *Nature Protocols,* 4**,** 44-57.

HUANG, S. & INGBER, D. E. 1999. The structural and mechanical complexity of cell-growth control. *Nat Cell Biol,* 1**,** E131-8.

HUANGFU, D., MAEHR, R., GUO, W., EIJKELENBOOM, A., SNITOW, M., CHEN, A. E. & MELTON, D. A. 2008. Induction of pluripotent stem cells by defined factors is greatly improved by small-molecule compounds. *Nat Biotechnol,* 26**,** 795-7.

HUTCHISON, C. J. 2002. Lamins: Building blocks or regulators of gene expression? *Nat Rev Mol Cell Biol,* 3**,** 848-58.

INGBER, D. E. 1993. Cellular tensegrity: defining new rules of biological design that govern the cytoskeleton. *J Cell Sci,* 104 (Pt 3)**,** 613-27.

INGBER, D. E. 1998. Mechanotransduction through integrins and cytoskeletal tensegrity. *Molecular Biology of the Cell,* 9**,** 257A-257A.

INGBER, D. E. 2003a. Tensegrity I. Cell structure and hierarchical systems biology. *J Cell Sci,* 116**,** 1157-73.

INGBER, D. E. 2003b. Tensegrity II. How structural networks influence cellular information processing networks. *J Cell Sci,* 116**,** 1397-408.

INGBER, D. E. 2008. Tensegrity and mechanotransduction. *J Bodyw Mov Ther,* 12**,** 198-200.

ISHIZAKI, T., NAITO, M., FUJISAWA, K., MAEKAWA, M., WATANABE, N., SAITO, Y. & NARUMIYA, S. 1997. p160(ROCK), a Rho-associated coiled-coil forming protein kinase, works downstream of Rho and induces focal adhesions. *Febs Letters,* 404**,** 118-124.

ITO, Y., KIMURA, T., AGO, Y., NAM, K., HIRAKU, K., MIYAZAKI, K., MASUZAWA, T. & KISHIDA, A. 2011. Nano-vibration effect on cell adhesion and its shape. *Biomed Mater Eng,* 21**,** 149-58.

JAMES, A. W., LEUCHT, P., LEVI, B., CARRE, A. L., XU, Y., HELMS, J. A. & LONGAKER, M. T. 2010. Sonic Hedgehog influences the balance of osteogenesis and adipogenesis in mouse adipose-derived stromal cells. *Tissue Eng Part A,* 16**,** 2605-16.

JANG, W. G., KIM, E. J., KIM, D. K., RYOO, H. M., LEE, K. B., KIM, S. H., CHOI, H. S. & KOH, J. T. 2012. BMP2 protein regulates osteocalcin expression via Runx2-mediated Atf6 gene transcription. *J Biol Chem,* 287**,** 905-15.

JEON, E. J., LEE, K. Y., CHOI, N. S., LEE, M. H., KIM, H. N., JIN, Y. H., RYOO, H. M., CHOI, J. Y., YOSHIDA, M., NISHINO, N., OH, B. C., LEE, K. S., LEE, Y. H. & BAE, S. C. 2006. Bone morphogenetic protein-2 stimulates Runx2 acetylation. *J Biol Chem,* 281**,** 16502-11.

KAMKIN, A. & KISELEVA, I. 2008. *Mechanosensitive Ion Channels*, Springer, Netherlands.

KANCHANAWONG, P., SHTENGEL, G., PASAPERA, A. M., RAMKO, E. B., DAVIDSON, M. W., HESS, H. F. & WATERMAN, C. M. 2010. Nanoscale architecture of integrin-based cell adhesions. *Nature,* 468**,** 580-4.

KARAMBOULAS, C. & AILLES, L. 2013. Developmental signaling pathways in cancer stem cells of solid tumors. *Biochim Biophys Acta,* 1830**,** 2481-95.

KARAMICHOS, D., BROWN, R. A. & MUDERA, V. 2007. Collagen stiffness regulates cellular contraction and matrix remodeling gene expression. *J Biomed Mater Res A,* 83**,** 887-94.

KARAMICHOS, D., SKINNER, J., BROWN, R. & MUDERA, V. 2008. Matrix stiffness and serum concentration effects matrix remodelling and ECM regulatory genes of human bone marrow stem cells. *J Tissue Eng Regen Med,* 2**,** 97-105.

KAVERINA, I., KRYLYSHKINA, O., BENINGO, K., ANDERSON, K., WANG, Y. L. & SMALL, J. V. 2002. Tensile stress stimulates microtubule outgrowth in living cells. *J Cell Sci,* 115**,** 2283-91.

KILIAN, K. A., BUGARIJA, B., LAHN, B. T. & MRKSICH, M. 2010. Geometric cues for directing the differentiation of mesenchymal stem cells. *Proc Natl Acad Sci U S A,* 107**,** 4872-7.

KIM, J. H., LEE, T. H., SONG, Y. M., KIM, I. S., CHO, T. H., HWANG, S. J. & KIM, S. J. 2011. An implantable electrical bioreactor for enhancement of cell viability. *Conf Proc IEEE Eng Med Biol Soc,* 2011**,** 3601-4.

KIM, S. H., CHOI, Y. R., PARK, M. S., SHIN, J. W., PARK, K. D., KIM, S. J. & LEE, J. W. 2007. ERK 1/2 activation in enhanced osteogenesis of human mesenchymal stem cells in poly(lactic-glycolic acid) by cyclic hydrostatic pressure. *J Biomed Mater Res A,* 80**,** 826-36.

KIM, W. K., MELITON, V., BOURQUARD, N., HAHN, T. J. & PARHAMI, F. 2010. Hedgehog signaling and osteogenic differentiation in multipotent bone marrow stromal cells are inhibited by oxidative stress. *J Cell Biochem,* 111**,** 1199-209.

KIRKHAM, G. R., ELLIOT, K. J., KERAMANE, A., SALTER, D. M., DOBSON, J. P., EL HAJ, A. J. & CARTMELL, S. H. 2010. Hyperpolarization of human mesenchymal stem cells in response to magnetic force. *IEEE Trans Nanobioscience,* 9**,** 71-4.

KLEIN-NULEND, J., BAKKER, A. D., BACABAC, R. G., VATSA, A. & WEINBAUM, S. 2013. Mechanosensation and transduction in osteocytes. *Bone,* 54**,** 182-90.

KO, K. S. & MCCULLOCH, C. A. 2000. Partners in protection: interdependence of cytoskeleton and plasma membrane in adaptations to applied forces. *J Membr Biol,* 174**,** 85-95.

KOCK, L., VAN DONKELAAR, C. C. & ITO, K. 2012. Tissue engineering of functional articular cartilage: the current status. *Cell Tissue Res,* 347**,** 613-27.

KON, E., FILARDO, G., ROFFI, A., ANDRIOLO, L. & MARCACCI, M. 2012. New trends for knee cartilage regeneration: from cell-free scaffolds to mesenchymal stem cells. *Curr Rev Musculoskelet Med,* 5**,** 236-43.

KRUGER, E. A., IM, D. D., BISCHOFF, D. S., PEREIRA, C. T., HUANG, W., RUDKIN, G. H., YAMAGUCHI, D. T. & MILLER, T. A. 2011. In vitro mineralization of human mesenchymal stem cells on three-dimensional type I collagen versus PLGA scaffolds: a comparative analysis. *Plast Reconstr Surg,* 127**,** 2301-11.

KSHITIZ, PARK, J., KIM, P., HELEN, W., ENGLER, A. J., LEVCHENKO, A. & KIM, D. H. 2012. Control of stem cell fate and function by engineering physical microenvironments. *Integr Biol (Camb),* 4**,** 1008-18.

KUBINOVA, S. & SYKOVA, E. 2010. Nanotechnologies in regenerative medicine. *Minim Invasive Ther Allied Technol,* 19**,** 144-56.

KUO, J. C. 2013. Mechanotransduction at focal adhesions: integrating cytoskeletal mechanics in migrating cells. *J Cell Mol Med,* 17**,** 704-12.

LAMMERDING, J., FONG, L. G., JI, J. Y., REUE, K., STEWART, C. L., YOUNG, S. G. & LEE, R. T. 2006. Lamins A and C but not lamin B1 regulate nuclear mechanics. *J Biol Chem,* 281**,** 25768-80.

LAMMERDING, J., HSIAO, J., SCHULZE, P. C., KOZLOV, S., STEWART, C. L. & LEE, R. T. 2005. Abnormal nuclear shape and impaired mechanotransduction in emerin-deficient cells. *J Cell Biol,* 170**,** 781-91.

LANG, S. B. 1999. The history of pyroelectricity: from ancient Greece to space missions. *Ferroelectrics,* 230**,** 401-410.

LANGER, R. & VACANTI, J. P. 1993. Tissue engineering. *Science,* 260**,** 920-6.

LAUNEY, M. E., BUEHLER, M. J. & RITCHIE, R. O. 2010. On the Mechanistic Origins of Toughness in Bone. *Annual Review of Materials Research, Vol 40,* 40**,** 25-53.

LEUCHT, P., KIM, J. B., CURREY, J. A., BRUNSKI, J. & HELMS, J. A. 2007. FAK-Mediated mechanotransduction in skeletal regeneration. *PLoS ONE,* 2**,** e390.

LI, Z., YAO, S. J., ALINI, M. & STODDART, M. J. 2010. Chondrogenesis of human bone marrow mesenchymal stem cells in fibrin-polyurethane composites is modulated by frequency and amplitude of dynamic compression and shear stress. *Tissue Eng Part A,* 16**,** 575-84.

LIEDERT, A., CLAES, L. E. & IGNATIUS, A. 2008. Signal transduction pathways involved in mechanotransduction in osteoblastic and mesenchymal stem cells. *Mechanosensitivity in Cells and Tissues.*

LIM, K. T., KIM, J., SEONWOO, H., CHANG, J. U., CHOI, H., HEXIU, J., CHO, W. J., CHOUNG, P. H. & CHUNG, J. H. 2013. Enhanced osteogenesis of human alveolar bone-derived mesenchymal stem cells for tooth tissue engineering using fluid shear stress in a rocking culture method. *Tissue Eng Part C Methods,* 19**,** 128-45.

LIVAK, K. J. & SCHMITTGEN, T. D. 2001. Analysis of relative gene expression data using real-time quantitative PCR and the 2(-Delta Delta C(T)) Method. *Methods,* 25**,** 402-8.

LODISH, H., BERK, A., KAISER, C. A., KRIEGER, M., BRETSCHER, A., PLOEGH, H. & AMON, A. 2013. *Molecular Cell Biology,* New York, USA, Macmillan Higher Education.

MAMMOTO, T. & INGBER, D. E. 2010. Mechanical control of tissue and organ development. *Development,* 137**,** 1407-20.

MANIOTIS, A. J., BOJANOWSKI, K. & INGBER, D. E. 1997a. Mechanical continuity and reversible chromosome disassembly within intact genomes removed from living cells. *J Cell Biochem,* 65**,** 114-30.

MANIOTIS, A. J., CHEN, C. S. & INGBER, D. E. 1997b. Demonstration of mechanical connections between integrins cytoskeletal filaments, and nucleoplasm that stabilize nuclear structure. *Proceedings of the National Academy of Sciences of the United States of America,* 94**,** 849-854.

MARKLEIN, R. A. & BURDICK, J. A. 2010. Controlling stem cell fate with material design. *Adv Mater,* 22**,** 175-89.

MAROLT, D., CAMPOS, I. M., BHUMIRATANA, S., KOREN, A., PETRIDIS, P., ZHANG, G., SPITALNIK, P. F., GRAYSON, W. L. & VUNJAK-NOVAKOVIC, G. 2012. Engineering bone tissue from human embryonic stem cells. *Proc Natl Acad Sci U S A,* 109**,** 8705-9.

MARTIN, C., CHEN, S., MAYA-MENDOZA, A., LOVRIC, J., SIMS, P. F. & JACKSON, D. A. 2009. Lamin B1 maintains the functional plasticity of nucleoli. *J Cell Sci,* 122**,** 1551-62.

MARTINS, R. P., FINAN, J. D., GUILAK, F. & LEE, D. A. 2012. Mechanical regulation of nuclear structure and function. *Annu Rev Biomed Eng,* 14**,** 431-55.

MASON, C. & DUNNILL, P. 2008. A brief definition of regenerative medicine. *Regenerative Medicine,* 3**,** 1-5.

MATHEWS, D. J., DONOVAN, P., HARRIS, J., LOVELL-BADGE, R., SAVULESCU, J. & FADEN, R. 2006. Science and law. Integrity in international stem cell research collaborations. *Science,* 313**,** 921-2.

MATSUZAKA, K., WALBOOMERS, X. F., YOSHINARI, M., INOUE, T. & JANSEN, J. A. 2003. The attachment and growth behavior of osteoblast-like cells on microtextured surfaces. *Biomaterials,* 24**,** 2711-9.

MAUL, T. M., HAMILTON, D. W., NIEPONICE, A., SOLETTI, L. & VORP, D. A. 2007. A new experimental system for the extended application of cyclic hydrostatic pressure to cell culture. *J Biomech Eng,* 129**,** 110-6.

MCBEATH, R., PIRONE, D. M., NELSON, C. M., BHADRIRAJU, K. & CHEN, C. S. 2004. Cell shape, cytoskeletal tension, and RhoA regulate stem cell lineage commitment. *Dev Cell,* 6**,** 483-95.

MCMURRAY, R. J., GADEGAARD, N., TSIMBOURI, P. M., BURGESS, K. V., MCNAMARA, L. E., TARE, R., MURAWSKI, K., KINGHAM, E., OREFFO, R. O. & DALBY, M. J. 2011. Nanoscale surfaces for the long-term maintenance of mesenchymal stem cell phenotype and multipotency. *Nat Mater,* 10**,** 637-44.

MCNAMARA, L. E., BURCHMORE, R., RIEHLE, M. O., HERZYK, P., BIGGS, M. J., WILKINSON, C. D., CURTIS, A. S. & DALBY, M. J. 2012. The role of microtopography in cellular mechanotransduction. *Biomaterials,* 33**,** 2835-47.

MEINKOTH, J. L., ALBERTS, A. S., WENT, W., FANTOZZI, D., TAYLOR, S. S., HAGIWARA, M., MONTMINY, M. & FERAMISCO, J. R. 1993. Signal-Transduction through the Camp-Dependent Protein-Kinase. *Molecular and Cellular Biochemistry,* 128**,** 179-186.

MELOCHE, S. & POUYSSEGUR, J. 2007. The ERK1/2 mitogen-activated protein kinase pathway as a master regulator of the G1- to S-phase transition. *Oncogene,* 26**,** 3227-39.

MICOL, L. A., ANANTA, M., ENGELHARDT, E. M., MUDERA, V. C., BROWN, R. A., HUBBELL, J. A. & FREY, P. 2011. High-density collagen gel tubes as a matrix for primary human bladder smooth muscle cells. *Biomaterials,* 32**,** 1543-8.

MILLER, N. L., LAWSON, C., CHEN, X. L., LIM, S. T. & SCHLAEPFER, D. D. 2012. Rgnef (p190RhoGEF) knockout inhibits RhoA activity, focal adhesion establishment, and cell motility downstream of integrins. *PLoS ONE,* 7**,** e37830.

MIMEAULT, M., HAUKE, R. & BATRA, S. K. 2007. Stem cells: a revolution in therapeutics-recent advances in stem cell biology and their therapeutic applications in regenerative medicine and cancer therapies. *Clin Pharmacol Ther,* 82**,** 252-64.

MINARY-JOLANDAN, M. & YU, M. F. 2009. Nanoscale characterization of isolated individual type I collagen fibrils: polarization and piezoelectricity. *Nanotechnology,* 20**,** 085706.

MORANDO, S., VIGO, T., ESPOSITO, M., CASAZZA, S., NOVI, G., PRINCIPATO, M. C., FURLAN, R. & UCCELLI, A. 2012. The therapeutic effect of mesenchymal stem cell transplantation in experimental autoimmune encephalomyelitis is mediated by peripheral and central mechanisms. *Stem Cell Res Ther,* 3**,** 3.

MUDERA, V., CHEEMA, U., SHAH, R. & LEWIS, M. 2009. Improving biomaterials in tendon and muscle regeneration. *Cellular Response to Biomaterials*, 237-251.

MYCIELSKA, M. E. & DJAMGOZ, M. B. 2004. Cellular mechanisms of direct-current electric field effects: galvanotaxis and metastatic disease. *J Cell Sci,* 117, 1631-9.

NEUBURGER, M., HERGET, G. W., PLAUMANN, L., FALK, A., SCHWALB, H. & ADLER, C. P. 1998. Change in size, number and morphology of the nucleoli in human hearts as a result of hyperfunction. *Pathol Res Pract,* 194, 385-9.

NEUMANN, A. J., ALINI, M., ARCHER, C. W. & STODDART, M. J. 2013. Chondrogenesis of human bone marrow-derived mesenchymal stem cells is modulated by complex mechanical stimulation and adenoviral-mediated overexpression of bone morphogenetic protein 2. *Tissue Eng Part A,* 19, 1285-94.

NIKUKAR, H., REID, S., TSIMBOURI, P. M., RIEHLE, M. O., CURTIS, A. S. & DALBY, M. J. 2013. Osteogenesis of mesenchymal stem cells by nanoscale mechanotransduction. *ACS Nano,* 7, 2758-67.

NORIS-SUAREZ, K., LIRA-OLIVARES, J., FERREIRA, A. M., FEIJOO, J. L., SUAREZ, N., HERNANDEZ, M. C. & BARRIOS, E. 2007. In vitro deposition of hydroxyapatite on cortical bone collagen stimulated by deformation-induced piezoelectricity. *Biomacromolecules,* 8, 941-8.

OREFFO, R. O. & TRIFFITT, J. T. 1999. Future potentials for using osteogenic stem cells and biomaterials in orthopedics. *Bone,* 25, 5S-9S.

OSBORNE, C. S., CHAKALOVA, L., BROWN, K. E., CARTER, D., HORTON, A., DEBRAND, E., GOYENECHEA, B., MITCHELL, J. A., LOPES, S., REIK, W. & FRASER, P. 2004. Active genes dynamically colocalize to shared sites of ongoing transcription. *Nat Genet,* 36, 1065-71.

OSTLUND, C., FOLKER, E. S., CHOI, J. C., GOMES, E. R., GUNDERSEN, G. G. & WORMAN, H. J. 2009. Dynamics and molecular interactions of linker of nucleoskeleton and cytoskeleton (LINC) complex proteins. *J Cell Sci,* 122, 4099-108.

PAJEROWSKI, J. D., DAHL, K. N., ZHONG, F. L., SAMMAK, P. J. & DISCHER, D. E. 2007. Physical plasticity of the nucleus in stem cell differentiation. *Proc Natl Acad Sci U S A,* 104, 15619-24.

PATLA, I., VOLBERG, T., ELAD, N., HIRSCHFELD-WARNEKEN, V., GRASHOFF, C., FASSLER, R., SPATZ, J. P., GEIGER, B. & MEDALIA, O. 2010. Dissecting

the molecular architecture of integrin adhesion sites by cryo-electron tomography. *Nat Cell Biol,* 12**,** 909-15.

PATWARI, P. & LEE, R. T. 2008. Mechanical control of tissue morphogenesis. *Circ Res,* 103**,** 234-43.

PEDRINELLI, R., BALLO, P., FIORENTINI, C., DENTI, S., GALDERISI, M., GANAU, A., GERMANO, G., INNELLI, P., PAINI, A., PERLINI, S., SALVETTI, M. & ZACA, V. 2012. Hypertension and acute myocardial infarction: an overview. *J Cardiovasc Med (Hagerstown),* 13**,** 194-202.

PELLING, A. E., DAWSON, D. W., CARREON, D. M., CHRISTIANSEN, J. J., SHEN, R. R., TEITELL, M. A. & GIMZEWSKI, J. K. 2007a. Distinct contributions of microtubule subtypes to cell membrane shape and stability. *Nanomedicine,* 3**,** 43-52.

PELLING, A. E., VERAITCH, F. S., PUI-KEI CHU, C., NICHOLLS, B. M., HEMSLEY, A. L., MASON, C. & HORTON, M. A. 2007b. Mapping correlated membrane pulsations and fluctuations in human cells. *Journal of Molecular Recognition,* 20**,** 467-75.

PHIMPHILAI, M., ZHAO, Z., BOULES, H., ROCA, H. & FRANCESCHI, R. T. 2006. BMP signaling is required for RUNX2-dependent induction of the osteoblast phenotype. *J Bone Miner Res,* 21**,** 637-46.

PIERRES, A., BENOLIEL, A. M., TOUCHARD, D. & BONGRAND, P. 2008. How cells tiptoe on adhesive surfaces before sticking. *Biophys J,* 94**,** 4114-22.

PIERRES, A., MONNET-CORTI, V., BENOLIEL, A. M. & BONGRAND, P. 2009. Do membrane undulations help cells probe the world? *Trends Cell Biol,* 19**,** 428-33.

POON, E., KONG, C. W. & LI, R. A. 2011. Human pluripotent stem cell-based approaches for myocardial repair: from the electrophysiological perspective. *Mol Pharm,* 8**,** 1495-504.

PRE, D., CECCARELLI, G., GASTALDI, G., ASTI, A., SAINO, E., VISAI, L., BENAZZO, F., DE ANGELIS, M. G. C. & MAGENES, G. 2011. The differentiation of human adipose-derived stem cells (hASCs) into osteoblasts is promoted by low amplitude, high frequency vibration treatment. *Bone,* 49**,** 295-303.

RAPPAZ, B., BARBUL, A., HOFFMANN, A., BOSS, D., KORENSTEIN, R., DEPEURSINGE, C., MAGISTRETTI, P. J. & MARQUET, P. 2009. Spatial

analysis of erythrocyte membrane fluctuations by digital holographic microscopy. *Blood Cells Mol Dis,* 42**,** 228-32.

RASKA, I., SHAW, P. J. & CMARKO, D. 2006. Structure and function of the nucleolus in the spotlight. *Curr Opin Cell Biol,* 18**,** 325-34.

RATH, S. N., STROBEL, L. A., ARKUDAS, A., BEIER, J. P., MAIER, A. K., GREIL, P., HORCH, R. E. & KNESER, U. 2012. Osteoinduction and survival of osteoblasts and bone-marrow stromal cells in 3D biphasic calcium phosphate scaffolds under static and dynamic culture conditions. *J Cell Mol Med,* 16**,** 2350-61.

REHFELDT, F., ENGLER, A. J. & DISCHER, D. E. 2007a. Biomechanics of adult stem cell differentiation guided by matrix elasticity. *Biophysical Journal***,** 636A-636A.

REHFELDT, F., ENGLER, A. J., ECKHARDT, A., AHMED, F. & DISCHER, D. E. 2007b. Cell responses to the mechanochemical microenvironment--implications for regenerative medicine and drug delivery. *Adv Drug Deliv Rev,* 59**,** 1329-39.

REINISH, G. B. & NOWICK, A. S. 1975. Piezoelectric properties of bone as functions of moisture content. *Nature,* 253**,** 626-627.

REN, X. D., KIOSSES, W. B., SIEG, D. J., OTEY, C. A., SCHLAEPFER, D. D. & SCHWARTZ, M. A. 2000. Focal adhesion kinase suppresses Rho activity to promote focal adhesion turnover. *J Cell Sci,* 113 (Pt 20)**,** 3673-8.

RIBEIRO, A. J., TOTTEY, S., TAYLOR, R. W., BISE, R., KANADE, T., BADYLAK, S. F. & DAHL, K. N. 2012. Mechanical characterization of adult stem cells from bone marrow and perivascular niches. *J Biomech,* 45**,** 1280-7.

ROTHBALLER, A., SCHWARTZ, T. U. & KUTAY, U. 2013. LINCing complex functions at the nuclear envelope: what the molecular architecture of the LINC complex can reveal about its function. *Nucleus,* 4**,** 29-36.

RUBIN, C. T., CAPILLA, E., LUU, Y. K., BUSA, B., CRAWFORD, H., NOLAN, D. J., MITTAL, V., ROSEN, C. J., PESSIN, J. E. & JUDEX, S. 2007. Adipogenesis is inhibited by brief, daily exposure to high-frequency, extremely low-magnitude mechanical signals. *Proc Natl Acad Sci U S A,* 104**,** 17879-84.

RUPANI, A., BALINT, R. & CARTMELL, S. H. 2012. Osteoblasts and their applications in bone tissue engineering. *Cell Health and Cytoskeleton,* 4**,** 49-61.

RUST, P. A., KALSI, P., BRIGGS, T. W., CANNON, S. R. & BLUNN, G. W. 2007. Will mesenchymal stem cells differentiate into osteoblasts on allograft? *Clin Orthop Relat Res,* 457**,** 220-6.

SADIE-VAN GIJSEN, H., CROWTHER, N. J., HOUGH, F. S. & FERRIS, W. F. 2013. The interrelationship between bone and fat: from cellular see-saw to endocrine reciprocity. *Cell Mol Life Sci,* 70**,** 2331-49.

SANDRASAGRA, M. J. 2007. People: World's aging population will top 9 billion by 2050. *Global Information Network***,** 5-9.

SAWADA, Y. & SHEETZ, M. P. 2002. Force transduction by Triton cytoskeletons. *J Cell Biol,* 156**,** 609-15.

SAWADA, Y., TAMADA, M., DUBIN-THALER, B. J., CHERNIAVSKAYA, O., SAKAI, R., TANAKA, S. & SHEETZ, M. P. 2006. Force sensing by mechanical extension of the Src family kinase substrate p130Cas. *Cell,* 127**,** 1015-26.

SCADDEN, D. T. 2006. The stem-cell niche as an entity of action. *Nature,* 441**,** 1075-9.

SCHILLER, H. B. & FASSLER, R. 2013. Mechanosensitivity and compositional dynamics of cell-matrix adhesions. *Embo Reports,* 14**,** 509-19.

SCHMIDT, A. & HALL, M. N. 1998. Signaling to the actin cytoskeleton. *Annu Rev Cell Dev Biol,* 14**,** 305-38.

SCHMITTGEN, T. D. & LIVAK, K. J. 2008. Analyzing real-time PCR data by the comparative C(T) method. *Nature Protocols,* 3**,** 1101-8.

SCHOFIELD, A. V. & BERNARD, O. 2013. Rho-associated coiled-coil kinase (ROCK) signaling and disease. *Crit Rev Biochem Mol Biol,* 48**,** 301-16.

SCHULZ, T. J. & TSENG, Y. H. 2013. Brown adipose tissue: development, metabolism and beyond. *Biochem J,* 453**,** 167-78.

SCHWARTZ, M. A. 2010. Integrins and extracellular matrix in mechanotransduction. *Cold Spring Harb Perspect Biol,* 2**,** a005066.

SCHWARZ, U. S., ERDMANN, T. & BISCHOFS, I. B. 2006. Focal adhesions as mechanosensors: the two-spring model. *Biosystems,* 83**,** 225-32.

SELHUBER-UNKEL, C., ERDMANN, T., LOPEZ-GARCIA, M., KESSLER, H., SCHWARZ, U. S. & SPATZ, J. P. 2010. Cell adhesion strength is controlled by intermolecular spacing of adhesion receptors. *Biophys J,* 98**,** 543-51.

SEONG, J., WANG, N. & WANG, Y. 2013. Mechanotransduction at focal adhesions: from physiology to cancer development. *J Cell Mol Med,* 17**,** 597-604.

SHAUL, Y. D. & SEGER, R. 2007. The MEK/ERK cascade: from signaling specificity to diverse functions. *Biochim Biophys Acta,* 1773**,** 1213-26.

SHIH, Y. R., TSENG, K. F., LAI, H. Y., LIN, C. H. & LEE, O. K. 2011. Matrix stiffness regulation of integrin-mediated mechanotransduction during osteogenic differentiation of human mesenchymal stem cells. *J Bone Miner Res,* 26**,** 730-8.

SIKAVITSAS, V. I., BANCROFT, G. N., HOLTORF, H. L., JANSEN, J. A. & MIKOS, A. G. 2003. Mineralized matrix deposition by marrow stromal osteoblasts in 3D perfusion culture increases with increasing fluid shear forces. *Proc Natl Acad Sci U S A,* 100**,** 14683-8.

SIKAVITSAS, V. I., BANCROFT, G. N. & MIKOS, A. G. 2002. Formation of three-dimensional cell/polymer constructs for bone tissue engineering in a spinner flask and a rotating wall vessel bioreactor. *J Biomed Mater Res,* 62**,** 136-48.

SIRINOGLU DEMIRIZ, I., TEKGUNDUZ, E. & ALTUNTAS, F. 2012. What is the most appropriate source for hematopoietic stem cell transplantation? Peripheral stem cell/bone marrow/cord blood. *Bone Marrow Res,* 2012**,** 834040.

STEIN, G. S. & LIAN, J. B. 1993. Molecular mechanisms mediating proliferation/differentiation interrelationships during progressive development of the osteoblast phenotype. *Endocr Rev,* 14**,** 424-42.

STEWARD, R. L., JR., CHENG, C. M., WANG, D. L. & LEDUC, P. R. 2010. Probing cell structure responses through a shear and stretching mechanical stimulation technique. *Cell Biochem Biophys,* 56**,** 115-24.

STOLBERG, S. & MCCLOSKEY, K. E. 2009. Can Shear Stress Direct Stem Cell Fate? *Biotechnology Progress,* 25**,** 10-19.

SZABO, B., SELMECZI, D., KORNYEI, Z., MADARASZ, E. & ROZLOSNIK, N. 2002. Atomic force microscopy of height fluctuations of fibroblast cells. *Phys Rev E Stat Nonlin Soft Matter Phys,* 65**,** 041910.

TAKEUCHI, Y., SUZAWA, M., KIKUCHI, T., NISHIDA, E., FUJITA, T. & MATSUMOTO, T. 1997. Differentiation and transforming growth factor-beta receptor down-regulation by collagen-alpha 2 beta 1 integrin interaction is mediated by focal adhesion kinase and its downstream signals in murine osteoblastic cells. *Journal of Biological Chemistry,* 272**,** 29309-29316.

TAMMA, R., DELL'ENDICE, S., NOTARNICOLA, A., MORETTI, L., PATELLA, S., PATELLA, V., ZALLONE, A. & MORETTI, B. 2009. Extracorporeal shock waves stimulate osteoblast activities. *Ultrasound in Medicine and Biology,* 35**,** 2093-100.

TANG, N., ZHAO, Z., ZHANG, L., YU, Q., LI, J., XU, Z. & LI, X. 2012. Up-regulated osteogenic transcription factors during early response of human periodontal ligament stem cells to cyclic tensile strain. *Archives of Medical Science,* 8**,** 422-30.

TAY, C. Y., KOH, C. G., TAN, N. S., LEONG, D. T. & TAN, L. P. 2013. Mechanoregulation of stem cell fate via micro-/nano-scale manipulation for regenerative medicine. *Nanomedicine (Lond),* 8**,** 623-38.

TEH, T. K., TOH, S. L. & GOH, J. C. 2013. Aligned fibrous scaffolds for enhanced mechanoresponse and tenogenesis of mesenchymal stem cells. *Tissue Eng Part A,* 19**,** 1360-72.

THOMPSON, W. R., RUBIN, C. T. & RUBIN, J. 2012. Mechanical regulation of signaling pathways in bone. *Gene,* 503**,** 179-93.

TIRKKONEN, L., HALONEN, H., HYTTINEN, J., KUOKKANEN, H., SIEVANEN, H., KOIVISTO, A. M., MANNERSTROM, B., SANDOR, G. K., SUURONEN, R., MIETTINEN, S. & HAIMI, S. 2011. The effects of vibration loading on adipose stem cell number, viability and differentiation towards bone-forming cells. *J R Soc Interface,* 8**,** 1736-47.

TOUR, G., WENDEL, M. & TCACENCU, I. 2013. Human fibroblast-derived extracellular matrix constructs for bone tissue engineering applications. *J Biomed Mater Res A,* 101**,** 2826-37.

TSCHUMPERLIN, D. J., LIU, F. & TAGER, A. M. 2013. Biomechanical regulation of mesenchymal cell function. *Current Opinion in Rheumatology,* 25**,** 92-100.

TSIMBOURI, P. M., MCMURRAY, R. J., BURGESS, K. V., ALAKPA, E. V., REYNOLDS, P. M., MURAWSKI, K., KINGHAM, E., OREFFO, R. O., GADEGAARD, N. & DALBY, M. J. 2012. Using nanotopography and metabolomics to identify biochemical effectors of multipotency. *ACS Nano,* 6**,** 10239-49.

TSIMBOURI, P. M., MURAWSKI, K., HAMILTON, G., HERZYK, P., OREFFO, R. O., GADEGAARD, N. & DALBY, M. J. 2013. A genomics approach in determining nanotopographical effects on MSC phenotype. *Biomaterials,* 34**,** 2177-84.

TURNER, C. H. & PAVALKO, F. M. 1998. Mechanotransduction and functional response of the skeleton to physical stress: the mechanisms and mechanics of bone adaptation. *J Orthop Sci,* 3**,** 346-55.

VEMURI, M. C., CHASE, L. G. & RAO, M. S. 2011. Mesenchymal stem cell assays and applications. *Methods Mol Biol,* 698**,** 3-8.

VILLAVICENCIO, E. H., WALTERHOUSE, D. O. & IANNACCONE, P. M. 2000. The sonic hedgehog-patched-gli pathway in human development and disease. *American Journal of Human Genetics,* 67**,** 1047-54.

VOGEL, V. & SHEETZ, M. 2006. Local force and geometry sensing regulate cell functions. *Nat Rev Mol Cell Biol,* 7**,** 265-75.

WANG, N., BUTLER, J. P. & INGBER, D. E. 1993. Mechanotransduction across the cell surface and through the cytoskeleton. *Science,* 260**,** 1124-7.

WANG, N., NARUSE, K., STAMENOVIC, D., FREDBERG, J. J., MIJAILOVICH, S. M., TOLIC-NORRELYKKE, I. M., POLTE, T., MANNIX, R. & INGBER, D. E. 2001. Mechanical behavior in living cells consistent with the tensegrity model. *Proc Natl Acad Sci U S A,* 98**,** 7765-70.

WANG, N., TYTELL, J. D. & INGBER, D. E. 2009. Mechanotransduction at a distance: mechanically coupling the extracellular matrix with the nucleus. *Nat Rev Mol Cell Biol,* 10**,** 75-82.

WANG, Y. K. & CHEN, C. S. 2013. Cell adhesion and mechanical stimulation in the regulation of mesenchymal stem cell differentiation. *J Cell Mol Med,* 17**,** 823-32.

WARD, D. F., JR., WILLIAMS, W. A., SCHAPIRO, N. E., WEBER, G. L., CHRISTY, S. R., SALT, M., KLEES, R. F., BOSKEY, A. & PLOPPER, G. E. 2007. Focal adhesion kinase signaling controls cyclic tensile strain enhanced collagen I-induced osteogenic differentiation of human mesenchymal stem cells. *Mol Cell Biomech,* 4**,** 177-88.

WATT, F. M. & HOGAN, B. L. 2000. Out of Eden: stem cells and their niches. *Science,* 287**,** 1427-30.

WESTHOFF, M. A., SERRELS, B., FINCHAM, V. J., FRAME, M. C. & CARRAGHER, N. O. 2004. SRC-mediated phosphorylation of focal adhesion kinase couples actin and adhesion dynamics to survival signaling. *Mol Cell Biol,* 24**,** 8113-33.

WESTPHAL, M., JUNGBLUTH, A., HEIDECKER, M., MUHLBAUER, B., HEIZER, C., SCHWARTZ, J. M., MARRIOTT, G. & GERISCH, G. 1997. Microfilament dynamics during cell movement and chemotaxis monitored using a GFP-actin fusion protein. *Curr Biol,* 7**,** 176-83.

WINKLER, T., VON ROTH, P., RADOJEWSKI, P., URBANSKI, A., HAHN, S., PREININGER, B., DUDA, G. N. & PERKA, C. 2012. Immediate and delayed transplantation of mesenchymal stem cells improve muscle force after skeletal muscle injury in rats. *J Tissue Eng Regen Med,* 6 Suppl 3**,** s60-7.

WU, D., GANATOS, P., SPRAY, D. C. & WEINBAUM, S. 2011. On the electrophysiological response of bone cells using a Stokesian fluid stimulus probe for delivery of quantifiable localized picoNewton level forces. *J Biomech,* 44**,** 1702-8.

WYSOCKI, A., BUTLER, M., SHAMLIYAN, T. & KANE, R. L. 2011. Whole-body vibration therapy for osteoporosis: state of the science. *Annals of Internal Medicine,* 155**,** 680-6, W206-13.

XIAO, G., JIANG, D., GOPALAKRISHNAN, R. & FRANCESCHI, R. T. 2002. Fibroblast growth factor 2 induction of the osteocalcin gene requires MAPK activity and phosphorylation of the osteoblast transcription factor, Cbfa1/Runx2. *J Biol Chem,* 277**,** 36181-7.

YEATTS, A. B., CHOQUETTE, D. T. & FISHER, J. P. 2013. Bioreactors to influence stem cell fate: augmentation of mesenchymal stem cell signaling pathways via dynamic culture systems. *Biochim Biophys Acta,* 1830**,** 2470-80.

YU, J., VODYANIK, M. A., SMUGA-OTTO, K., ANTOSIEWICZ-BOURGET, J., FRANE, J. L., TIAN, S., NIE, J., JONSDOTTIR, G. A., RUOTTI, V., STEWART, R., SLUKVIN, II & THOMSON, J. A. 2007. Induced pluripotent stem cell lines derived from human somatic cells. *Science,* 318**,** 1917-20.

YUAN, L., SAKAMOTO, N., SONG, G. & SATO, M. 2013. High-level Shear Stress Stimulates Endothelial Differentiation and VEGF Secretion by Human Mesenchymal Stem Cells. *Cellular and Molecular Bioengineering,* 6**,** 220-229.

ZHAI, W., LU, H., WU, C., CHEN, L., LIN, X., NAOKI, K., CHEN, G. & CHANG, J. 2013. Stimulatory effects of the ionic products from Ca-Mg-Si bioceramics on both osteogenesis and angiogenesis in vitro. *Acta Biomater,* 9**,** 8004-14.

ZHANG, C., LI, J., ZHANG, L., ZHOU, Y., HOU, W., QUAN, H., LI, X., CHEN, Y. & YU, H. 2012. Effects of mechanical vibration on proliferation and osteogenic differentiation of human periodontal ligament stem cells. *Arch Oral Biol,* 57**,** 1395-407.

ZHOU, T., BENDA, C., DUNZINGER, S., HUANG, Y., HO, J. C., YANG, J., WANG, Y., ZHANG, Y., ZHUANG, Q., LI, Y., BAO, X., TSE, H. F., GRILLARI, J., GRILLARI-VOGLAUER, R., PEI, D. & ESTEBAN, M. A. 2012. Generation of human induced pluripotent stem cells from urine samples. *Nature Protocols,* 7**,** 2080-9.

ZHOU, Y., GUAN, X., ZHU, Z., GAO, S., ZHANG, C., LI, C., ZHOU, K., HOU, W. & YU, H. 2011. Osteogenic differentiation of bone marrow-derived mesenchymal stromal cells on bone-derived scaffolds: effect of microvibration and role of ERK1/2 activation. *Eur Cell Mater,* 22**,** 12-25.

ZHU, X. H. 2010. Piezoelectric Ceramics Materials: Processing, Properties, Characterization, and Applications. *Piezoelectric Materials: Structure, Properties and Applications***,** 1-36.

ZIEGLER, W. H., GINGRAS, A. R., CRITCHLEY, D. R. & EMSLEY, J. 2008. Integrin connections to the cytoskeleton through talin and vinculin. *Biochem Soc Trans,* 36**,** 235-9.

ZOJA, C., GARCIA, P. B., ROTA, C., CONTI, S., GAGLIARDINI, E., CORNA, D., ZANCHI, C., BIGINI, P., BENIGNI, A., REMUZZI, G. & MORIGI, M. 2012. Mesenchymal stem cell therapy promotes renal repair by limiting glomerular podocyte and progenitor cell dysfunction in adriamycin-induced nephropathy. *Am J Physiol Renal Physiol,* 303**,** F1370-81.

ZUK, P. A., ZHU, M., ASHJIAN, P., DE UGARTE, D. A., HUANG, J. I., MIZUNO, H., ALFONSO, Z. C., FRASER, J. K., BENHAIM, P. & HEDRICK, M. H. 2002. Human adipose tissue is a source of multipotent stem cells. *Mol Biol Cell,* 13**,** 4279-95.

ZUK, P. A., ZHU, M., MIZUNO, H., HUANG, J., FUTRELL, J. W., KATZ, A. J., BENHAIM, P., LORENZ, H. P. & HEDRICK, M. H. 2001. Multilineage cells from human adipose tissue: implications for cell-based therapies. *Tissue Eng,* 7**,** 211-28.